INTERACTIONS AND DYNAMICS OF THE TYPE IV PILUS ALIGNMENT SUBCOMPLEX PROTEINS, PILN AND PILO

INTERACTIONS AND DYNAMICS OF THE TYPE IV PILUS ALIGNMENT SUBCOMPLEX PROTEINS, PILN AND PILO

By

TIFFANY LEE LEIGHTON, B.Sc., M.Sc.

A Thesis Submitted to the School of Graduate Studies in Partial Fulfillment of the Requirements for the Degree

Doctor of Philosophy

McMaster University DOCTOR OF PHILOSOPHY (2016)
Hamilton, Ontario (Biochemistry and Biomedical Sciences)

TITLE: Interactions and dynamics of the type IV pilus alignment subcomplex proteins, PilN and PilO

AUTHOR: Tiffany L. Leighton, B.Sc. (Trent University), M.Sc. (McMaster University)

SUPERVISOR: Dr. Lori L Burrows

NUMBER OF PAGES: 226

This thesis is dedicated to my family.
With all my love.

LAY ABSTRACT

Pseudomonas aeruginosa is an opportunistic bacterium, able to infect individuals with weakened immune systems. It attaches to and moves along surfaces using long, thin, sticky, retractable fibres known as type IV pili. Similar to a grappling gun, a functional type IV pilus system requires four subcomplexes working in unison to allow for the extension, adherence, and retraction of pilus fibres, which pulls the cell forward towards the point of attachment. Two key proteins, PilN and PilO, are bound to each other and allow for efficient extension and retraction of the pilus fibre. This study focused on characterization of the interactions of PilN and PilO, and on understanding whether dynamic rearrangements of the interfaces between these proteins is required for proper function of the system. We show that although these proteins have extensive interaction interfaces, single residue substitutions in either of them can disrupt the ability of the bacteria to properly extend and/or retract their pili. This work furthers our understanding of the structures and regions of interaction between PilN and PilO, providing information that might allow disruption of these interfaces to block bacterial attachment or motility, both of which are important for infection.

ABSTRACT

Type IV pili (T4P) are long, thin, flexible surface appendages used by various bacteria for surface adhesion, cell-cell aggregation, DNA uptake, biofilm formation and motility. *Pseudomonas aeruginosa* is a Gram-negative opportunistic pathogen, and uses T4P as a key virulence factor to infect immunocompromised individuals. Four subcomplexes make up a functional T4P system in *P. aeruginosa* and the role of the alignment subcomplex is to physically connect the outer membrane pore with the inner membrane motor, allowing for efficient extrusion of the pilus fibre from the cell. Two alignment subcomplex proteins, PilN and PilO, form heterodimers and are required for proper function of the system. These proteins may be able to transduce signals between various T4P components to indicate extension and/or retraction of the pilus fibre. This thesis focused on characterization of the interaction interfaces between PilN and PilO, and on understanding the dynamics required for proper function of the system. We show that although PilN and PilO make extensive interaction contacts throughout their lengths, single point substitutions at key residues can successfully disrupt the function of the T4P system. Crosslinking PilN and PilO as homo- or heterodimers can disrupt motility and surface piliation, indicating that interfaces between these proteins must be dynamic to allow proper T4P function. A high resolution X-ray crystal structure of PilO was solved and exhibits new structural features previously unidentified. This work furthers our understanding

of the structures and regions of interaction between PilN and PilO, as well as defining a role for these proteins in extension and retraction.

ACKNOWLEDGEMENTS

First and foremost I would like to thank my amazing supervisor and role model, Dr. Lori Burrows. Your guidance, patience, and advice over the past four years, have played an instrumental role in my success. You told me to do something scary every day and to push myself in both my work and personal life, which has helped me to grow as both a scientist and as an individual. Thank you for your continued support, I really couldn't have done this without you.

To my committee members both past and present, Dr. Murray Junop, Dr. Lynne Howell, and Dr. Alba Guarné, I want to thank you all for your encouragement and passion for science. Dr. Junop, I am so lucky to have had the opportunity to work with you and your wonderful lab group over the past six years. Mac, Seiji, Beverly, Chris, and your other amazing students (too many to name over the years) have been wonderful teachers and friends, a testament to your patience and guidance. Dr. Howell you've been like a second supervisor to me through this degree, and I cannot thank you enough for the constant support and constructive criticisms during this journey. Last but certainly not least Dr. Alba Guarné, although you were a late addition to my committee, thank you for your constant enthusiasm, helpful suggestions, and your fresh perspectives. My committee surpassed all expectations, and I feel grateful to have had such strong, positive, humorous, and brilliant scientists influencing me.

I want to thank all my friends and mentors in the Burrows lab; even if I had tried, I could not have chosen a more amazing group of people to spend

these years with. In no particular order…Dr. Ryan, Sara, Ylan, Ryan B, Hanjeong, Uyen, Martin, Tori, and Tyson, you are some of the most brilliant, funny, and amazing individuals that I have met and had the pleasure to work with. There are so many great times between family fun days, trips to the Phoenix, deep conversations over coffee, and wine days (who could forget those!). Thanks for the memories and I wish you all nothing but the best.

Last but certainly not least I want to thank my amazing family. There was no better feeling than knowing that I had a personal cheering section behind me, rooting me on every step of the way. Mom and Dad, you've provided me with a constant stream of encouragement, love, and support my entire life, and I couldn't have embarked on this incredible journey without you. Now at its end, I never thought that I would be standing without one of you by my side; dad I miss you, and I think about you every day. To my brother Darrell and my sister-in-law Carmen, you have both been such an amazing support team, constantly making me laugh and listening to my various science woes. To Tristan, my friend, my confidant, my partner in crime, thank you for not only putting up with me but also being there to support me when I needed it most. Thank you for listening to each one of my presentations (sometimes multiple times) and asking me all the right questions (I do!). There was never a better, more supportive, and encouraging family than mine.

TABLE OF CONTENTS

LAY ABSTRACT ..... **iv**

ABSTRACT ..... **v**

ACKNOWLEDGEMENTS ..... **vii**

TABLE OF CONTENTS ..... **ix**

LIST OF FIGURES ..... **xiii**

LIST OF TABLES ..... **xvi**

LIST OF ABBREVIATIONS ..... **xvii**

CHAPTER ONE **1**

Preface **2**

Overview **3**

Type IV pili classification **4**

The type II secretion system **5**

Functions of type IV pili **7**

Type IV pili gene organization in *P. aeruginosa* **8**

Type IV pilus system assembly in *P. aeruginosa* **11**

The secretin: a gate to the outside 12

The pilus fibre: the rope and grappling hook 14

The motor: powering the grappling hook 17

The alignment subcomplex: threading the needle 20

PilM 22

PilN 24

PilO 26

PilP 27

Proposed functions of the alignment subcomplex 28

Hypothesis and Research Aims **31**

CHAPTER TWO **34**

Preface **35**

Title page and author list **36**

Abstract **37**

Importance **38**

Introduction **38**

Experimental procedures **44**

Strains, media and growth conditions 44

Bacterial Two Hybrid (BTH) β-galacotsidase Activity Assay 44

Generation of pilN and pilO mutations on the chromosome of *P. aeruginosa* PAK 45
Generation of *pilT* mutants 46
Twitching motility assays 47
Sheared surface protein preparation 48
Preparation of whole cell lysates 48
Western blot analysis 49
Results 49
PilO forms homodimers and heterodimers, while PilN forms only heterodimers 49
The transmembrane segments of PilNO are important for their interaction 52
Point mutations in the coiled coils of PilN or PilO disrupt their interaction in the BTH assay 53
Substitutions in PilN and PilO disrupt the dynamics of the T4P system 58
The core domain of PilN is more sensitive to perturbation than the coiled-coil region 60
Non-piliated mutants can assemble pili in a retraction deficient background 61
Discussion 62
Acknowledgements 69
Supplementary 70

CHAPTER THREE 80
Preface 81
Title page and author list 82
Abstract 83
Introduction 84
Results 88
Selection of residues for Cys substitution 88
Formation of Cys cross-linked PilNO and PilOO dimers *in vivo* 92
Disulfide bond formation between PilN and/or PilO disrupts T4P function 96
Lack of piliation is caused by inefficient assembly 98
Specific single Cys mutations affect function of the T4P system 99
Single Cys substitutions allow for *in vivo* homodimer formation but only a subset have functional consequences 101
Heterodimer formation of $PilN^{R142C}$ and $PilO^{D175C}$ is abolished in a *pilM* background 101
Heterodimer formation of $PilN^{R142C}$ and $PilO^{D175C}$ is also abolished in a *pilP* background 104

Other T4P components do not modulate the PilNO interface 105
Discussion 108
PilN and PilO may form dimers of dimers *in vivo* 108
PilN and PilO homodimers may represent a functional – rather than assembly intermediate – state of the T4P system 111
Modulation of the PilNO core interface by the other alignment subcomplex components 114
Experimental Procedures 117
Strains, media and growth conditions 117
Generation of Cys mutants 118
Generation of *pilN* and *pilO* Cys mutations onto the chromosome of *P. aeruginosa* PAK 118
Preparation of whole cell lysates 119
Western blot analysis 119
Expression and purification of $PilN_{\Delta 44}$ and $PilO_{\Delta 51}$ 120
Twitching motility assays 122
Sheared surface protein preparation 122
In vivo disulfide crosslinking analysis 123
Generation of PilN and PilO Cys pairs in various T4P component mutant backgrounds 123
Acknowledgements 129
Conflict of Interest 129

CHAPTER FOUR 130
Preface 131
Title page and author list 132
Abstract 133
Introduction 134
Experimental procedures 137
Strains, media and growth conditions 137
Expression and purification of $PilN_{\Delta 44}/PilO_{\Delta 51}/PilP_{\Delta 18}$ 138
TEV Digestion 140
Reductive Methylation 140
Crystallization and structural determination 142
Mass Spectrometry of the $PilN_{\Delta 44}/PilO_{\Delta 51}/PilP_{\Delta 18}$ complex 143
PilO bioinformatics analysis 143
Twitching motility assays 145
Sheared surface protein preparation 145
Preparation of whole cell lysates 146

Western blot analysis 146
Results 147
A new 1.7 Å crystal structure of $PilO_{\Delta 109}$ reveals novel secondary structure characteristics 147
The predicted dimer interface for $PilO_{\Delta 109}$ is more similar to the EspM from *V. cholera*, than the previous PilO structure 154
Two highly conserved hydrophobic areas correspond to unstructured loop regions 156
Two residues in the second PilO hydrophobic region are required for T4P function 159
Discussion 161
Acknowledgments 164
Supplementary data 165
CHAPTER FIVE 173
Discussion 174
PilNO interaction interfaces contribute to pilus extension/retraction 174
A new model of PilNO interactions 175
Seven PilNO tetramers likely surround a 14-membered secretin with 7-fold symmetry 180
Future directions 183
PilNO core interactions 183
Crosslinking of the PilN and PilO coiled-coils 184
Small molecule inhibitors of PilNO interactions 185
Additional roles of PilN and PilO in signalling 186
PilNOP structural studies 187
Significance and conclusions 190
REFERENCES 192

LIST OF FIGURES

CHAPTER ONE - Introduction…… 1
Figure 1.1 Electron Microscopy of polar T4P on *P. aeruginosa*…… 3
Figure 1.2 Gene organization and cartoon schematic of the type IVa pilus system in *P. aeruginosa*…….. 10
Figure 1.3 Domain schematic and structural models of alignment subcomplex proteins in *P. aeruginosa*..…… 21

CHAPTER TWO - Novel role for PilNO in type IV pilus retraction revealed by alignment subcomplex mutations…… 34
Figure 2.1 The type IV pilus system in *Pseudomonas aeruginosa*……. 41
Figure 2.2 A PilO chimera disrupts PilNO heterodimer formation in the BTH system……. 51
Figure 2.3 Model of a PilNO heterodimer……. 54
Figure 2.4 Specific mutations in the coiled-coil region of PilN disrupt PilNO interaction……... 57
Figure 2.5 Specific *pilN* and *pilO* point mutations on the *P. aeruginosa* PAK chromosome affect piliation and twitching motility…….. 59
Figure 2.6 PilN ES132-133VA and MR141-142KL assemble pili in retraction-deficient backgrounds……... 62
Figure S2.1 Amino acid sequences and secondary structures of PilN and PilO…….. 75
Figure S2.2 All BTH fusion constructs are stable…….. 76
Figure S2.3 Intracellular levels of alignment subcomplex proteins and PilA are unaffected by PilN and PilO chromosomal mutations…….. 77
Figure S2.4 Twitching motility of PilN and PilO mutants compared to wild-type…….. 78
Figure S2.5 Interaction between PilM and PilN in the BTH system is altered when the TMS of PilN is replaced with that of PilO…… 79

CHAPTER THREE - *In vivo* capture of the type IV pilus system PilN and PilO homo- and heterodimers by Cys crosslinking…….. 80
Figure 3.1 Locations of residues chosen for Cys substitution mutagenesis in PilN and PilO…….. 89
Figure 3.2 Formation of disulfide-bonded homo- and heterodimers *in vivo*... 91
Figure 3.3 Confirmation of homo- and heterodimer formation of PilN and

PilO using Cys crosslinking analysis *in vitro*…….…… 95
Figure 3.4 Functional consequences of covalent dimer formation in wild type and retraction deficient backgrounds…… 97
Figure 3.5 $PilN^{R142C}$ and $PilO^{D175C}$ single Cys substitutions cause T4P dysfunction in wild-type and retraction deficient backgrounds..... 100
Figure 3.6 Heterodimer formation is abolished in *pilM* or *pilP* backgrounds……. 103
Figure 3.7 Disruption of *pilA, pilB, pilC, pilT,* and *pilU* in $PilN^{R142C}$/$PilO^{D175C}$, $PilO^{A158C/I178C}$, & $PilO^{Y154C/I178C}$ backgrounds……... 106
Figure 3.8 Dimerization of $PilN^{R142C}$/$PilO^{D175C}$, $PilO^{A158C/I178C}$, & $PilO^{Y154C/I178C}$ is unaffected by loss of non-alignment subcomplex components…… 107
Figure 3.9 Model of the interaction between PilN and PilO with other T4P components…….. 113

CHAPTER FOUR – Analysis of *Pseudomonas aeruginosa* PilO based on a new high-resolution structure: conserved, unstructured regions are important for type IV pilus function…….. 130
Figure 4.1 Structure and topology diagram of $PilO_{\Delta109}$……. 150
Figure 4.2 Comparison of the PilO structures…… 152
Figure 4.3 The predicted dimeric interface of the $PilO_{\Delta109}$ structure is more similar to EpsM from *V. cholera*, than the previous PilO structure……... 155
Figure 4.4 Highly conserved residues in unstructured regions on the $PilO_{\Delta109}$ structure were chosen for site directed mutagenesis…. 158
Figure 4.5 PilO R169D and I170A are able to disrupt T4P function……... 160
Figure S4.1 $PilN_{\Delta44}$/$PilO_{\Delta51}$/$PilP_{\Delta18}$ copurify from a gel filtration column as a stable heterotrimer following reductive methylation…….. 168
Figure S4.2 Mass spectrometry (MALDI-TOF/TOF) results indicate successful methylation of the $PilN_{\Delta44}$/$PilO_{\Delta51}$/$PilP_{\Delta18}$complex….. 169
Figure S4.3 Mass spectrometry (MALDI-TOF/TOF) results indicate only PilO fragments were present in the crystals…… 170
Figure S4.4 Predicted $PilO_{\Delta109}$ structure dimerization interfaces…….. 171
Figure S4.5 All alignment subcomplex proteins are stable with PilO mutations…… 172

CHAPTER FIVE – Discussion, future directions, and conclusions…… 173
Figure 5.1 Architectural model of the type IV pilus system..……... 177
Figure 5.2 Model of the alignment subcomplex proteins…… 179
Figure 5.3 Cartoon models of the possible PilMNOP transenvelope complex conformations……. 182

LIST OF TABLES

CHAPTER ONE – Introduction…… 1
Table 1.1 List of homologous assembly proteins in the T4P and T2S systems……... 6

CHAPTER TWO - Novel role for PilNO in type IV pilus retraction revealed by alignment subcomplex mutations…… 34
Table 2.1 Summary of PilN and PilO mutants and their phenotypes…….. 56
Table S2.1 Bacterial strains & vectors…… 70
Table S2.2 Oligonucleotide primer sequences…….. 73

CHAPTER THREE - *In vivo* capture of the type IV pilus system PilN and PilO homo- and heterodimers by Cys crosslinking……..…. 80
Table 3.1 Bacterial strains…….. 126
Table 3.2 Oligonucleotide primer sequences……. 128

CHAPTER FOUR - Analysis of *Pseudomonas aeruginosa* PilO based on a new high-resolution structure: conserved, unstructured regions are important for type IV pilus function…….. 130
Table 4.1 Data collection and refinement statistics for $PilO_{\Delta 109}$……. 149
Table 4.2 Summary of PilO mutants and their phenotypes…… 160
Table S4.1 Bacterial Strains & Vectors…… 165
Table S4.2 Oligonucleotide Primer Sequences…….. 166

LIST OF ABBREVIATIONS

AMIN	amidase N-terminal domain
Ap	ampicillin
ATP	adenosine triphosphate
BCIP	5-bromo-4-chloro-3-indolylphosphate
BME	β-mercaptoethanol
bp	base pair
BTH	bacterial two-hybrid
cryo-EM	cryo-electron microscopy
Cb	carbapenem
C-terminal	carboxyl-terminal
CC	coiled-coils
c-di-GMP	3', 5'-cyclic-di-gluanylate
Cys	cysteine
Da	Dalton
DGC	diguanylate cyclase
DNA	deoxyribonucleic acid
EM	electron microscopy
EPS	exopolysaccharide
FPLC	Fast protein liquid chromatography
FRT	flippase recognition target
g	gravity
Gm	gentamicin
Gsp	general secretory pathway
h	hour(s)
HTS	high throughput screening
IM	inner membrane
IPTG	isopropyl β-D-thiogalactopyranoside
kb	kilobase
kDa	kilodaltons
Kn	kanamycin
LB	Luria-Bertani medium
LDAO	lauryldimethylamine-oxide
min	minute(s)
N-terminal	amino-terminal
NBT	nitro-blue tetrazolium
NMR	Nuclear magnetic resonance

OD	optical density
OM	outer membrane
ONPG	ortho-Nitrophenyl-β-galactoside
PAGE	polyacrylamide gel electrophoresis
PBS	phosphate buffered saline
PCR	polymerase chain reaction
PDB	Protein Data Bank
PEG	polyethylene glycol
PG	peptidoglycan
pH	power of hydrogen
pI	isoelectric point
PIA	*Pseudomonas* isolation agar
PP	periplasm
RMSD	root-mean-square deviation
s	second
SS	species specific
SDS	sodium dodecyl sulfate
T2S	type II secretion
T2SS	type II secretion system
T3S	type III secretion
T3SS	type III secretion system
T4S	type IV secretion
T4P	type IV pili/pilus
T4PS	type IV pilus system
T4aP	type IV a pili/pilus
T4bP	type IV b pili/pilus
TEM	transmission electron microscopy
TEV	tobacco etch virus
TMS	transmembrane segment(s)

CHAPTER ONE

Introduction

Preface

Chapter One was adapted in part from the following publication:

Leighton TL, Buensuceso RN, Howell PL, and Burrows LL. 2015. Biogenesis of *Pseudomonas aeruginosa* type IV pili and regulation of their function. Environ Microbiol 17(11): 4148-63. DOI:10.1111/1462-2920.12849

Sections and figures herein were created primarily by TLL and LLB.

Environmental Microbiology, volume 17(11), 2015, 4148-63, DOI:10.1111/1462-2920.12849

Overview

Type IV pili (T4P) are long, thin (5-8 nm diameter) hair-like appendages found on bacterial and archael cell surfaces (1,2) (Figure 1.1). They play roles in surface attachment and adhesion, cell-cell aggregation, biofilm formation, and motility (1-5). Type IV pili are important for virulence, as mutants lacking T4P are impaired for host cell colonization and thus less infectious (6,7). Pili are assembled at the cytoplasmic membrane by intricate nanomachines whose molecular mechanisms and regulation are not yet fully understood.

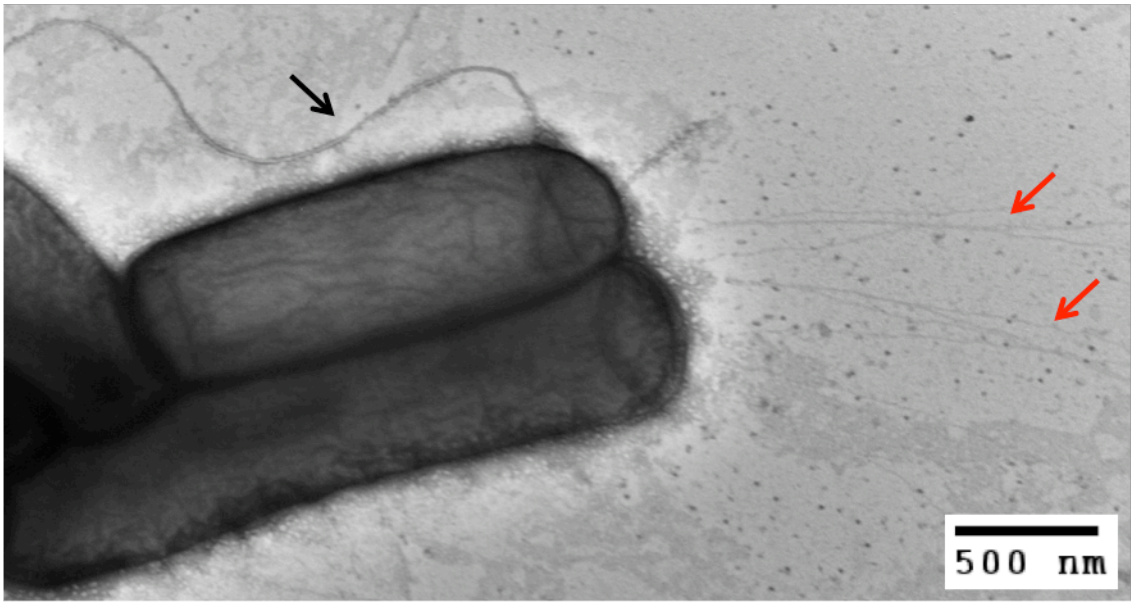

Figure 1.1. Electron Microscopy of polar T4P on *P. aeruginosa.* Wild-type cells of *P. aeruginosa* stained with 1% uranyl acetate and visualized using transmission electron microscopy (TEM) showing the type IV pili (red arrows) and the flagellum (black arrow). Magnification 25,000x.

Pseudomonas aeruginosa is an environmental bacterium and is typically

associated with opportunistic and nosocomial infections. It primarily affects immunocompromised individuals, such as those with severe burns, cancer, HIV/AIDS and cystic fibrosis (8). Virulence in *P. aeruginosa* depends on various mechanisms including the T4P system (9), which is specifically involved through the extension and retraction of the pilus fibres (9-11). T4P are able to coordinate virulence via both the type II secretion (T2S) and type III secretion (T3S) systems by bringing the cell body close to the host cell surface, making the T4P system an attractive target for novel therapeutics that could effectively disarm the bacteria.

Type IV pili classification

Type IV pili are divided into two major subfamilies, type IVa (T4aP) and type IVb pili (T4bP), characterized by differences in the major and minor pilin subunits which make up the fibre, and among assembly system components (4,12,13). T4aP are the best-studied subfamily, and are widely distributed amongst Gram-negative bacteria, including *Pseudomonas* (14,15), *Myxococcus* (16), and *Neisseria* (17,18). In contrast, T4bP are primarily found on enteric bacteria such as *Vibrio cholerae, Salmonella enterica,* and enteropathogenic and enterotoxogenic *Escherichia coli* (ETEC and EHEC respectively), which colonize the human gut (19-21). Interestingly, T4P are also found in Gram-positive bacteria such as *Clostridium difficile*, but exhibit mixed traits of both T4aP and T4bP, suggesting all T4P have evolved in bacteria from a common ancestor (22). The T4aP system in *P. aeruginosa* is the focus of this thesis and will henceforth

be called T4P for simplicity.

The type II secretion system

Another important virulence factor used by many Gram-negative bacteria is the T2S system. Folded proteins are exported via this system from the periplasm into the extracellular milieu outside the cell (23-26). Although the outputs of these systems are different, extensive bioinformatics and structural studies revealed that the T2S and T4P systems are evolutionarily related (23). Both systems have a similar architecture, with inner and outer membrane components that together span the cell envelope. An inner membrane platform protein is found at the base of the apparatus, connected to a cytoplasmic ATPase that provides the energy for secretion. There is an outer membrane secretin oligomer that forms a gated channel, and this is connected to the inner membrane components via an inner membrane alignment subcomplex. A small fibrillar structure called a pseudopilus is assembled at the base of the apparatus and is proposed to function like a piston to push its folded protein substrates out of the cell (27). Insights into the roles of T4P components can be provided through bioinformatics analysis and structural studies of well-studied T2S system orthologues.

P. aeruginosa has two T2S systems: the Xcp (extracellular protein) system capable of secreting a large array of proteins, and the Hxc (homologous to Xcp) which has only one known substrate so far (27). Unfortunately, a standardized

nomenclature for structurally and functionally similar T2S and T4P proteins has not been universally adopted. For the purposes of this thesis we will use the general secretory pathway (Gsp) nomenclature when describing T2S proteins from various species (28). The nomenclature for functionally equivalent proteins in the T2S and T4P system of *P. aeruginosa* is summarized in Table 1.1 (23,24).

Table 1.1. List of homologous assembly proteins in the T4P & T2S systems.

	T4PS	T2S
Pilus fibre (major & minor pilin components)	PilA FimU PilV PilW PilX PilE	GspG GspH GspI GspJ GspK -
Motor subcomplex	PilC PilB PilT PIlU	GspF GspE - -
Alignment subcomplex	PilM PilN PilO PilP	GspL (cytoplasmic) GspL (periplasmic) GspM GspC
Secretin subcomplex	PilQ PilF	GspD GspS

Functions of type IV pili

Unlike most other bacterial surface filaments, with the exception of F-pili which may retract via a mechanism that remains undefined (29), T4P are dynamic and can be rapidly extended and retracted (30). Through their ability to repeatedly extend, adhere and retract, T4P confer unique locomotion modalities including twitching, swarming, walking and sling shot motilities (31-33). These modalities use T4P alone or in combination with other surface appendages such as the flagellum to achieve movement.

The best characterized of these forms of motility in *P. aeruginosa* is twitching motility, which is flagellum-independent (5). Twitching motility involves three distinct stages: extension of the pilus fibre, nonspecific adherence to a surface and then retraction of the fibre back into the bacterium, which winches the cell forwards towards the point of attachment (14,30,34,35). While adhesion is relatively non-specific, previous work has shown the ability of T4P from *P. aeruginosa* to follow a polysaccharide-fibre trail (formed by the Psl polysaccharide) and similarly *M. xanthus* T4P can directly bind to exopolysaccharides (EPS)(36,37). During twitching, a social form of motility, *P. aeruginosa* cells cluster into tight cell-cell aggregates and form spearhead-shaped rafts, which expand outwards from the colony centre (38,39). Studies of fluorescently labelled *P. aeruginosa* cells demonstrate that pili can be extended and retracted at a rate of 0.5 μm/sec (30), corresponding to a retraction rate of approximately 1000 pilin subunits/s (35). Retraction of the pili can produce forces

in excess of 100 pN per filament (34,35), thus making T4P the strongest molecular motors reported to date.

In addition to their role in motility and adhesion to surfaces, T4P are also involved in a number of other processes including cell-cell aggregation (5,10), DNA uptake (40), and biofilm formation (10).

Type IV pili gene organization in *P. aeruginosa*

There are over 40 genes involved in the assembly and regulation of the T4P system in *P. aeruginosa* (2,4). These genes can be divided into two groups: structural components that form the assembly machinery plus the pilus itself, and regulatory components which dictate how many pili to make, when to move, and where. Interestingly, some proteins fit into both categories, although their exact roles in these distinct processes are still being unravelled (41). In *Pseudomonas*, the T4aP biogenesis genes are scattered throughout the genome (Figure 1.2A), unlike T4bP genes which are typically arranged ‘en bloc’ (2). The core T4P biogenesis genes found in all Gram-negative bacteria include a pilin protein (the primary subunit of the pilus fibre), one or more pilin-like proteins (which prime assembly and/or act as adhesins), a prepilin peptidase (to process the prepilins into mature pilin subunits), a traffic ATPase (to power the system), a inner membrane (IM) platform protein (the site for pilus assembly/disassembly), and an integral outer membrane (OM) protein (which forms the pore through which the pilus passes) (2). In *P. aeruginosa,* an additional set of genes encoding the

alignment subcomplex components, located immediately upstream of the secretin gene, is required for efficient piliation. In the absence of any of the alignment subcomplex genes (*pilMNOP*), pili are not produced.

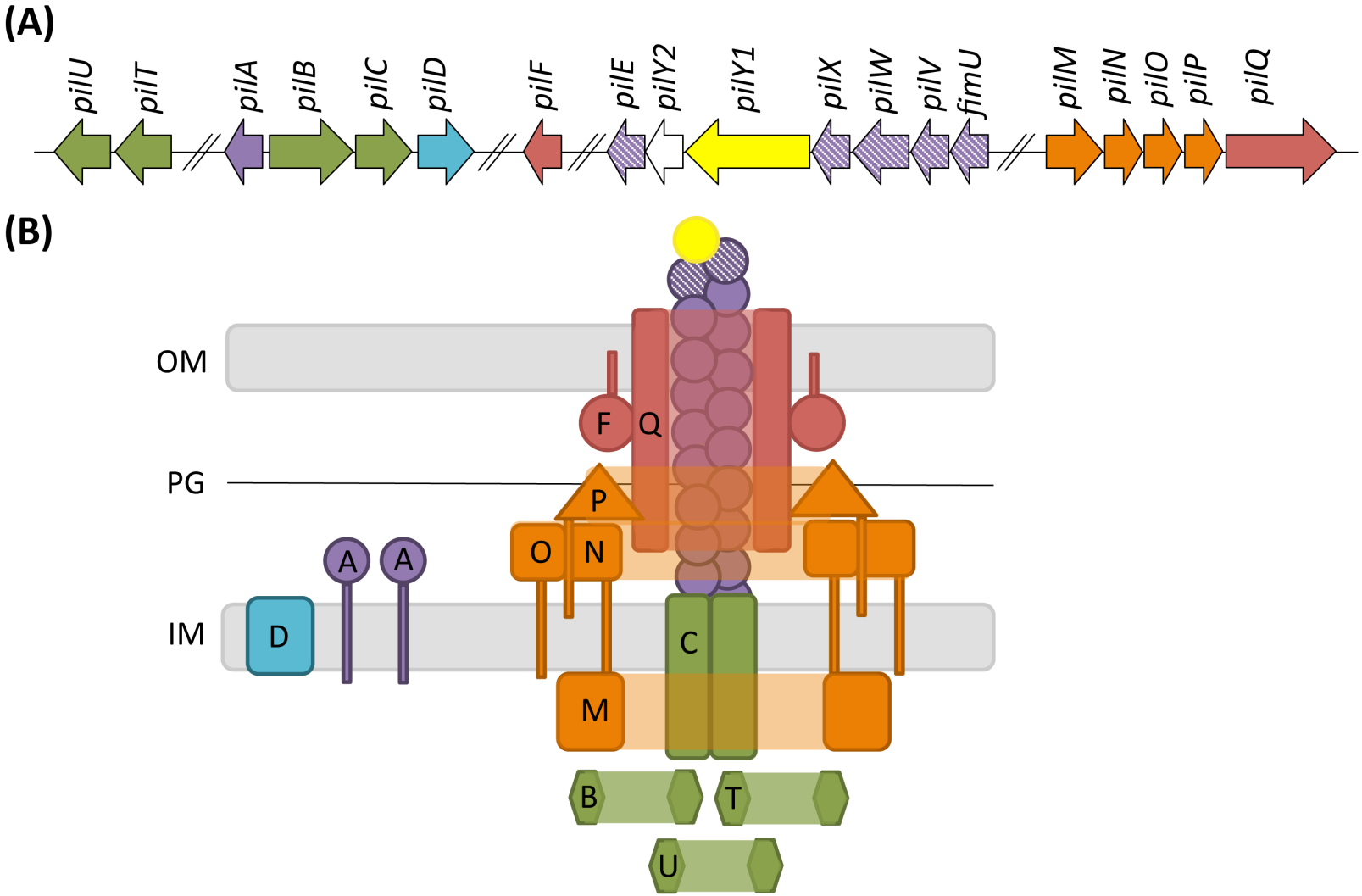
(A)
pilU
pilT
pilA
pilB
pilC
pilD
pilF
pilE
pilY2
pilY1
pilX
pilW
pilV
fimU
pilM
pilN
pilO
pilP
pilQ
(B)
OM
PG
IM
F
Q
P
O
N
A
A
D
C
M
B
T
U

Figure 1.2. Gene organization and cartoon schematic of the type IVa pilus system in *P. aeruginosa*. (A) Genetic organization of the T4P proteins colored by subcomplex. Components include the outer membrane (OM) secretin subcomplex: PilQ and PilF (red); the inner membrane (IM) motor subcomplex: PilC, PilB, PilT, and PilU (green); the IM alignment subcomplex: PilM, PilN, PilO, and PilP (orange); and the pilins and pilus fibre: PilA (purple). Minor pilins are indicated by the purple stripe, and PilY1 is shown in yellow at the tip of the pilus fibre. Slashes indicate genes are separated by a large distance. Genes are not to scale. **(B)** Cartoon model of T4P structural components with proteins labeled according to the Pil nomenclature. Peptidoglycan (PG) is shown as a single line in the periplasm. Not shown are FimV, PA0020 (predicted orthologue of TsaP), and PilY2.

Type IV pilus system assembly in *P. aeruginosa*

In *P. aeruginosa,* four subcomplexes spanning the entire bacterial cell envelope make up the T4P assembly system (Figure 1.2B). The OM secretin subcomplex is composed of an oligomer of 14 subunits of PilQ (42-44)(Koo et al., 2016 – in press) with its pilotin protein PilF, forming a gated pore through which the pilus is extruded (45,46). The TsaP protein, recently identified in *N. gonorrhoeae* and *M. xanthus,* contains a peptidoglycan (PG)-binding LysM motif, and may help anchor the secretin to the bacterial cell wall (47). *P. aeruginosa* PA0020 encodes a putative TsaP homologue; however when this gene is deleted in either the PAO1 or PAK strains, piliation and twitching motility were unaffected (Koo et al., 2016 – in press). The IM motor subcomplex is composed of an integral membrane ‘platform’ protein PilC, and three cytoplasmic ATPases,

PilBTU, which provide the energy for extension and retraction of the fibre (48,49). The secretin and motor subcomplexes are linked by the alignment subcomplex, PilMNOP (50,51), which may also include FimV – a large protein with periplasmic and cytoplasmic domains connected by a single transmembrane segment. Like TsaP, FimV has a peptidoglycan-binding LysM motif and is important for secretin formation (52). FimV has been proposed to help the multimeric secretin traverse the PG layer, and/or participate in regulation of pilus biogenesis (53), as discussed below. The PilMNOP proteins span from the cytoplasm to the periplasm and connect with the PilQ secretin via PilP, potentially controlling secretin gating (54,55). Together, the motor and the alignment subcomplexes comprise the IM platform. The final subcomplex is the helical pilus fibre, composed of major (PilA) and minor (FimU, PilVWXE) pilin subunits along with a non-pilin protein, PilY1 (5,13,56-58). Together with regulatory components, these subcomplexes form a functional T4P system.

The secretin: a gate to the outside

The T2S and T4P system secretins belong to a large family of pore-forming proteins also involved in T3S and the export of filamentous phage (59-61). Secretins form a gated 50-80 Å diameter channel that allows the polymerized fibre to pass through the outer membrane (62). In the absence of a pilus fibre, the secretin pore is closed by loops that are part of the secretin structure, or in some systems, by a plug protein that physically blocks the channel (62,63). These components inhibit the release of periplasmic proteins

while the secretin is in its resting state, unoccupied by pili (63). Secretins consist of two regions; a variable N terminal periplasmic region responsible for protein-protein and/or protein-peptidoglycan interactions and substrate recognition, and a highly conserved C-terminal domain that forms the physical pore in the membrane (54,64,65). The periplasmic region of the T4P PilQ secretin is divided into four subdomains, starting at the N terminus; SS1-SS2-N0-N1 (54). The N-terminal species-specific (SS) or beta domains of PilQ are structurally related to the Amidase N-terminal domain (AMIN), found in peptidoglycan hydrolases involved in cell division (66-68). The AMIN domain of AmiC, an *E. coli N*-acetylmuramoyl-L-alanine amidase responsible for the final stages of daughter cell separation, binds PG and is proposed to target the protein to the septum where it participates in daughter cell separation (68). In PilQ, the AMIN domains could help to target the secretin subunits to nascent poles as cell division is occurring, to allow for incorporation of the large multimeric secretin into the cell wall as the PG is newly synthesized (69,70). This domain could also play a role in anchoring the secretin and/or assembly system into the cell wall, acting with FimV to brace the assembly system against forces generated by retraction of the pilus fibre (47,52,71). The adjacent N0 region of PilQ plays an important role in protein-protein interactions, as it is the point of contact with the alignment subcomplex lipoprotein, PilP (54). N0, plus the N1 and/or secretin subdomains, may participate in the interaction between PilQ and its pilotin, PilF (72). Depending on the system, secretin localization to the OM and multimerization

can occur independently or in concert with various accessory proteins such as pilotins (45). Trafficking of a PilQ-PilF pair by the lipoprotein sorting machinery (Lol pathway) was suggested as one possible mechanism by which PilQ monomers could be shuttled to the outer membrane (72). PilF is likely inserted into the OM by Lol machinery, while PilQ may be spontaneously co-inserted or require other cellular machinery (72,73). Evidence from studies of *M. xanthus* led to the proposal of an 'outside-in' pathway of T4P system assembly, where the OM secretin first oligomerizes, then recruits alignment subcomplexes, which subsequently recruit the IM motor subcomplex (74). Whether this scenario holds true for the T4P system of *P. aeruginosa,* and how the system ends up in its final configuration at the cell poles, has yet to be elucidated.

The pilus fibre: the rope and grappling hook

The pilus fibre contains hundreds of subunits in a helical filament that is capable of rapid assembly and disassembly. PilA is the predominant subunit, though other essential pilin-like proteins known as minor pilins are incorporated into the filament at low abundance (12,75). A polycistronic operon encodes five minor pilins (FimU-PilVWXE) and two non-minor pilin proteins (PilY1 and PilY2; Figure 1.2A) (76). The minor pilins are proposed to form an initiation complex for pilus assembly, leading to their incorporation into the fibre, forming its tip (12,77,78). In the current model, minor pilins PilVWX and the ~125 kDa PilY1 protein are thought to form an IM subcomplex that recruits PilE. This complex is

then connected to PilA through interactions with both PilE and FimU (58). This pilus initiation structure (PilY1-PilVWX-PilE-FimU-PilA) is proposed to prime the subsequent polymerization of hundreds of PilA subunits, forming a helical filament that elongates from its base. Minor pilin FimU couples the major pilin to the minor pilin-PilY1 complex (58), similar to its T2S homologue GspH, which is proposed to connect a minor pseudopilin priming complex to the major pseudopilin (79). This hypothesis is supported by data showing that either the minor pilins or minor pseudopilins of *P. aeruginosa* can prime pilus assembly (58). Structures of *P. aeruginosa* major and some minor pilins (PilA, FimU, and PilE) have been solved, and reveal similar architectures (56,58,80,81). Pilins have a long, S-shaped, hydrophobic N-terminal α-helix, followed by a variable C-terminal β-sheet region composed of 4-7 antiparallel β-strands (56,82). Most major (and specific minor) pilins have two Cys residues in the C-terminal region, forming a disulfide bond that staples the C terminus of the proteins to the β-sheet (82). The loop formed by this bond stabilizes the interaction between adjacent subunits, as mutating the Cys residues prevents assembly (83), and treating assembled pili with a reducing agent causes their rapid disintegration (84).

PilY1, encoded with the minor pilin genes, is essential for pilus assembly (85). PilY1 was initially proposed to be an adhesin (57) but its role in pilus-mediated adherence was hard to test, since *pilY1* mutants lack surface pili (9,85). In a recent study, atomic force microscopy was used to test the contribution of PilY1 to pilus-mediated adherence. Overexpression of PilY1 did not increase

adherence (86), prompting the authors to conclude that PilY1 is not directly involved in surface adhesion; however, they did not test whether their overexpression of PilY1 alone – without its minor pilin partners – actually changed the amount of PilY1 on the cell surface. Expressing PilY1 alone alters the stoichiometry between it and PilVWX (81), which could affect PilY1 surface display. A more recent study (87) suggested that overexpression of PilY1 alone significantly increases the amount recovered in cell surface fractions, even in the absence of pili; however, the potential pilus-independent mechanism of PilY1 secretion remains unknown.

A crystal structure of the C-terminal domain of PilY1 (~60 kDa of 125 kDa) revealed a beta propeller fold and a novel calcium-binding motif (88). When this motif was mutated to a configuration mimicking the calcium-bound state, PilY1 opposed retraction, while a calcium-free mimetic state increased the amount of retraction relative to control (88). A second calcium-binding site was subsequently identified in the N-terminal domain of PilY1, and pull-down experiments showed that integrin binding was regulated by both sites (89). Integrins and integrin-like proteins are present on many different cell types in the plant, insect, and animal kingdoms, and are common targets for bacterial pathogens (90,91). Binding of PilY1 to integrins expressed on target cells could allow *P. aeruginosa* to sense attachment and pull itself towards the host. A recent study proposed a more general mechanosensory role for PilY1 in modulating virulence (92). Shear forces generated upon attachment to a surface were

suggested to deform the mechanosensitive Von Willebrand Factor-like domain in the N-terminal region of PilY1 – possibly leading to cleavage by unknown proteases – signalling successful surface engagement and inducing a virulence program (92). Interestingly, PilY1 was required for surface-activated virulence independent of pilus expression, as other pili-less mutants remained virulent as long as PilY1, PilW and PilX were present (92). Even when not incorporated into the pilus, PilY1 participates in surface-activated virulence, likely by acting upstream of the diguanylate cyclase (DGC) SadC, responsible for modulating cellular levels of 3',5'-cyclic-di-guanylate (c-di-GMP) (93-95). PilY1's potential regulatory roles are discussed in detail below. At this point, the exact role(s) of PilY1 in the T4P system of *P. aeruginosa,* and how they are integrated with its biology, remain areas of intense study.

The motor: powering the grappling hook

Like a molecular grappling hook, the T4P system functions through rounds of pilus extension, adherence, and retraction, winching the cell towards the point of attachment (30). This motion can be jerky and erratic, hence the term 'twitching' motility (14). The pilus is responsible for attachment, but cytoplasmic ATPases provide the driving force behind its extension and retraction. *P. aeruginosa* has three hexameric motor ATPases, PilB, PilT and PilU (5,48,96-98) that hydrolyze ATP to provide energy for pilus extension and retraction. It is likely that the ATPases contribute to assembly/disassembly of pilin subunits through their interactions with the IM platform proteins (PilMNOP, and/or PilC) (99). Direct

interaction between PilB and the N-terminal domain of PilC was demonstrated by co-affinity purification (49). It was hypothesized in that study that the C-terminal cytoplasmic domain of PilC may interact with the retraction ATPases, PilT and/or PilU based on the phenotypes of PilC point mutants, though solubility issues with the C-terminal domain of PilC have made it difficult to test this hypothesis. More recent structural modelling in the T4P system of *M. xanthus* have provided strong evidence that the PilM ring in the cytoplasm can only accommodate a single ATPase hexamer at one time, therefore interaction of the two ATPases with each PilC subdomain simultaneously is unlikely (71). The interaction between PilC and the hexameric ATPases (34,99,100) is thought to transduce mechanical energy from conformational changes occurring upon ATP hydrolysis through the IM platform, leading to the addition or removal of pilin subunits from the fibre (101,102). The structure of PilT was solved to 2.6 Å resolution, with and without the non-hydrolyzable ATP analog β,γ-methylene-adenosine 5′-triphosphate (AMP-PCP) (99). Each subunit of PilT consists of N- and C-terminal domains separated by a flexible linker, with the active site at the interface between these two domains, similar to other T4P-associated ATPases (102-105). Although no structures of *P. aeruginosa* PilB and PilU are yet available, both are predicted to have similar structural features, with sequence identity among the three ATPases ranging from 20-40%. A unique internal region of 40 residues in PilB located between the N- and C-terminal domains that is not functionally conserved with the other two ATPases, was recently shown to be the site of interaction for a

D3112 bacteriophage-encoded protein, gp05 (also called Tip – twitching inhibitory protein) (106). Binding of Tip to PilB caused delocalization of fluorescently tagged PilB from the poles of the cell, disrupting surface piliation and motility in *P. aeruginosa* (106). Although not determined in that study, delocalization of PilB by Tip could be caused by disruption of PilB hexamer formation, or by loss of its interaction with PilC (49).

Whereas most T4P systems function with two ATPases, all three are required for twitching motility in *P. aeruginosa* (96,97,107). PilB and PilT function in extension and retraction, respectively, but the function of the third ATPase, PilU, remains enigmatic (3). Unlike *pilB* and *pilT* mutants that have surface piliation phenotypes reflective of their role in T4P extension and retraction respectively, *pilU* mutants are nearly incapable of twitching, but have approximately wild-type levels of surface pili and are sensitive to killing by pilus-specific bacteriophages (97). These phenotypes suggest that *pilU* mutants continue to assemble and retract surface pili. However, given that *pilU* mutants do not twitch, it is likely that PilU coordinates PilT-mediated retraction to ensure that it occurs at only one pole at a time, to prevent futile tugs-of-war. The link between PilU and PilT function is strengthened by the idea that PilU arose through a gene-duplication event, as *pilT* and *pilU* are adjacent on the *P. aeruginosa* chromosome. In *N. gonorrhoeae,* there are multiple PilU homologues, all of which have been implicated in fine-tuning of pilus retraction (108). The presence of multiple PilU orthologues might reflect the more complex problem of

controlling directional motility in a coccoid bacterium with peritrichous pili.

In *M. xanthus,* the extension and retraction ATPases are primarily found at the leading and lagging poles, respectively (109). During reversals in motility, the ATPases switch places, the lagging pole becomes the new leading pole, and motion proceeds in a new direction (109). This oscillation of the ATPases has been linked to the chemosensory system which regulates the reversals in *M. xanthus* (110). *P. aeruginosa* PilU is unipolar, unlike PilB and PilT that are found at both poles (48). PilU might differentiate the leading and the lagging poles to control the direction of motility.

The alignment subcomplex: threading the needle

With the platform and the motor of the system located in the cytoplasm and IM, and the secretin in the OM, connection of these subassemblies is required for efficient pilus biogenesis. Four genes, *pilMNOP*, form a polycistronic operon with *pilQ,* and their products span the cytoplasm (PilM), inner membrane and periplasm (PilNOP), effectively linking the motor and the secretin. The PilMNOP proteins are composed of various domains/regions that mediate interactions between one another and various other T4P proteins (Figure 1.3A).

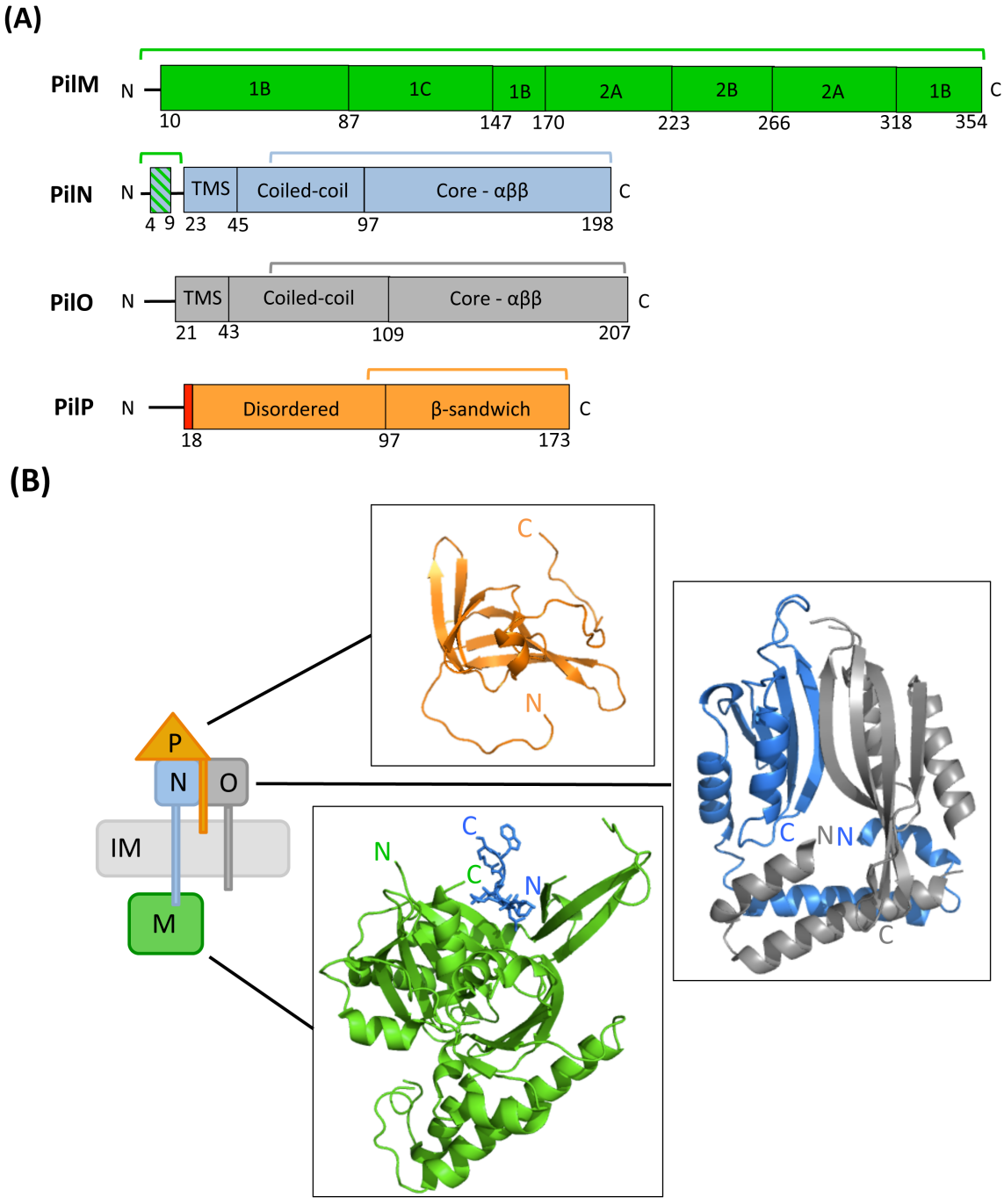

Figure 1.3. Domain schematic and structural models of alignment subcomplex proteins in *P. aeruginosa*. (A) PilMNOP domain/region boundaries are defined with approximate residue numbers. PilM domains (1B,

1C, 2A, and 2B) are labelled according to FtsA domain definitions (111,112). PilM binding site on PilN, indicated by blue/green stripes. Approximate PilN and PilO transmembrane segment (TMS) regions shown. Red bar indicates the location of the highly conserved PilP lipobox. Brackets above indicate approximate size present in structural models below. **(B)** Cartoon representation of the alignment subcomplex proteins arrangement in the inner membrane (IM), labelled according to Pil nomenclature. Ribbon diagram representations mapping the N- and C-termini, secondary structure elements and structural domains of: C-terminal fragment of $PilP_{\Delta 71}$ (orange) (PDB 2LC4 (55)), $PilN_{\Delta 57}$ (blue) and $PilO_{\Delta 68}$ (grey) using a Phyre^2 (113) model of PilN generated using the $PilO_{\Delta 68}$ homodimer (PDB 2RJZ (51)) as a template, and PilM:$PilN_{1\text{-}12}$ (green and blue, respectively) (PDB 5EOU (111)).

PilM

A crystal structure of the cytoplasmic protein PilM from *T. thermophilus,* bound to a short fragment of the N-terminus of PilN, confirmed bioinformatic predictions that PilM was an actin-like protein with structural similarities to cell division proteins FtsA and MreB, as well as to GspL and BfpC from the T2S and T4bP systems, respectively (113-115). Structures of *P. aeruginosa* PilM and a PilMN chimera that was C-terminally linked to the first twelve residues of PilN (PilM:$PilN_{1\text{-}12}$) were recently solved (Figure 1.3B) (111). Interestingly, the stoichiometry of PilM varied depending on whether PilM was expressed alone (dimeric) or fused to the N terminus of PilN (monomeric). The N terminus of *P. aeruginosa* PilN (which included the short, highly conserved PilN sequence – ^{4}INLLPW^9 (51)) binds tightly to a small groove on the surface of PilM (111,114).

However, in the dimeric form – where PilM was crystallized in the absence of PilN – the PilN binding pocket was still occupied. The residues bound in this pocket were mapped to the N terminus of the adjacent PilM subunit. A highly conserved N-terminal ^{1}MXXIFXK^{7} motif was identified in this segment, with similar motifs found in PilM-like orthologs from various species (111). PilM self-interaction was further analyzed through the use of a bacterial two-hybrid (BTH) system and mutational analysis that confirmed that PilM residues 1-7 were important for homodimerization (111). These data indicate that the binding of the N terminus of PilN to PilM prevents PilM self-association. Whether these two states have physiological relevance remains to be verified.

PilM contains four subdomains, 1B, 1C, 2A, and 2B, named according to previously described FtsA domain definitions (Figure 1.3A) (112). The 1B and 2A subdomains bind the phosphates of ATP, as well as creating a peptide-binding interface found in all Actin/Hsp70/Hexokinase superfamily members (111). Upon binding PilN, domain 1C undergoes a dramatic movement of 25^{o} that pinches the PilN N-terminal peptide between the 1B and 2A domains. Although absent in GspL and BfpC, the 2B subdomain of PilM binds the remainder of the ATP ligand, but is unable to hydrolyze it (111,113,115). Binding of *P. aeruginosa* PilM to ATP likely modulates the PilMN interaction, and may ultimately alter the interaction of PilM with other T4P components, specifically the ATPases PilB and PilT as suggested by BTH data (below) (111). Interestingly, the PilM and PilN homologues in the T2S system are expressed as a single polypeptide (GspL),

which would preclude dissociation during cycles of protein secretion (23,113,116-118). The suggestion that PilM may have the capacity to reversibly dissociate from PilN during T4P function is under investigation.

Previous work in the T2S and T4bP systems suggested that PilM might bind to other T4P components, such as the IM platform protein and the cytoplasmic ATPase(s) (113,119-121). BTH assays confirmed interactions of PilM with PilN, and additional T4P components PilC, PilB and PilT. These interactions were further confirmed through pull-downs, in which the PilMN chimera co-purified with PilB and PilT (111). If PilM was able to selectively modulate the binding of the extension/retraction ATPases, it could suggest that PilM is not a passive cytoplasmic scaffold, but rather a dynamic component of the T4P system.

PilN

Initial sequence analysis and secondary structure predictions for PilN suggested strong similarity to PilO, despite their limited 16% sequence identity (51). PilN is predicted to be an integral membrane protein with a single TMS, followed in the periplasm by a coiled-coil and core domain composed of two αββ repeats (Figure 1.3A) (50,51). The short cytoplasmic N-terminus of PilN contains a high degree of sequence conservation in PilN homologs, with the greatest similarity between PilN residues 4-9, a strongly conserved INLLPW consensus motif (51). Using an N-terminal PilN peptide, it was confirmed that these residues are essential for the PilMN interactions and proper T4P function (54).

In addition to binding PilM, PilN also interacts with the other two components of the alignment subcomplex, PilO and PilP. Although they form heterodimers, the interaction interfaces between PilN and PilO have not been well defined. Studies in both the T4P and T2S systems indicate PilN and PilO-like proteins are dependent on one another for stability; in the absence of one, the other is susceptible to degradation (50,51,117,118). In *P. aeruginosa*, the large electrostatic difference between the coiled-coils of PilN and PilO (pIs of 10.2 and 4.2 respectively) may drive heterodimerization of these proteins (51). Similarly, their *V. cholerae* T2S system homologues GspL (periplasmic domain) and GspM have pIs of 9.3 and 4.7, respectively (51). Mapping of the interactions between PilN- and PilO-like proteins in the T2SS of *V. cholerae* and *Dickeya dadantii* implicated the TMS, the coiled-coils, and the core domains in their interaction (118,122,123). These results suggest an extensive interaction interface between PilN and PilO capable of mediating heterodimer formation, but also interaction with PilP (50,54,55).

Recently, a structure of PilN from the T4P system of *Thermus thermophilus* was solved using X-ray crystallography, revealing a significant difference in the order of secondary structural elements in its core domain (αβ**α**β-αββ), compared to the prediction for PilN of *P. aeruginosa* (αββ-αββ) (51,124). The α-helical insertion could be a species-specific element, as sequence conservation in that region is relatively low when compared to other PilN homologs (124). Due to the low overall sequence identity between PilN from *T.*

thermophilus and *P. aeruginosa*, as well as the presence of extra secondary structure elements, the *Thermus* structure did not yield a high confidence model using the *P. aeruginosa* sequence. *P. aeruginosa* PilN is predicted to have a similar structural organization to PilO, thus we used the truncated *P. aeruginosa* PilO homodimer structure (51) to generate a high confidence Phyre^2 (125) model of a $PilN_{\Delta 57}$ monomer, and used the crystallographic PilO homodimer interface to model a PilNO heterodimer (Figure 1.3B). The accuracy of this heterodimer model is tested and discussed in Chapters 2 and 3. With its ability to bind all of the other alignment subcomplex proteins, PilN forms a critical connection between the cytoplasmic and OM components of the T4P system, and may be a key player in a signal transduction network that regulates the extension/retraction state of the system.

PilO

Like PilN, PilO is a bitopic inner membrane protein with a short cytoplasmic region, a TMS, and a periplasmic coiled-coil and core domain (Figure 1.3A) (51). A PilO family sequence alignment revealed a high degree of sequence similarity in the periplasmic region, with the most highly conserved sequence, LPRIVTL, identified in the core domain of PilO, between residues 167-173 (51). The role of these residues has yet to be elucidated.

Although PilN and PilO interact to form heterodimers capable of interaction with PilP, PilO can also form homodimers (54,55). The structure of a PilO dimer with a N-terminal truncation of 68 residues (missing the cytoplasmic tail, the TMS,

and part of the first coiled-coil) has been solved (51). In this structure, the truncated coiled-coils are folded back on themselves at a flexible linker, creating an artificial interface since they are not anchored into the inner membrane (Figure 1.3B). The core domain of PilO consists of a modified ferredoxin fold (αββ-αββ), wherein the two α-helices are packed onto a four-stranded antiparallel β-sheet (51). Despite the nearly complete lack of sequence identity, the structure of PilO and the homologous protein from the T2SS in *V. cholerae,* GspM, are remarkably similar (51,126). Although homodimerization has been reported for PilO-like proteins in the T2SS (122), the *in vivo* homodimerization of PilO has been observed only under conditions where the protein is overexpressed, suggesting instead that under physiological conditions, PilO forms heterodimers with PilN. The PilNO heterodimer (Figure 1.3B) is thought to be the functionally relevant state, since it can interact with PilP, while a PilO homodimer cannot (54,55).

PilP

PilP, the final component of the alignment subcomplex, is an inner membrane-associated lipoprotein (55). The N terminus of PilP contains a highly conserved lipobox sequence, LAGC, between residues 15-18 (Figure 1.3A) (55). Much of the N-terminus of PilP (residues 1-90) is predicted to be intrinsically disordered, while the C terminus of the protein, 93-169, is ordered. As determined using solution nuclear magnetic resonance (NMR) spectroscopy, the core domain of PilP (residues 72-169) is folded into a short 3_{10} helix followed by seven antiparallel β-strands arranged into two β-sheets, forming a modified β-

sandwich (Figure 1.3B) (55). Structurally, PilP from *P. aeruginosa* is very similar to its homologue from *N. meningitidis* (127), and to GspC family proteins from the T2SS (55). One major difference between PilP and GspC is that while PilP is tethered to the periplasmic side of the IM via its lipidated Cys, GspC is anchored into the membrane via a TMS (55,128). The equivalent protein in the T4aP system of *T. thermophilus*, PilW, is also an integral membrane protein instead of a lipoprotein, possibly an adaptation to its high temperature growth environment and related differences in membrane fluidity (129).

Although disordered when expressed alone, the N-terminal segment of PilP can interact with PilN and PilO, as confirmed by pull-down assays using PilP residues 19-83 (54,55,65). The C-terminal β sandwich domain of PilP (likely β strands 1-2 or 6-7 located on the edges of the β sandwich) interacts with the N0 domain of PilQ, the OM secretin monomer (54,130), completing the transenvelope subcomplex from the cytoplasm (PilM) through the periplasm (PilN and PilO) to the OM (via PilP and PilQ interaction).

Proposed functions of the alignment subcomplex

The alignment subcomplex has a number of proposed and complementary roles. Alignment of the IM motor with the OM secretin would allow for efficient extension of the pilus fibre through the pore, similar to threading a needle. In the absence of any of the alignment subcomplex proteins, pili are not recoverable from the surface of the cells except in a retraction-deficient background when the

retraction ATPase (PilT) is disrupted (49,50). This finding indicates a basal level of pilus assembly occurs without PilMNOP, but with them, the system is far more efficient (49). The presence of all alignment subcomplex proteins are required to maintain a transenvelope network which couples the IM components to the OM secretin, allowing for proper function of the T4P system.

As suggested above, this subcomplex might also transduce signals via conformational changes from the IM motor to the OM secretin, or vice versa. These signals could indicate “active” (during extension or retraction) or “resting” states of the system. In the T2SS of *D. dadantii,* the GspL and GspM proteins – functionally analogous to PilMN and PilO, respectively – undergo dramatic rotational rearrangements, allowing them to switch between homo- or heterodimeric states (122). “Partner switching” as it was coined, has not been shown for the T4P system but the idea is intriguing, and could be a way to switch between the “open” and “closed” or “active” and “resting” states of the system.

Recent work has proposed a role for the alignment subcomplex proteins in another signalling pathway, involved in biofilm formation and other surface behaviours (87). In many bacterial species, c-di-GMP is a master regulator of the transition between motile and stationary lifestyles (131,132). High levels of c-di-GMP synthesized by a diguanylate cyclase, SadC, inhibit flagellum-mediated swarming motility and promote biofilm formation, hallmarks of a sessile bacterial lifestyle (133,134). Previous work has confirmed the role of a T4P protein, PilY1, in modulating levels of c-di-GMP by functioning upstream of SadC (94). In

mutants lacking one or all of the alignment subcomplex components, PilMNOP, overexpression of PilY1 (which normally represses swarming motility) failed to affect swarming (87). This phenotype was not observed in other T4P mutants (e.g. *pilC* or *fimV*) indicating lack of T4P formation was not the cause of the phenotype. These findings indicate that PilMNOP may play a role in transducing a signal between the surface-expressed PilY1 protein, and the IM component SadC, which can ultimately decrease flagellar motility and up-regulate biofilm formation. However, the exact mechanism by which this signal transduction occurs remains unclear.

Finally, the alignment subcomplex may help to concentrate PilA subunits at the base of the apparatus. Upon disassembly of the pilus fibre, PilA subunits are re-deposited into the IM at approximately 1000 subunits per second (34,35) where they are free to diffuse (74). Since PilA subunits are recycled in further rounds of pilus assembly (30), retaining them near the assembly platform via interactions with PilNOP (54,124) could increase local concentrations and assembly efficiency. With the secretin predicted to contain 14 subunits of PilQ (42-44)(Koo et al., 2016 – in press), and the organization of the *pilMNOPQ* operon, which suggests 1:1:1:1:1 stoichiometry, it is likely that there are 14 sets of PilMNOP proteins surrounding the pilus fibre (54).

Hypothesis and Research Aims

Almost a decade of detailed structural and biochemical studies revealed that the alignment subcomplex proteins are the connection between the inner and outermost components of the T4P system. PilMNOP participate in various protein-protein interactions with many other T4P components including the ATPases, the platform protein, the major pilin subunit, and the OM secretin. However, our knowledge of the specific interaction interfaces among the alignment subcomplex proteins, and how they may change during function of this highly dynamic machine, remains unclear. The aim of this research was to use molecular, biochemical, and structural approaches to gain a better understanding of how these components interact, with the long-term goal of disrupting pilus function by perturbing those interactions. The overarching hypothesis of this work is that dynamic interactions of the alignment subcomplex proteins – specifically PilN and PilO – contribute to assembly and disassembly of T4P in *P. aeruginosa.*

The specific research aims of this thesis were:

1. **To probe PilN and PilO interaction interfaces via site directed mutagenesis to better understand their roles in pilus extension/retraction.**

   Previous studies showed that the periplasmic regions of PilN and PilO are sufficient for heterodimer formation. However, recent work in the

T4PS of *N. meningitidis* and the T2SS of *D. dadantii* showed interactions between the TMS of PilN- and PilO-like proteins (122,135), suggesting more complex interaction interfaces than were previously envisaged. In Chapter 2, the core, the coiled-coils, and the TMS of PilN and PilO from *P. aeruginosa* were tested for their role in interaction and proper function of the T4P system.

2. **To investigate whether PilN and PilO form both homo- and heterodimers under physiological conditions, and determine if T4P function requires that those interactions be dynamic.**

"Partner switching" whereby PilN- and PilO-like proteins undergo rotational movements resulting in swapping between homo- or heterodimerization were reported for the T2SS (122). Although PilO forms homodimers *in vitro,* whether a similar PilNO homo- and heterodimer switching phenomenon occurs in the T4P system of *P. aeruginosa* has not been examined. This hypothesis is explored in Chapter 3.

3. **To characterize the structure of PilO and examine the importance of highly conserved, unstructured regions on T4P function.**

The most highly conserved sequence in PilO, ^{167}LPRIVTL^{173}, falls in a region of the protein predicted to be largely unstructured (51). PilO co-purifies with PilN and PilP as a stable heterotrimer (55). Using soluble

periplasmic fragments of PilNOP, we made multiple attempts to obtain a structure of the heterotrimer to visualize the interfaces between these components. In one case, we obtained crystals containing only PilN and PilO that diffracted well but were unable to solve using molecular replacement due to pseudotranslational non-crystallographic symmetry. In another, we isolated a different crystal form that diffracted to high resolution but contained only PilO. Using these latter data, a new, higher-resolution PilO structure was solved, and the involvement of highly conserved residues located in the core of PilO in T4P function was investigated in Chapter 4.

CHAPTER TWO

Novel role for PilNO in type IV pilus retraction revealed by alignment subcomplex mutations

Preface

Chapter two consists of the following publication:

Leighton TL, Dayalani N, Sampaleanu LM, Howell PL, and Burrows LL. 2015. Novel role for PilNO in type IV pilus retraction revealed by alignment subcomplex mutations. J. Bacteriol. 197(13): 2229-38.

Attributions: ND was an undergraduate thesis student mentored by TLL. Constructs were created and cloned by TLL, ND, and LMS. Experiments were designed by TLL and LLB, and performed by TLL. The manuscript was written by TLL, LLB, and PLH.

Title page and author list

Novel role for PilNO in type IV pilus retraction revealed by alignment subcomplex mutations.

Leighton TL[1], Dayalani N[1], Sampaleanu LM[2], Howell PL[2,3] & Burrows LL[1]*

[1] Department of Biochemistry and Biomedical Sciences and the Michael G. DeGroote Institute for Infectious Disease Research, McMaster University, ON, CAN.

[2] Program in Molecular Structure & Function, The Hospital for Sick Children and the [3]Department of Biochemistry, University of Toronto, ON, CAN.

*To whom correspondence should be addressed:

Dr. Lori L. Burrows, 4H18 Health Sciences Centre, 1200 Main St. West, Hamilton, ON, L8N 3Z5 CANADA, Tel: (905)-525-9140 ext: 22029, Fax: (905) 522-9033, E-mail: burrowl@mcmaster.ca

Dr. P. Lynne Howell, 20-9-715 Peter Giligan Centre for Research and Learning, 686 Bay St., Toronto, ON M5G 0A4 CANADA, Tel: (416) 813-5378, Fax: (416) 813-5022, E-mail: howell@sickkids.ca

Running Title: Novel role for PilNO in type IV pilus retraction

Abstract

Type IV pili (T4P) are surface-exposed fibres that mediate adhesion, biofilm formation and twitching motility. A conserved alignment subcomplex of the PilMNOP proteins is required for function of the T4P system. Three potential interaction interfaces between PilNO were identified: the core, the coiled-coil (CC) and the transmembrane segment (TMS). A model of a PilNO heterodimer was used to select 10 residues for mutation to probe the PilNO interaction interface using a bacterial two-hybrid (BTH) system. Mutations made in the oppositely charged CC's and the TMS disrupted PilNO heterodimer formation. Up to 6 combined mutations in the core region failed to disrupt PilNO interaction, implying that this region is less critical. Each of the 10 mutations was introduced onto the chromosome of *Pseudomonas aeruginosa* at the native *pilN* or *pilO* loci, and effects on T4P function determined. Our analyses revealed that specific mutations in each of the three regions – including core mutations that failed to disrupt interactions in the BTH system – altered surface piliation and impaired twitching motility without affecting protein stability. Some mutants were piliated but non-motile, suggesting that PilNO participate in both extension and retraction of T4P. Our findings support a model of multiple, precise interaction interfaces between PilNO, and highlight potential target sites for novel small molecule inhibitors of the T4P system of *P. aeruginosa*.

Importance

Pseudomonas aeruginosa is an opportunistic pathogen that uses type IV pili (T4P) for host attachment. The T4P machinery is composed of four cell envelope-spanning subcomplexes. PilN and PilO heterodimers are part of the alignment subcomplex and essential for T4P function. Three potential PilNO interaction interfaces (the core-core, coiled-coil, and transmembrane segment interfaces) were probed using site-directed mutagenesis followed by functional assays in an *Escherichia coli* two-hybrid system and in *P. aeruginosa*. Several mutations blocked T4P assembly and/or motility, including two that revealed a novel role for PilNO in pilus retraction, while other mutations affected extension dynamics. These critical PilNO interaction interfaces represent novel targets for small-molecule inhibitors with the potential to disrupt T4P function.

Introduction

Alarming increases in antibiotic resistance have prompted the search for alternative strategies to combat bacterial infection (136). Genomic-based strategies targeting essential bacterial processes have been informative, but less successful than once predicted due to high mutation rates leading to resistance (137). Alternative strategies – such as phage therapy and ‘antivirulence’ drugs that target bacterial factors involved in pathogenesis – show promise. They effectively disarm the bacteria, which are then more easily cleared by the host immune system. The targeting of non-vital cellular processes decreases selection

pressure, making mutation-based resistance to these therapies less likely (138). The type III secretion system (T3SS) field has had success with this strategy, where promising molecules – some of which showed broad-spectrum activity for various bacterial pathogens – were identified through whole-cell-based high-throughput screens (139-141).

Type IV pili (T4P) are common virulence factors (6,7,142) and another attractive target for therapeutics against bacterial infection. They are long, thin (5-8nm diameter) hair-like appendages which extend from the bacterial surface and promote attachment, cell-cell aggregation, biofilm formation, and twitching motility (1-5,10). T4P are produced by a wide variety of bacteria and archaea, including the opportunistic pathogen, *Pseudomonas aeruginosa*, which infects individuals with severe burns, cystic fibrosis, or immunodeficiencies (8). Mutants lacking T4P are impaired in host colonization and infectivity (7). T4P-mediated twitching motility is a form of flagellum-independent surface translocation that results from repeated rounds of pilus extension, adhesion, and retraction (14,30). Upon pilus retraction, the cell body is winched towards the point of attachment (1,13,30).

The T4P system is comprised of four subcomplexes that together span the entire Gram-negative cell envelope (Figure 2.1A) (4). The outer membrane (OM) subcomplex is composed of an oligomer of 12-14 secretin subunits, PilQ (44), bound to a pilotin protein, PilF, forming a pore through which the pilus exits the cell (45,46,72). Recently, a T4P secretin-associated protein called TsaP (PA0020 in *P. aeruginosa*), containing a peptidoglycan-binding motif and important for

assembly of functional T4P, was identified in *Neisseria gonorrhoeae* and *Myxococcus xanthus* (47). TsaP potentially anchors the secretin to the peptidoglycan to resist retraction forces, though this is still to be investigated in *P. aeruginosa*. There are two inner membrane (IM) subcomplexes – the motor and alignment subcomplexes – that together make up the IM platform. The motor subcomplex is composed of a platform protein, PilC, and associated cytoplasmic ATPases (PilBTU in *P. aeruginosa*) that provide the mechanical forces that lead to pilus extension/retraction (48,49). The secretin and the motor subcomplexes are linked by the alignment subcomplex, PilMNOP, which may also play a role in secretin gating (23,54). The final subcomplex is the pilus fibre itself, composed of major and minor pilin subunits plus the adhesion, PilY1 (5,13,56-58). Together with a number of regulatory proteins whose functions are poorly understood, these subcomplexes form a fully functional T4P system (41,75,143,144).

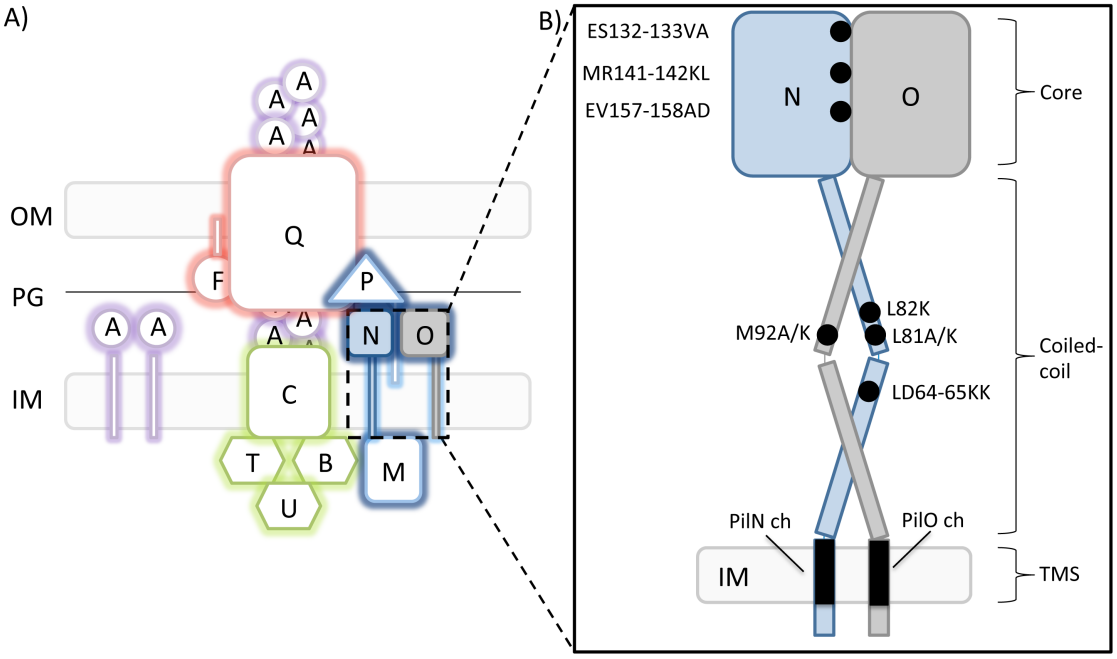

Figure 2.1. The type IV pilus system in *Pseudomonas aeruginosa* (adapted from (4)). (A) Components of the type IV pilus proteins are labeled according to the *Pseudomonas aeruginosa* nomenclature. Components include the outer membrane (OM) secretin subcomplex (red), the inner membrane (IM) motor subcomplex (green), the IM alignment subcomplex (dark blue), and the pilus fibre (purple). **(B)** Cartoon representation of two alignment subcomplex components, PilN (blue) and PilO (grey), indicating the approximate locations of residue substitutions (black circles/rectangle). The three regions examined in this study are indicated on right: the core region, the coiled-coil (CC) region, and the transmembrane segment (TMS).

The alignment subcomplex is composed of four proteins, PilMNOP. PilM is a cytoplasmic protein with an actin-like fold, similar to bacterial cytoskeleton proteins FtsA and MreB (23,114). A narrow crevice on PilM binds a conserved motif in the N-terminus of PilN in *P. aeruginosa* (51) and *Thermus thermophilus* (114). PilN and PilO are bitopic IM proteins with similar topologies (51)(51)(51). Both have short cytoplasmic N termini, a single transmembrane segment (TMS), two extended α-helices connected by a short linker forming a coiled coil (CC), and a C-terminal core domain composed of dual ferredoxin-like αββ motifs (see supplementary Figure S2.1) (51). In the crystal structure of a PilO homodimer missing the N-terminal 68 residues, the truncated coiled-coil segment is folded up against the core domain (51). A recent analysis of the crystal structure of a C-terminal fragment (residues 94 to 207) of *T. thermophilus* PilN revealed a dual αββ motif with an extra α-helix insertion that is not present in orthologs from mesophilic bacteria, resulting in a secondary structure order of αβαβ-αββ (114). PilN and PilO form stable heterodimers and are dependent upon one another for stability *in vivo* (51). The fourth component of the alignment subcomplex is the inner-membrane lipoprotein PilP, which binds the PilNO heterodimer through its extended N-terminal segment (55). Previous studies reported an interaction between PilP and PilQ in *N. meningitidis* (65), and more recently, interaction of the C-terminal β-domain of *P. aeruginosa* PilP with the N0 domain of PilQ was demonstrated by co-purification experiments (54). Together, the PilMNOP

subcomplex connects the inner and outer membrane T4P subcomplexes and is essential for pilus function.

Disruption of a key protein homodimer by small molecules was shown to block formation of the type IV secretion (T4S) system and to diminish virulence of *Brucella* spp. (62,145). Toward our goal of designing inhibitors of T4P function in *P. aeruginosa*, here we examined the contributions of the core, coiled-coil and transmembrane segments of PilNO in their interaction and function. Point mutations in the coiled-coil region disrupted PilNO heterodimer formation in a bacterial two-hybrid (BTH) assay, as did swapping of their transmembrane segments. In contrast, up to six combined point mutations in the core region had no effect. When the same mutations were introduced at their native loci on the *P. aeruginosa* chromosome, many - including those that failed to disrupt PilNO interactions in the BTH assay - altered twitching motility and surface piliation. Chromosomal mutations thus provided key information about T4P system dynamics that could not be predicted from the results of the pairwise BTH assay. Our findings support a model in which multiple, precise PilNO interaction interfaces are critical for subcomplex dynamics and highlight potential target sites for inhibitor design.

Experimental procedures

Strains, media and growth conditions

E. coli and *P. aeruginosa* were grown at 37 °C in LB supplemented with antibiotics at the following final concentrations when necessary (μg•mL^{-1}): ampicillin (Ap), 100; carbapenem (Cb), 200; kanamycin (Kn), 50; gentamicin (Gm), 15 for *E. coli* and 30 for *P. aeruginosa*, unless otherwise specified. Plasmids were transformed by heat shock into chemically competent cells. All constructs were verified by DNA sequencing (MOBIX).

Bacterial Two Hybrid (BTH) β-galacotsidase Activity Assay

Chemically competent *E. coli* BTH101 was co-transformed with various combinations of pUT18C and pKT25 protein fusions, and tested for activity using a 96-well plate-based assay as previously described (146) with modifications. Briefly, BTH101 cells co-transformed with T18-PilN and T25-PilO fusion constructs were grown at 30 °C in LB supplemented with Ap and Kn, shaking at 260 rpm overnight. LB broth containing antibiotics and 0.5 mM Isopropyl β-D-1-thiogalacto-pyranoside (IPTG; Sigma-Aldrich), were inoculated with a 1:5 dilution of an overnight culture and grown at 30 °C, 260 rpm shaking, to an optical density at 600 nm (OD_{600}) of ~0.6 and standardized. Cells were harvested by centrifugation for 3 min at 2292 x *g* in a microcentrifuge, washed with 500 μl 1X phosphate buffered saline (PBS; 0.14M NaCl, 2.68mM KCl, 8.1mM Na_2HPO_4, 1.47mM KH_2PO_4), and resuspended in 400 μL of 1X PBS. The cells were lysed

using MP Bio Lysing Matrix silica beads and the FastPrep®-24 instrument (MP Biomedicals) for 20 s following manufacturer's instructions. Tubes were centrifuged to remove the matrix and cell debris, and the supernatant collected. Fifty µL of the supernatant was added to a 96-well microplate containing 50 µL of 2x Assay Buffer (200 mM sodium phosphate buffer, pH 7.3, 2 mM $MgCl_2$, 100 mM β-mercaptoethanol, 1.33 mg/ml o-nitrophenyl-β-D-galactopyranoside (ONPG; Sigma-Aldrich)) per well. The plate was incubated for 30 min at 37 °C, on a rocking platform. The reaction was stopped with the addition of 150 µL of 1 M sodium carbonate, and absorbance at 420 nm and 550 nm was measured using a Multiscan GO microplate reader (Thermo Scientific). The specific β-galactosidase activity was converted to Miller Units using the following equation where A is absorbance, and T is time in minutes:

$$Activity\ (Miller\ Units) = 1000\ x \frac{A420 - (1.75\ x\ A550)}{T\ x\ 0.1\ x\ A600}$$

All assays were performed in triplicate and at least 3 independent experiments were performed for each transformant.

Generation of pilN and pilO mutations on the chromosome of P. aeruginosa PAK

pilN and *pilO* mutants were constructed using a Flp-FRT (FLP recombination target) system as previously described (147)(147)(147). Briefly, suicide vectors which contained the target gene, *pilN* or *pilO*, containing the desired mutations plus the flanking genes (pEX18Gm::*pilMNO* and pEX18Gm::*pilNOP*, respectively), were introduced into *E. coli* SM10 cells. The constructs were transferred by conjugation in a 1:9 ratio of *P. aeruginosa* to *E.*

coli. The mixed culture was pelleted for 3 min at 2292 x *g* in a microcentrifuge, and the pellet was resuspended in 50 µL of LB, spot-plated on LB agar, and incubated overnight at 37 °C. *P. aeruginosa* PAK strains which contained either *pilN::FRT* or *pilO::FRT* mutations were used as recipients for pEX18Gm::*pilMNO* or pEX18Gm::*pilNOP* constructs, respectively in mating experiments (50)(50)(50). After mating, cells were scraped from the LB agar plate, resuspended in 1 mL of LB and the *E. coli* SM10 donor was counterselected by plating on *Pseudomonas* isolation agar (PIA; Difco) containing Gm (100 µg•mL^{-1}). Gm-resistant *P. aeruginosa* isolates were streaked on LB no salt plates with sucrose (1% w/v bacto-tryptone, 0.5% w/v bacto-yeast extract, 5% w/v sucrose) then incubated for 16 h at 30 °C. Select colonies were cultured in parallel on LB and LB plates supplemented with Gm. Gm-sensitive colonies were screened by PCR using *pilN* or *pilO* primer pairs to confirm replacement of the FRT-disrupted gene, and PCR products of the expected size were sequenced to confirm incorporation of the desired mutations.

Generation of pilT mutants

pilT mutants were constructed using the Flp-FRT recombination system as previously described (147). Briefly, a suicide vector containing the target gene (*pilT*) disrupted by a gentamicin resistance cassette flanked by FRT sites (pEX18AP::*pilT*::GmFRT) (148) was introduced into chemically competent *E. coli* SM10 cells. The constructs were transferred to *P. aeruginosa* PAK strains containing *pilN* mutations (ES132-133VA, MR141-142KL, EV157-158AD), by

biparental mating as described above. *E. coli* SM10 was counterselected by plating on *Pseudomonas* isolation agar (PIA; Difco) containing Gm (100 μg•mL^{-1}). Gm-resistant isolates were selected, and streaked on LB no salt plates with sucrose then incubated for 16 h at 30 °C. Select colonies were plated in parallel on LB plates supplemented with Cb and LB plates with Gm, and Gm-resistant, Cb-sensitive colonies selected. Removal of the integrated Gm cassette by Flp recombinase-catalyzed excision was achieved by conjugally transferring the Flp-expressing pFLP2 from *E. coli* SM10 into *P. aeruginosa* as previously described (147). *E. coli* SM10 was counter-selected by plating on *Pseudomonas* isolation agar (Difco) containing Cb. pFLP2 was cured by streaking Cb-resistant isolates on LB-no salt plates containing 5% (w/v) sucrose, and incubating for 16 h at 30 °C. Select colonies were streaked in parallel on LB plates, LB plus Cb plates and LB plus Gm plates. Cb- and Gm-sensitive colonies were selected and the *pilT*::FRT mutation confirmed by PCR and DNA sequencing.

Twitching motility assays

Twitching assays were performed as previously described (149). Briefly, single colonies were stab inoculated to the bottom of a 1% LB agar plate. The plates were incubated for 36 h at 37 °C. Post incubation, the agar was carefully removed and the adherent bacteria stained with 1% (w/v) crystal violet dye, followed by washing with tap water to remove unbound dye. Twitching zone areas were measured using ImageJ software (NIH) (150). All experiments were performed in triplicate with at least three independent replicates.

Sheared surface protein preparation

Surface pili and flagella were analyzed as described previously (149). Briefly, strains of interest were streaked in a grid-like pattern on LB agar plates and incubated at 37 °C for 16 h. Using a glass cover slip, the bacteria were gently scraped from the surface of the agar and resuspended in 4.5 mL of 1X PBS. Surface appendages were sheared by vortexing for 30 s. Suspensions were transferred to 1.5 mL Eppendorf tubes and pelleted by centrifugation for 5 min at 11,688 x *g*. The supernatant was transferred to fresh tubes and centrifuged for 20 min to remove remaining cellular debris. The supernatant was transferred to new tubes and 1/10 volume of 5 M NaCl and 30% (w/v) polyethelene glycol 8000 (PEG 8000, Sigma Aldrich) were added to precipitate soluble proteins. Tubes were incubated on ice for 90 min. Proteins were collected by centrifugation for 30 min at 11,688 x *g* and the supernatant was discarded. The pellet was resuspended in 150 µL of 1X SDS sample buffer (125mM Tris, pH 6.8, 2% β-mercaptoethanol, 20% glycerol (v/v), 4% SDS (w/v) and 0.001% bromophenol blue (w/v)). Samples were boiled for 10 min and separated on 15% SDS-PAGE gels. Proteins were visualized by staining with Coomassie brilliant blue (0.1% Coomassie Brilliant Blue R-250, 50% methanol and 10% glacial acetic acid).

Preparation of whole cell lysates

Cultures were grown overnight at 37 °C in LB supplemented with appropriate antibiotics to an OD_{600} of 0.6. A 1 mL aliquot of cells was collected by centrifugation at 2292 x *g* for 3 min in a microcentrifuge. The cell pellet was

resuspended in 100 µL of 1X SDS sample buffer and boiled for 10 min. Whole cell lysate samples were separated on 15% SDS-PAGE gels and subject to Western blot analysis.

Western blot analysis

Whole cell lysate samples were separated on 15% SDS-PAGE gels and transferred to nitrocellulose membranes for 1 h at 225 mA. Membranes were blocked using a 5% (w/v) low fat skim milk powder in 1x PBS for 1 h at room temperature on a shaking platform, followed by incubation with the appropriate antisera for 2 h at room temperature, at a dilutions as follows: PilM 1/2500, PilNOP 1/1000 and PilA 1/5000. The membranes were washed twice in 1x PBS for 5 min then incubated in goat-anti-rabbit IgG-alkaline phosphatase conjugated secondary antibody (Bio-Rad) at a dilution of 1/3000 for 1 h. The membranes were washed twice in 1x PBS for 5 min, and visualized with alkaline phosphatase developing reagent (Bio-Rad) following the manufacturer's protocol.

Results

PilO forms homodimers and heterodimers, while PilN forms only heterodimers

Using a bacterial adenylate cyclase two-hybrid (BTH) system amenable to examining potential interactions of membrane-bound proteins (146,151), we examined interactions between both truncated and full-length versions of PilN and PilO (Figure 2.2A). Truncated constructs encompassed the core and CC

domains but lacked the TMS and cytoplasmic N termini (Figure 2.2B; see also supplementary Figure S2.1). Stable expression of all fusions was confirmed via Western blotting with specific antisera to PilN or PilO (see supplementary Figure S2.2). Interactions between the periplasmic regions of PilN and PilO ($PilN_{\Delta 44}$ and $PilO_{\Delta 51}$, respectively) – previously established by co-purification and gel filtration (51,55) – were confirmed, as were interactions between the full-length proteins (Figure 2.2A) (51,55). In addition to forming heterodimers with $PilN_{\Delta 44}$ and $PilO_{\Delta 51}$ fragment formed homodimers. Unexpectedly, full-length PilO did not homodimerize in the BTH assay, with β-galactosidase activities similar to those seen with the negative control (Figure 2.2A). Neither truncated nor full-length PilN formed homodimers in this assay (Figure 2.2A).

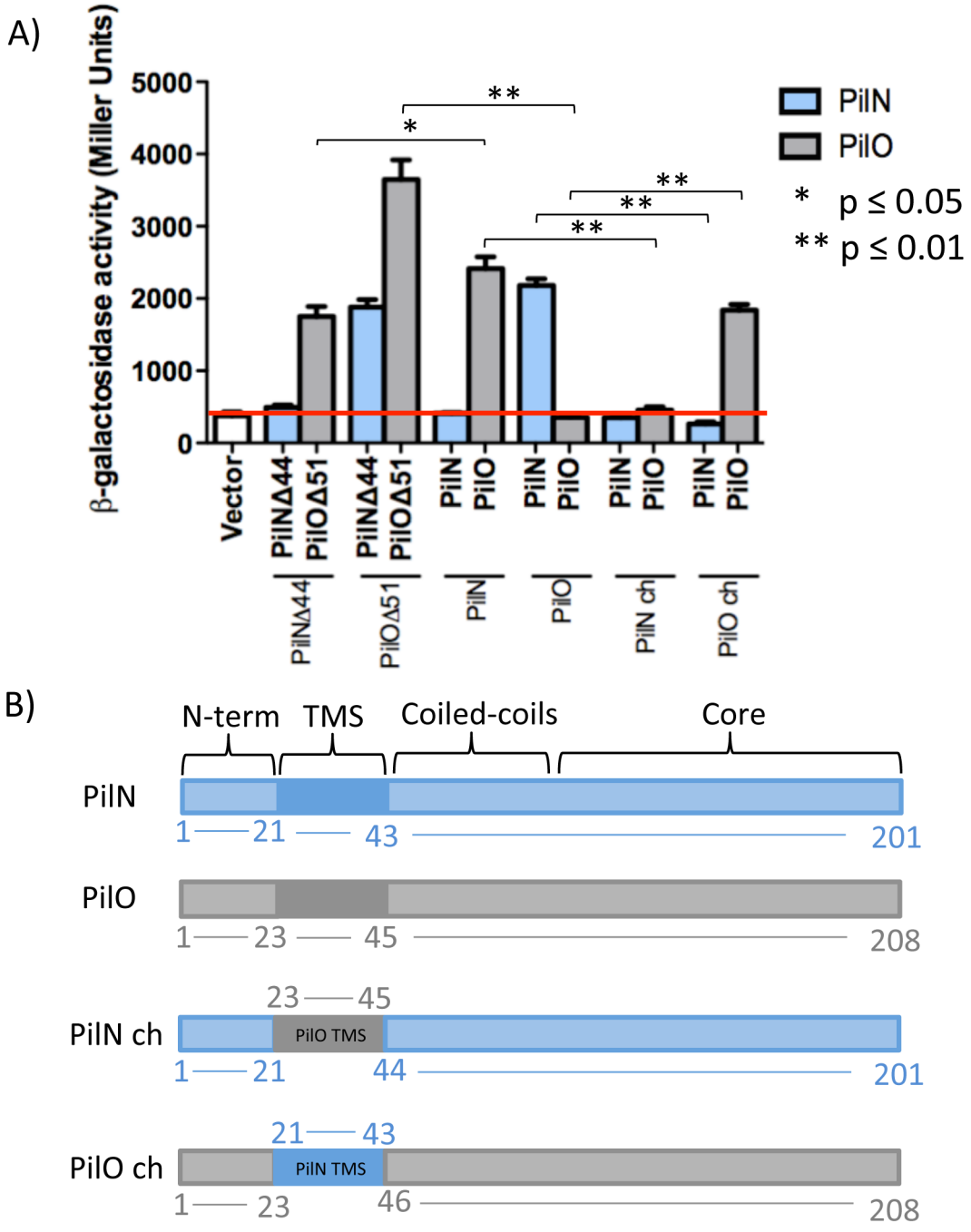

Figure 2.2. A PilO chimera disrupts PilNO heterodimer formation in the BTH system. (A) N-terminal truncations of PilN and PilO ($PilN_{\Delta 44}$ and $PilO_{\Delta 51}$) and full-length versions of PilN, PilO and a PilO chimera (PilO Ch) were fused at their N-

termini to either the T18 or T25 fragments of adenylate cyclase from *B. pertussis*. Interaction of PilN and PilO was detected using both truncated and full-length versions, whereas only the truncated version of PilO formed homodimers. Swapping of the TMS from PilO with that of PilN resulted in a loss of interaction with PilN but restored the interaction with PilO. Experiments performed in triplicate (N=3). Horizontal red line indicates β-galactosidase activity of the vector only negative control (white bar). ** $p \leq 0.01$ **(B)** Cartoon schematic of the PilO chimera construct with boundaries indicated for PilN (blue) and PilO (grey).

The transmembrane segments of PilNO are important for their interaction

Although we showed previously (55) that the periplasmic regions of PilN and PilO are sufficient for their interaction, evidence from the *Neisseria* T4P system and for functionally equivalent components GspLM from the T2SS of *Dickeya dadantii* indicated that TMS likely participate in PilNO interactions (122,135). Contributions of the *P. aeruginosa* PilN and PilO TMS to their interactions were examined using chimeras. The PilN chimera construct consisted of full-length PilN in which the TMS (residues 21 to 43) was replaced with that of PilO (residues 23 to 45). In the PilO chimera, the TMS (residues 23 to 45) was swapped for that of PilN (residues 21 to 43) (Figure 2.2B). Although homodimerization of full-length PilO was negative in the BTH assay, the PilO chimera could interact with wild-type PilO but lost the ability to interact with PilN (Figure 2.2A). Full-length PilN did not homodimerize, and the PilN chimera failed to interact with either PilN or PilO in this assay (Figure 2.2A).

Point mutations in the coiled coils of PilN or PilO disrupt their interaction in the BTH assay

Attempts to purify soluble *P. aeruginosa* PilN for structural studies, or to obtain an X-ray crystal structure of the PilNO heterodimer, have so far been unsuccessful. While a structure of a *T. thermophilus* PilN periplasmic fragment is available (124) its primary sequence identity with *P. aeruginosa* PilN is very low, and the arrangements of their secondary structure elements differ, precluding use of *T. thermophilus* PilN as a template to produce a high-confidence structural model. Instead, the truncated *P. aeruginosa* PilO homodimer structure (51) was used to generate a high-confidence Phyre^2 (125) model of a PilNO heterodimer (Figure 2.3A). The model was used to design a series of single or double point substitutions meant to disrupt hydrophobic or charged interactions at the core-core or coiled-coil interfaces (Figure 2.1B and Tables 2.1 and 2.2). Because the PilNO heterodimer, like the PilO homodimer, is predicted to have a large buried surface area – 2,082 Å^2 for the PilO$_{\Delta 68}$ homodimer (51) – some mutations were generated in pairs to rapidly exclude those with no effect. Residues at the predicted core-core interface between PilN α4 and PilO β4 or between PilN β3 and PilO α4, with estimated distances of less than 12 Å between Cα atoms, were selected for mutagenesis (Figure 2.3B and Tables 2.1 and 2.2). Coiled-coil residues were selected based on their conservation in orthologs from other T4P-expressing bacteria (Figure 2.3C and Tables 2.1 and 2.2). The mutations were introduced into the full-length T18-PilN and T25-PilO constructs, and stable

expression of mutant fusions was verified by Western blotting (see supplementary Figure S2.2). In the BTH assay, none of the core mutations (PilN ES132-133VA, MR141-142KL, and EV156-157AD) nor a combination of all these mutations (PilN Triple) disrupted the PilNO interaction (Figure 2.4, gray bars). In the coiled-coil region, PilN L81K and LD64-65KK and PilO M92K disrupted the PilNO interaction (Figure 2.4, black bars). These data suggested that, in addition to the TMS, the coiled-coil region was involved in PilNO interactions.

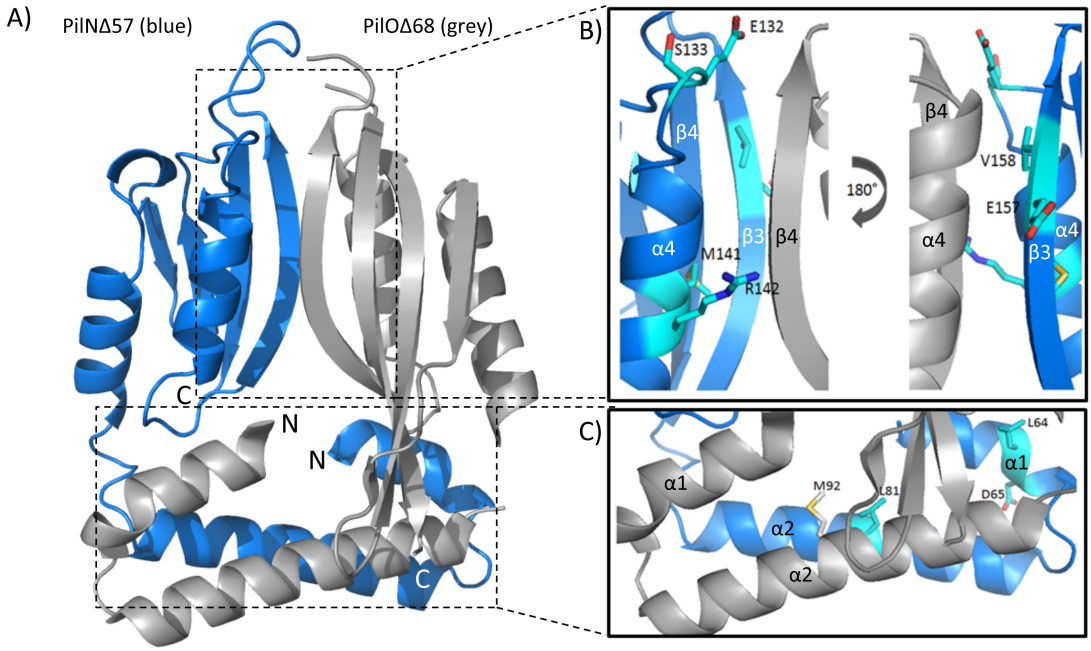

Figure 2.3. Model of a PilNO heterodimer. (A) A ribbon diagram representation mapping the N- and C-termini, secondary structure elements and structural domains of $PilN_{\Delta 57}$ (blue) $PilO_{\Delta 68}$ (grey) using a Phyre^2 (125) model of PilN generated using the $PilO_{\Delta 68}$ homodimer (PDB 2RJZ (51)(51)(51)) as a template.

(B) Close up of the core-core domain, which consists of PilN α-helices 3-4 and β-strands 1-4, and PilO α-helices 3-4 and β-strands 1-5. Shown are the residues on PilN chosen for substitution; α4 helix: E132, S133, M141, R142; β3 strand: E157, V158. **(C)**: Close up of the PilNO coiled-coils, which consist of α-helices 1-2. Shown are the residues chosen for substitution; PilN α1 helix: L64, D65; α2 helix: L81, L82; PilO α2 helix M92.

Table 2.1: Summary of PilN and PilO mutants and their phenotypes.

Mutation PilN	**Location**	**BTH PilO Interaction**	**Twitching motility**	**Surface Pili**
ES132-133VA	Core	Yes	Yes	Yes
MR141-142KL	Core	Yes	No	No
EV157-158AD	Core	Yes	No	No
Triple [ESMREV132-133-141-142-157-158VAKLAD]	Core	Yes	No	No
L81K	Coiled-coils	No	Yes - reduced	Yes - hyper
L81A	Coiled-coils	Yes	Yes	Yes
L82K	Coiled-coils	Yes	Yes	Yes
LD64-65KK	Coiled-coils	No	No	Yes – reduced
Mutation PilO	**Location**	**BTH PilN Interaction**	**Twitching motility**	**Surface Pili**
M92A	Coiled-coils	Yes	Yes	Yes
M92K	Coiled-coils	No	Yes - reduced	Yes - hyper
Chimera	TMS	No	Yes - reduced	Yes

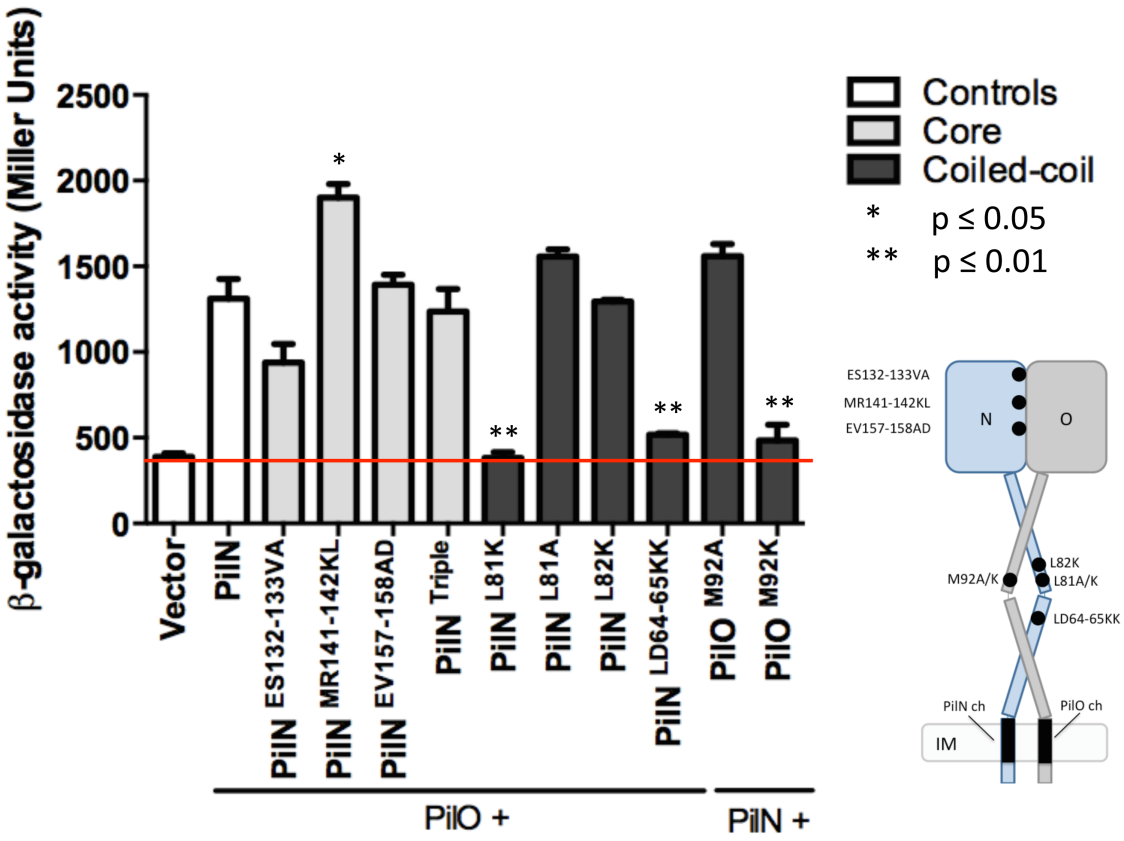

Figure 2.4. Specific mutations in the coiled-coil region of PilN disrupt PilNO interaction. Core mutations (grey bars), PilN ES132-133VA, MR141-142KL, and EV157-158AD were tested individually and in combination (Triple), but failed to disrupt interaction between full length PilN and PilO. Mutations in the coiled-coils (black bars) PilN L81K, LD64-65KK and PilO M92K disrupted the interaction, whereas PilN L81A, L82K, and PilO M92A had no effect. Experiments performed in triplicate (N=3). Horizontal red line indicates β-galactosidase activity of vector only negative control (white bar). Positive control was full-length PilN and PilO interaction. * $p \leq 0.05$, ** $p \leq 0.01$.

Substitutions in PilN and PilO disrupt the dynamics of the T4P system

PilMNOP are encoded in a single operon and their stability is sensitive to perturbations in stoichiometry (50). To retain their native context, all point substitutions and the chimeric mutations swapping the TMSs of PilN and PilO were integrated into the *P. aeruginosa* chromosome at their original loci. After the stable expression of all alignment subcomplex proteins and the major pilin PilA was verified using specific antisera (see supplementary Figure S2.3A), the mutants were assessed for surface pilus expression and twitching motility.

We predicted that mutations failing to disrupt heterodimerization in the BTH assay (PilN ES132-133VA, MR141-142KL, EV157-158AD, Triple, L81A, and L82K and PilO M92A) would confer a wild-type phenotype, while those that prevented interactions (PilN L81K and LD64-65KK and the PilN chimera and PilO M92K and the PilO chimera) would prevent pilus assembly and, thus, motility. Mutants PilN ES132-133VA, L81A, and L82K and PilO M92A had phenotypes similar to the wild-type phenotype, but, surprisingly, core mutants PilN MR141-142KL and EV157-158AD - and consequently, the Triple mutant that contains those mutations - were unable to twitch due to a lack of pili (Figure 2.5A). Coiled-coil mutants PilN L81K and PilO M92K that failed to interact in the BTH assay unexpectedly had wild-type or greater levels of pili but only ~60% of the wild-type level of twitching motility, a statistically significant decrease ($p \leq 0.01$) (Figure 2.5A; see also supplementary Figure S2.4). These phenotypes were consistent with defects in pilus retraction. The PilN LD64-65KK coiled-coil mutant and the

PilN chimera had only a small amount of pili and no twitching motility, while the PilO chimera had levels of pili similar to the wild-type level but was significantly impaired in its ability to twitch, at ~50% of the level seen with the wild-type control ($p \leq 0.01$) (Figure 2.5A; see also supplementary Figure S2.4). These data indicate that specific residues at the core-core and coiled-coil interfaces, and in the TMS, play diverse roles in function of the PilN and PilO proteins and that interaction (or lack thereof) in the BTH assay does not necessarily correlate with dysfunction in the native context.

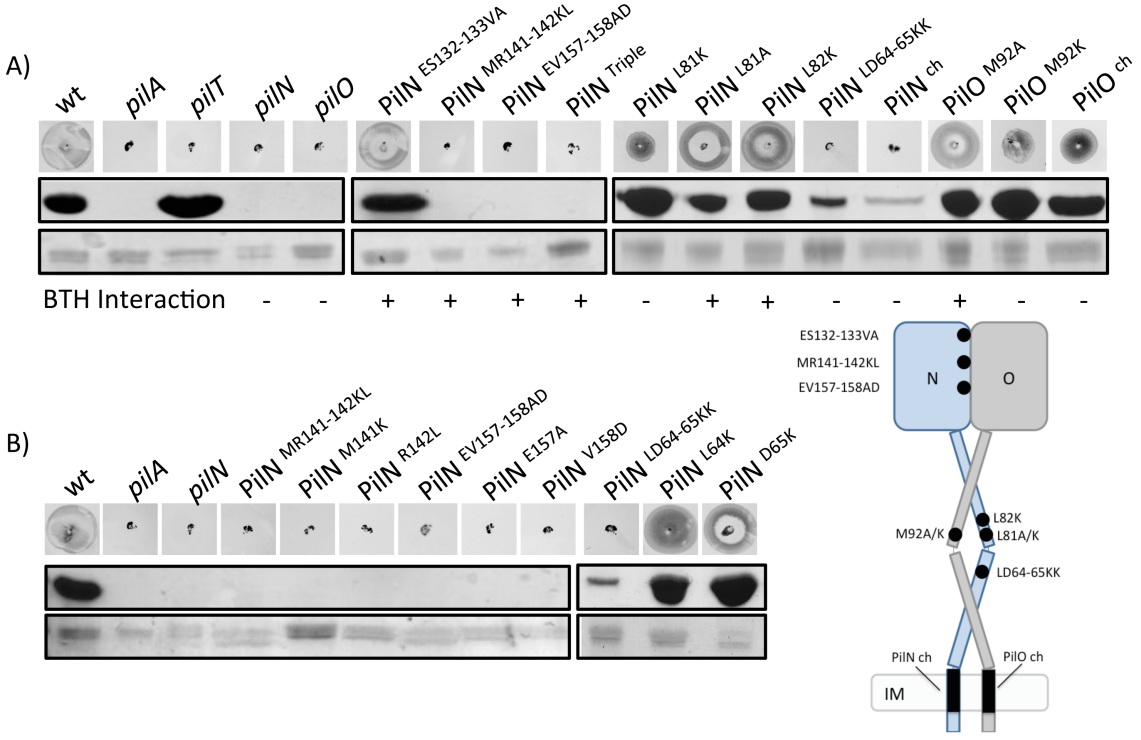

Figure 2.5. Specific *pilN* and *pilO* point mutations on the *P. aeruginosa* PAK chromosome affect piliation and twitching motility. (A) PilN and PilO mutants plus (wt), non-piliated (*pilA*), hyperpiliated (*pilT*), and negative controls (*pilN* and

p*ilO* respectively), were tested for twitching motility (top), and sheared surface pili (bottom). Boxes: Twitching motility zones from each mutant stained with 1% (w/v) crystal violet. Rows: Sheared surface proteins were separated on 15% SDS-PA gel stained with Coomassie brilliant blue to visualize pilins (top) and flagellins (loading control - bottom) for each PilN and PilO mutant. The interaction (+) or lack of interaction (-) for each mutant in BTH assay is summarized below. **(B)** Single point substitutions were created for mutants MR141-142KL, EV157-158AD and LD64-65KK and the mutants subjected to twitching motility (top), and sheared surface pilin assays (bottom).

The core domain of PilN is more sensitive to perturbation than the coiled-coil region

To further dissect the residues in the PilN MR141-142KL, EV157-158AD, and LD64-65KK mutants that were responsible for aberrant function, single mutations from each pair were introduced into the *P. aeruginosa* chromosome at the pilN locus. Single substitutions had no effect on the stable expression of alignment subcomplex components or intracellular levels of PilA (see supplementary Figure S2.3B). Single mutants M141K, R142L, E157A, and V158D recapitulated the double-mutant phenotype, with no pili and motility, while single mutants L64K and D65K had wild-type levels of pili and twitching motility (Figure 2.5B; see also supplementary Figure S2.4) and regained the ability to interact with PilO in the BTH assay (see supplementary Figure S2.5). Therefore, single substitutions in the core domain of PilN independently disrupted T4P

function, while the combination of coiled-coil mutations was necessary to produce the observed functional defects.

Non-piliated mutants can assemble pili in a retraction deficient background

In a *pilT* mutant lacking the retraction ATPase, all pili that are assembled become trapped on the surface of the bacteria (152). In a retraction-deficient background, mutants lacking individual components of the alignment subcomplex assemble fewer pili than a *pilT* control (49). We hypothesized that PilN MR141-142KL and EV157-158AD mutants may assemble pili in a retraction-deficient background, similar to a *pilN* deletion mutant. The PilT retraction ATPase was inactivated in PilN ES132-133VA, MR141-142KL, and EV157-158AD mutants. As predicted, PilN MR141-142KL and EV157-158AD assembled a small amount of pili when retraction was disabled (Figure 2.6), a lesser amount than the PilN ES132-133VA control (which has pili; Figure 2.5A) or the wild-type. Interestingly, the PilN point mutants assembled fewer pili than a mutant in which *pilN* was completely deleted (Figure 2.6). These data suggest that small changes in the PilN MR141–142KL and EV157-158AD mutant interface with PilO severely restrict pilus assembly and that the resulting imbalance between extension and retraction leads to bald cells.

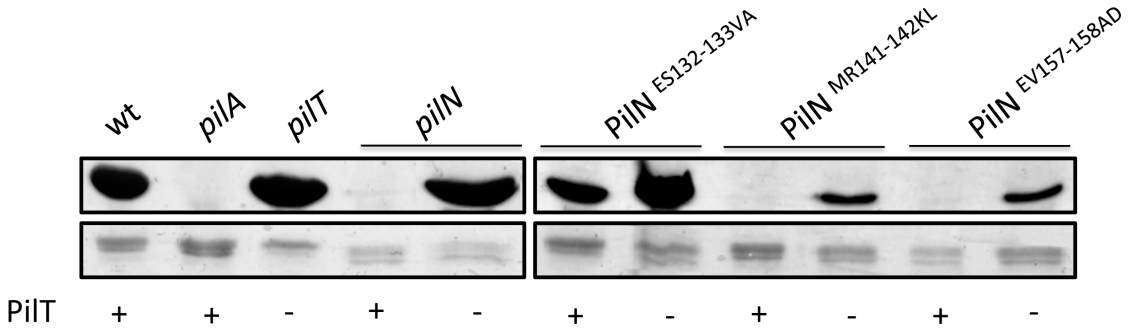

Figure 2.6. PilN ES132-133VA and MR141-142KL assemble pili in retraction-deficient backgrounds. PilN mutants ES132-133VA, MR141-142KL, and EV157-158AD were tested in a retraction-deficient background for their ability to assemble pili. Mutants were compared to (wt), non-piliated (*pilA*), hyperpiliated (*pilT*), a PilN mutant (*pilN*) and a PilN/PilT double mutant (p*ilN*/*pilT*). Sheared surface proteins were separated on 15% SDS-PA gel stained with Coomassie brilliant blue to visualize pilins (top) and flagellins (loading control - bottom) of each PilN mutant.

Discussion

Various functions for the T4P alignment subcomplex PilMNOP have been proposed, including a possible role in relaying signals from the cytoplasmic motor components to the secretin complex in the OM (50,54,55). Here we provide evidence suggesting that the highly conserved components PilN and PilO contribute to both extension and retraction of the pilus fibre. PilNO interactions are precise - because they can be altered by mutation of single residues, resulting in loss of function - and specific - since extension or retraction can be independently perturbed, depending on the location and nature of the mutation.

Structural and functional similarities between the type II secretion (T2S) and T4P systems have long been recognized (153). Despite minimal sequence identity between homologous components of the alignment subcomplexes in the two systems, atomic resolution structures revealed a high degree of structural similarity, suggesting conservation of function (51,55,113,116,124,126). Previous studies suggested that multiple segments of GspL and GspM, the T2S equivalents of PilN and PilO, participate in their interaction (122,135). Our BTH assay results confirmed the presence of heterodimeric interactions between the periplasmic domains PilN and PilO (core plus coiled coil) (see supplementary Figure S2.1), as well as the full-length, membrane-bound forms (50,55). The increased β-galactosidase activity observed for full-length versus truncated PilNO suggested that the TMSs contribute to the interaction. Although full-length PilO did not homodimerize in the BTH assay, a PilO chimera with the PilN TMS gained the ability to interact with full-length PilO, while losing the ability to interact with PilN (Figure 2.2A), suggesting that the TMS modulates the interaction. Failure of PilO to homodimerize in the BTH assay may relate to the low isoelectric point (pI 4.2) of its coiled-coil region (51), which could cause charge repulsion, increasing the distance between the T18 and T25 fusion tags and preventing enzyme reconstitution. A similar phenomenon could explain the lack of PilN homodimerization in the BTH assay due the high (10.2) pI in this region of the protein (51), although it seems less likely given that even the truncated form of PilN failed to interact with itself (Figure 2.2A). The PilN chimera (which has the

TMS of PilO) failed to interact with full-length PilO, or with full-length PilN (Figure 2.2A). Given that their TMSs should be compatible, failure of the PilN chimera to interact with PilN (Figure 2.2A) did not match our prediction but suggests that additional contacts in the coiled-coil and core regions are required to stabilize TMS interactions. These findings are consistent with BTH data for *N. meningitidis* T4P components, in that the PilN ortholog interacts with PilO but not with itself, and with previous genetic and biochemical data showing that PilN is misfolded and unstable in the absence of PilO (50,51,55,135). In contrast, PilN from the *T. thermophilus* T4P system (124) and GspL in the T2S system (154-156) form homodimers. In the *T. thermophilus* model, homodimers of PilMN were hypothesized to form the initial transmembrane platform for assembly, followed by docking of PilO onto PilN to form PilNO heterodimers (124). Partner switching between the homo- and heterodimer states of GspL and GspM (PilMN and PilO, respectively) in the T2S system has been reported and has functional implications (122,156). Whether the interactions among components of the T4P alignment subcomplex are dynamic is under investigation.

Defects in pilus retraction, such as those caused by inactivation of the retraction ATPase, PilT, cause a hyperpiliated phenotype (157). Loss of the PilT paralogue PilU (97), or point mutations in the anti-retraction factor PilY1 (88) or the platform protein PilC (49), can also result in piliated cells that have reduced motility. We identified two new mutations in PilNO (PilN L81K and PilO M92K)

that resulted in a loss of twitching motility but increased piliation, suggesting they have a role in pilus retraction. These apposing residues are located in the α2-helices of the coiled-coil (CC-2) region (Figure 2.3C), which are hypothesized to be key sites of interaction between the two proteins due to their large differences in pI (51). The residues of interest likely form a key hydrophobic contact, since PilN L81A - but not L81K - retains wild-type function; similarly, PilO M92A has normal function, while M92K disrupts twitching (Figure 2.5A).

Substituting the TMS of PilN for that of PilO in *P. aeruginosa* caused a marked reduction in motility (see supplementary Figure S2.4) without decreasing piliation (Figure 2.5A), also characteristic of a retraction defect. Although T4P dynamics were clearly impaired, the PilO chimera retained the ability to heterodimerize with PilN in *P. aeruginosa*, as evidenced by the stability of the proteins (see Figure S2.3A in the supplemental material) and their ability to assemble pili (Figure 2.5A). When the TMS of PilN was replaced with that of PilO, the PilN chimera was unable to homo- or heterodimerize in the BTH assay and in *P. aeruginosa* led to trace amounts of surface pili and no motility. The PilN chimera was detrimental to T4P assembly, potentially due to decreased interaction with its cytoplasmic partner, PilM (see supplementary Figure S2.5).

The contributions of the TMS of inner membrane components to their interactions have been largely overlooked in the T4P and T2S systems due to past focus on biochemical and structural analysis of soluble cytoplasmic or periplasmic fragments. In the T2S system of *D. dadantii*, multiple interactions

between the TMSs of GspL and GspM, plus a third integral IM protein, GspC (the equivalent of PilP), were demonstrated using pull-down assays, BTH assays, and Cys crosslinking (122). The mechanism of T2S pseudopilus disassembly is unknown, but in the case of T4P, the phenotypes of the coiled-coil and TMS mutants support the conclusion that precise PilNO interactions contribute to pilus disassembly, as well as assembly.

Multiple mutations at the PilNO core-core interface had no effect on interaction in the pairwise BTH assay, so we were surprised when four of six mutations at this surface severely reduced pilus assembly when introduced into *P. aeruginosa* (Figure 2.4 and 2.5A). These results validate the utility of the PilNO Phyre^2 model in selection of functionally significant residues and stress the importance of testing the effects of mutations in a native, multiprotein complex context. PilN mutations MR141-142KL and EV157-158AD are located on α4 and α3, respectively, while the PilN ES132-133VA pair, which had no effect on function, is located in an unstructured region at the top of α4 (Figure 2.3B). Loss of function might relate to subtle shifts in the core-core interface, such that it is no longer correctly oriented for optimal pilus assembly. Alternatively, these mutations could affect interactions of the PilNO heterodimer with the lipoprotein, PilP, which has a long unstructured N-terminal region that is unstable in the absence of the PilNO heterodimer (55). PilP was stable in all mutants examined (see supplementary Figure S2.3), but the MR141-142KL and EV157-158AD substitutions may affect its interactions with the PilNO heterodimer, reducing pilus

assembly. PilN MR141-142KL and EV157-158AD double mutants and their single-mutant derivatives assemble pili on the surface only when retraction is blocked (Figure 2.6), implying inefficient pilus extension, or a reduced ability to counteract retraction (49,158). Correct orientation of PilNOP interfaces could be important for optimal PilP and PilQ (49,159) interactions and control of secretin gating (55,65,160).

The PilN LD64-65KK mutation located in the first α-helix (CC-1 region) (Figure 2.3C) disrupted PilNO interactions in the BTH assay and, in *P. aeruginosa*, decreased the amount of surface piliation and twitching motility (Figure 2.4 and 2.5A), without affecting the stability of the alignment subcomplex proteins (see supplementary Figure S2.3A). This defect was less pronounced than those caused by the core mutations. Mutation of both residues in PilN LD64-65KK was necessary to produce the observed phenotype (Figure 2.5B), suggesting that this part of the coiled-coil region is more permissive for substitution; of note, its contribution to function would have been missed had only single-residue substitutions been tested.

From these data, we propose a model in which the TMSs of PilN and PilO initiate their heterodimerization. PilN and PilO contacts are subsequently stabilized through interactions of their oppositely charged coiled-coil regions, as predicted for EpsLM in the *Vibrio* T2S system (51). The PilNO heterodimer then interacts with PilP (55), creating, with PilM bound to PilN's N terminus (51,114), a transenvelope complex upon PilP's interaction with PilQ (54). Without the correct

contacts in these regions, cytoplasmic components such as PilM may be unable to accurately relay conformational changes arising from the activity of IM platform components, including the PilB and PilT ATPases. This model could explain why the PilN chimera was more detrimental to the function of the system than the PilO chimera, as the TMS swap in PilN might alter relay of conformational changes from PilM. In the T2S and the type IVb pilus (T4bP) systems, PilB-like ATPases have been cocrystallized with their PilM homologs, confirming interactions between these components (115,120,161). Alternatively, communication between the PilMNOP subcomplex and PilQ could be altered such that the secretin is not appropriately gated to allow for normal pilus assembly/disassembly dynamics (62,145). Finally, since interaction between components of the alignment subcomplex and pilin subunits has been confirmed in both T2S and T4P systems (54,124,135,162), changes in those interactions may also contribute to loss of function.

Together, our findings suggest that precise PilNO interactions play a critical role in T4P dynamics, supporting the idea that the alignment subcomplex is not simply a static connector of inner and outer membrane components. Depending on their location and nature, small changes can cause a range of effects from subtle (less piliation, reduced motility) to drastic (no piliation or hyperpiliation, loss of motility). The data emphasize the importance of studying protein-protein interactions in their native context and stoichiometry, since chromosomal mutations provided key information on dynamics that could not

have been predicted from BTH assay results. Our discovery that mutating even a single residue at a critical contact point can render the T4P system dysfunctional is encouraging from the perspective of drug development. Small-molecule disruption of protein-protein interactions has been successful in the T3S and T4S systems (139-141,163,164) but can be challenging due to the potentially large interaction interfaces involved. This work shows that, despite their large predicted buried surface areas, there are critical interfaces of PilNO that can be targeted to block piliation and/or motility without completely disrupting their interactions, suggesting that inhibitors could have a high likelihood of success.

Acknowledgements

This work was supported by an Operating Grant MOP-93585 from *the Canadian Institutes of Health Research* to L.L.B and P.L.H. P.L.H. is the recipient of a Tier I Canada Research Chair.

Supplementary

Table S2.1: Bacterial Strains & Vectors

Strain	Description	Source/ Reference
***E. coli* strains**		
DH5α	F-, φ80lacZ, M15, Δ(lacZYA-argF), U169, recA1, endA1, hsdR17(rk-,mk+), phoAsupE44, thi-1, gyrA96, relA1, λ-	Invitrogen
BTH101	F-, cya-99, araD139, galE15, galK16, rpsL1 (StrR), hsdR2, mcrA1, mcrB1, relA1	Euromedex
SM10	thi-1, thr, leu, tonA, lacy, supE, recA, RP4-2-Tcr::Mu, Km^r; mobilizes plasmids into *P. aeruginosa* via conjugation	**(165)**
***P. aeruginosa* strains**		
PAK	Wild-type	J. Boyd
ΔpilM	Deletion of *pilM*	**Ayers et al. (50)**
pilN::FRT	FRT scar at position 124 within *pilN*	**Ayers et al. (50)**
pilO::FRT	FRT scar at position 328 within *pilO*	**Ayers et al. (50)**
pilP::FRT	FRT scar at position 86 within *pilP*	**Ayers et al. (50)**
pilT::FRT	FRT scar at position 540 within *pilT*	**Whitchurch et al. (96)**
pilN::FRT/pilT::FRT	FRT scar at position 124 within *pilN* and FRT scar at position 540 within *pilT*	H. Takhar, et al.**(49)**
pilA::FRT	FRT scar at SphI site within *pilA*	**Kus et al. (166)**
pilN ES132-133VA	*pilN ES132-133VA*	This study
pilN ES132-133VA/pilT::FRT	*pilN ES132-133VA* with FRT scar at position 540 within *pilT*	This study
pilN MR141-142KL	*pilN MR141-142KL*	This study
pilN MR141-142KL /pilT::FRT	*pilN MR141-142KL* with FRT scar at position 540 within *pilT*	This study
pilN M141K	*pilN M141K* single mutation of *pilN MR141-142KL*	This study
pilN R142L	*pilN R142L* single mutation of *pilN MR141-142KL*	This study
pilN EV157-158AD	*pilN EV157-158AD*	This study
pilN EV157-158AD /pilT::FRT	*pilN EV157-158AD* with FRT scar at position 540 within *pilT*	This study
pilN E157A	*pilN E157A* single mutation of *pilN EV157-*	This study

	158AD	
pilN V158D	*pilN V158D* single mutation of *pilN EV157-158AD*	This study
pilN Triple	Triple mutation *pilN ESMREV132-133-141-142-157-158VAKLAD*	This study
pilN L81K	*pilN L81K*	This study
pilN L81A	*pilN L81A*	This study
pilN L82K	*pilN L82K*	This study
pilN LD64-65KK	*pilN LD64-65KK*	This study
pilN L64K	*pilN L64K* single mutation of *pilN LD64-65KK*	This study
pilN D65K	*pilN D65K* single mutation of *pilN LD64-65KK*	This study
pilN chimera	*pilN chimera* – residues 23-45 replaced with *pilO* residues 21-43	This study
pilO M92A	*pilO M92A*	This study
pilO M92K	*pilO M92K*	This study
pilO chimera	*pilO chimera* – residues 21-43 replaced with *pilN* residues 23-45	This study
Vectors	Description	Source/Reference
pEX18Gm	Suicide vector used for gene replacement, Gm^R	**Hoang et al. (147)**
pFLP2	2.6-kb BamHI–SphI fragment from pALB2 ligated into the SmaI site, Ap^R	**Hoang et al. (147)**
pKT25	Kn^R	**Karimova et al. (151)**
pUT18C	Ap^R	**Karimova et al. (151)**
pUT18C::*pilNΔ44*	Ap^R	Howell Lab
pKT25::*pilNΔ44*	Kn^R	Howell Lab
pUT18C::*pilOΔ51*	Ap^R	Howell Lab
pKT25::*pilOΔ51*	Kn^R	Howell Lab
pUT18C::*pilN*	Ap^R	This study
pKT25::*pilN*	Kn^R	This study
pUT18C::*pilO*	Ap^R	This study
pKT25:: *pilO*	Kn^R	This study
pUT18C::*pilN ES132-133VA*	*pilN ES132-133VA*, Ap^R	This study
pUT18C::*pilN MR141-142KL*	*pilN MR141-142KL*, Ap^R	This study
pUT18C::*pilN EV157-158AD*	*pilN EV157-158AD*, Ap^R	This study
pUT18C::*pilN Triple*	*pilN ESMREV132-133-141-142-157-158VAKLAD*, Ap^R	This study

pUT18C::*pilN L81K*	*pilN L81K*, Ap^R	This study
pUT18C::*pilN L81A*	*pilN L81A*, Ap^R	This study
pUT18C::*pilN L82K*	*pilN L82K*, Ap^R	This study
pUT18C::*pilN LD64-65KK*	*pilN LD64-65KK*, Ap^R	This study
pUT18C::*pilN chimera*	*pilN chimera* – residues 23-45 replaced with *pilO* residues 21-43 , Ap^R	This study
pKT25::*pilO M92A*	*pilO M92A*, Kn^R	This study
pKT25::*pilO M92K*	*pilO M92K*, Kn^R	This study
pKT25::*pilO chimera*	*pilO chimera* – residues 21-43 replaced with *pilN* residues 23-45 , Kn^R	This study
pkT25::*pilM*	Kn^R	This study
pEX18Gm::*pilMNO - pilN ES132-133VA*	Suicide vector containing PAK *pilMNO* with *pilN ES132-133VA*, Gm^R	This study
pEX18Gm::*pilMNO - pilN MR141-142KL*	Suicide vector containing PAK *pilMNO* with *pilN MR141-142KL*, Gm^R	This study
pEX18Gm::*pilMNO - pilN M141K*	Suicide vector containing PAK *pilMNO* with *pilN M141K* single mutation of *pilN MR141-142KL*, Gm^R	This study
pEX18Gm::*pilMNO - pilN R142L*	Suicide vector containing PAK *pilMNO* with *pilN R142L* single mutation of *pilN MR141-142KL*, Gm^R	This study
pEX18Gm::*pilMNO - pilN EV157-158AD*	Suicide vector containing PAK *pilMNO* with *pilN EV157-158AD*, Gm^R	This study
pEX18Gm::*pilMNO - pilN E157A*	Suicide vector containing PAK *pilMNO* with *pilN E157A* single mutation of *pilN EV157-158AD*, Gm^R	This study
pEX18Gm::*pilMNO - pilN V158D*	Suicide vector containing PAK *pilMNO* with *pilN V158D* single mutation of *pilN EV157-158AD*, Gm^R	This study
pEX18Gm::*pilMNO - pilN Triple*	Suicide vector containing PAK *pilMNO* with *pilN ESMREV132-133-141-142-157-158VAKLAD*, Gm^R	This study
pEX18Gm::*pilMNO - pilN L81K*	Suicide vector containing PAK *pilMNO* with *pilN L81K*, Gm^R	This study
pEX18Gm::*pilMNO - pilN L81A*	Suicide vector containing PAK *pilMNO* with *pilN L81A*, Gm^R	This study
pEX18Gm::*pilMNO - pilN L82K*	Suicide vector containing PAK *pilMNO* with *pilN L82K*, Gm^R	This study
pEX18Gm::*pilMNO - pilN LD64-65KK*	Suicide vector containing PAK *pilMNO* with *pilN LD64-65KK*, Gm^R	This study
pEX18Gm::*pilMNO – pilN L64K*	Suicide vector containing PAK *pilMNO* with *pilN L64K* single mutation of *pilN LD64-65KK*, Gm^R	This study
pEX18Gm::*pilMNO – pilN D65K*	Suicide vector containing PAK *pilMNO* with *pilN D65K* single mutation of *pilN*	This study

	LD64-65KK, Gm^R	
pEX18Gm::*pilMNO – pilN chimera*	Suicide vector containing PAK *pilMNO* with *pilN* chimera - residues 23-45 replaced with *pilO* residues 21-43, Gm^R	This study
pEX18Gm::*pilNOP - pilO M92A*	Suicide vector containing PAK *pilNOP* with *pilO M92A*, Gm^R	This study
pEX18Gm::*pilNOP - pilO M92K*	Suicide vector containing PAK *pilNOP* with *pilO M92K*, Gm^R	This study
pEX18Gm::*pilNOP - pilO chimera*	Suicide vector containing PAK *pilNOP* with *pilO* chimera - residues 21-43 replaced with *pilN* residues 23-45, Gm^R	This study
pEX18Ap::*pilT::Gm::FRT*	Suicide vector containing *pilT* disrupted with FRT-flanked gentamicin cassette at position 540, Ap^R and Gm^R	(148)

Table S2.2: Oligonucleotide Primer Sequences

Name	Oligonucleotide Sequence (5' – 3')
PilOΔ51F	TATATAACTCTAGAGATGAGTGACATGCAGGCTCAGCT CGAAC
PilOΔ51R	TATATATAGAATTCTTCATTTCTTCAGCCCCTTGTCGTTG TAGC
PilNΔ44F	TATATAACTCTAGAGATGGCGGCCATCGAGAAC
PilNΔ44R	TATATATAGAATTCTTCATTTCTTGGCTCCTTGCGC
Bth PilOF	TATATAACTCTAGAGATGAGTCTGGCCAGTTCCCTGGA AAGTC
Bth PilOR	TATATATAGAATTCTTCATTTCTTCAGCCCCTTGTCGTTG TAGC
Bth PilNF	TATATAACTCTAGAGATGGCACGGATCAACCTTCTACCC TGG
Bth PilNR	TATATATGGAATTCGTCATTTCTTGGCTCCTTGCGCAAC CCC
Bth PilMF	TAT ATA TAT CTA GAG GTG CTA GGG CTC ATA AAG AAG AAA G
Bth PilMR	TAT TAT AAG AAT TCG TCA GTC GAA ACT CCT CAA CGC C
PilN ES132-133VA F	CCGGCGCGGCCGTGGCCAACAACCGCGTTTCC
PilN ES132-133VA R	GGAAACGCGGTTGTTGGCCACGGCCGCGCCGG
PilN MR141-142KL F	CCGCGTTTCCAATCTCAAGCTCAACATGGACGCGTCCG AGTGGC
PilN MR141-142KL R	GCCACTCGGACGCGTCCATGTTGAGCTTGAGATTGGAA ACGCGG
PilN M141K F	CGCGTTTCCAATCTCAAGCGCAACATGGACGCG
PilN M141K R	CGCGTCCATGTTGCGCTTGAGATTGGAAACGCG
PilN R142L F	CGGTTTCCAATCTCATGCTCAACATGGACGCGGTCCG

PilN R142L R	CGGACCGCGTCCATGTTGAGCATGAGATTGGAAACCG
PilN EV157-158AD F	CCGCCCCGACCCTGAACGCGGACAAGGCGGTGACCC
PilN EV157-158AD R	GGGTCACCGCCTTGTCCGCGTTCAGGGTCGGGGCGG
PilN E157A F	CGACCCTGAACGCGGTCAAGGCGGTG
PilN E157A R	CACCGCCTTGACCGCGTTCAGGGTCG
PilN V158D F	CGACCCTGAACGAGGATAAGGCGGTGACCCA
PilN V158D R	TGGGTCACCGCCTTATCCTCGTTCAGGGTCG
PilN L81K F	GCGAACTGAAGTCGCGGCGCCAGCAAAAGCTCGAGCG GATGAAGAT
PilN L81K R	GATCTTCATCCGCTCGAGCTTTTGCTGGCGCCGCGACT TCAGTTCGC
PilN L81A F	CGCCAGCAATTGGCCGAGCGGATGAAG
PilN L81A R	CTTCATCCGCTCGGCCAATTGCTGGCG
PilN L82K F	GCGAACTGAAGTCGCGGCGCCAGCAATTGAAGGAGCG GATGAAGAT
PilN L82K R	GATCTTCATCCGCTCCTTCAATTGCTGGCGCCGCGACT TCAGTTCGC
PilN LD64-65KK F	GCGCAAGGAAATCGTCGTAAAGAAGGCCCGGATCAAG GAAATCAGC
PilN LD64-65KK R	CGCTGATTTCCTTGATCCGGGCCTTCTTTACGACGATTT CCTTGCGC
PilN L64K F	CGCAAGGAAATCGTCGTAAAAGACGCCCGGATCAAG
PilN L64K R	CTTGATCCGGGCGTCTTTTACGACGATTTCCTTGCG
PilN D65K F	AAGGAAATCGTCGTACTCAAAGCCCGGATCAAGGAA
PilN D65K R	TTCCTTGATCCGGGCTTTGAGTACGACGATTTCCTT
PilO M92A F	GCCTACAAGGCACAGATGAAGGAGGCGGAAGAGTCCT TTGGCGCC
PilO M92A R	GGCGCCAAAGGACTCTTCCGCCTCCTTCATCTGTGCCT TGTAGGC
PilO M92K F	GCCTACAAGGCACAGATGAAGGAGAAGGAAGAGTCCT TTGGCGCC
PilO M92K R	GGCGCCAAAGGACTCTTCCTTCTCCTTCATCTGTGCCT TGTAGGC
PilM F	TATATATATGTGCTAGGGCTCATAAAGAAG
PilP R	TATATATGGAATTCGTCAGGAGCGTTCCTTGAGAGTCA G

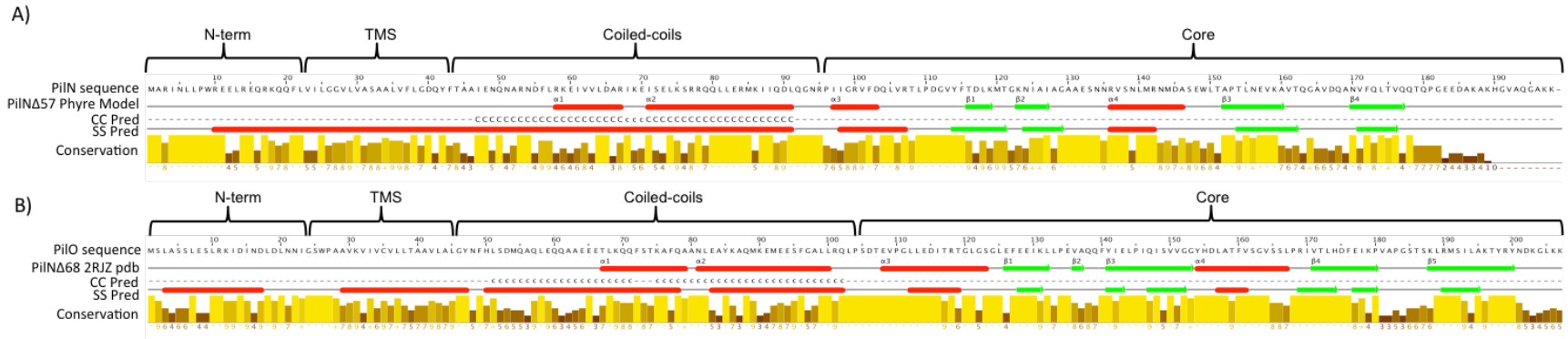

Figure S2.1. Amino acid sequences and secondary structures of PilN and PilO. The sequence alignments for **(A)** PilN and **(B)** PilO are shown. The predicted cytoplasmic N-terminal regions (N-term), the transmembrane segments (TMS), the coiled-coils (CC) and the core regions used in this study are indicated above with open brackets. The sequence conservation of the PilN and PilO families from a subset of Pseudomonads (*P. aeruginosa* PAK, *P. fulva* 12-X, *P. stutzeri* A1501*, P. syringae* pv. phaseolicola 1448A*,* & *P. protegens* CHA0) are indicated by the bars. High conservation of the residues are indicated by a high bar and a bright yellow color, whereas low conservation is displayed as a low bar and a dark brown color. The α-helices (red rectangles) and β-strands (green arrows) present in the PilOΔ68 structure (PDB 2RJZ (51)), the $PilN_{\Delta 57}$ Phyre[2] homology model, and in the secondary-structure predictions (SS pred) are shown. The predicted CC regions (CC pred) are indicated with the letter “c”, with the size indicating the confidence of these predictions with “C” and “c” representing stronger and weaker predictions, respectively. The sequences were gathered from the Pseudomonas Genome Database (167) and this figure was prepared using Jalview 2.8.2 (168,169).

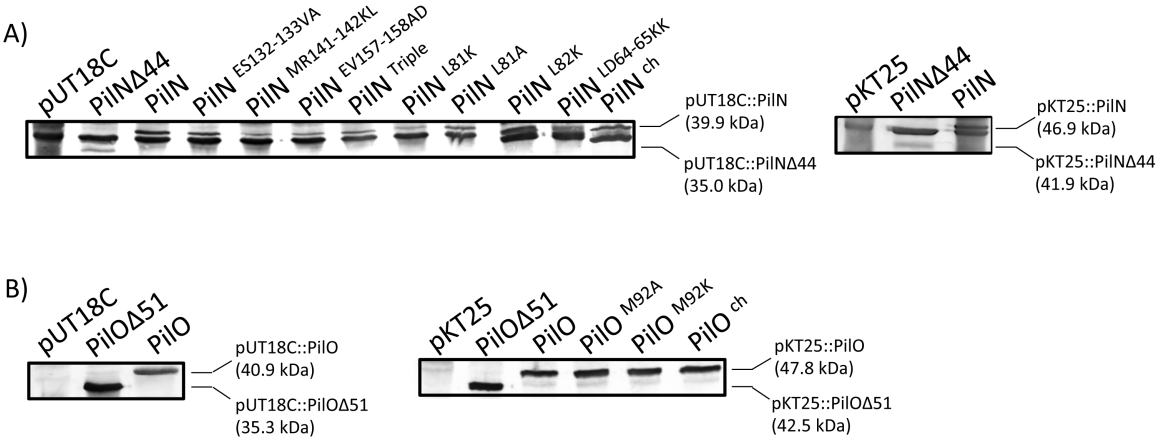

Figure S2.2. All BTH fusion constructs are stable. Fusion constructs were tested for expression and stability via Western blotting using protein specific antisera for **(A)** PilN mutants and the PilN chimera (PilN ch), or **(B)** PilO mutants and the PilO chimera (PilO ch) in each vector.

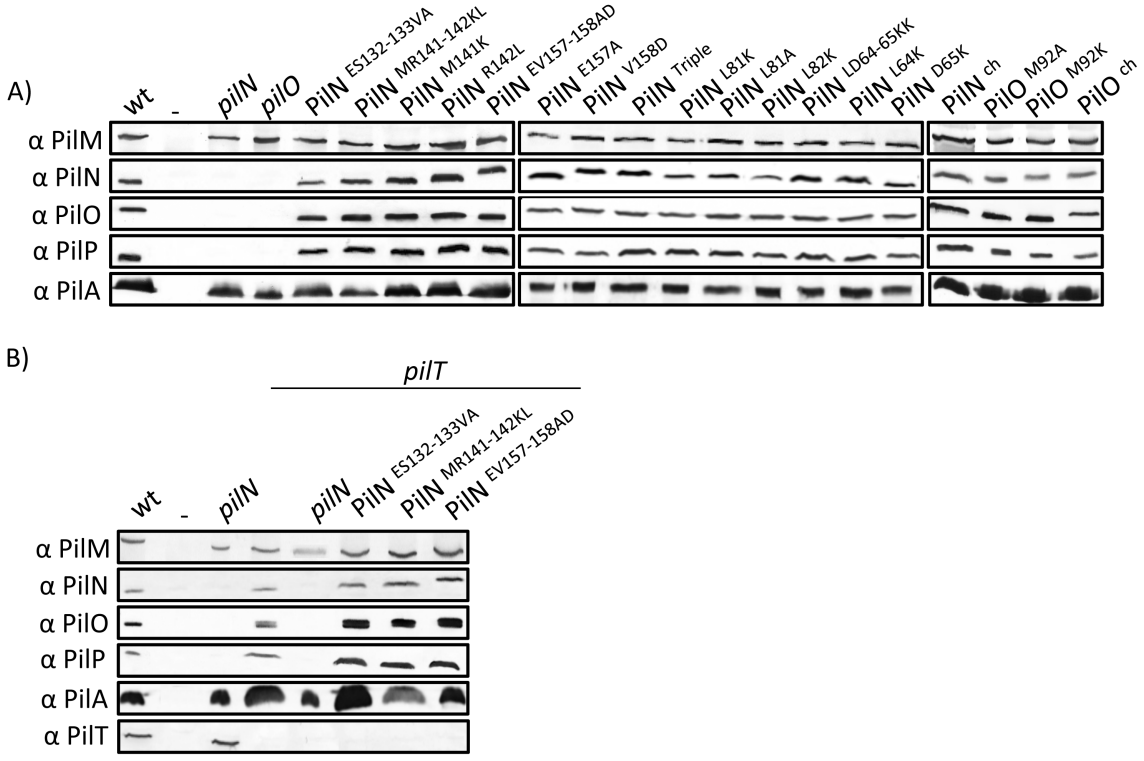

Figure S2.3. Intracellular levels of alignment subcomplex proteins and PilA are unaffected by PilN and PilO chromosomal mutations. (A) All PilN and PilO mutations were introduced into the chromosome of *P. aeruginosa* and PilMNOPA proteins were tested for stability via Western blotting using protein specific antisera as designated on left. **(B)** PilN mutants ES132-133VA, MR141-142KL, and EV157-158AD were created in a retraction deficient background (*pilT*) and tested for stability via Western blotting using protein specific antisera for PilMNOPAT as designated on left.

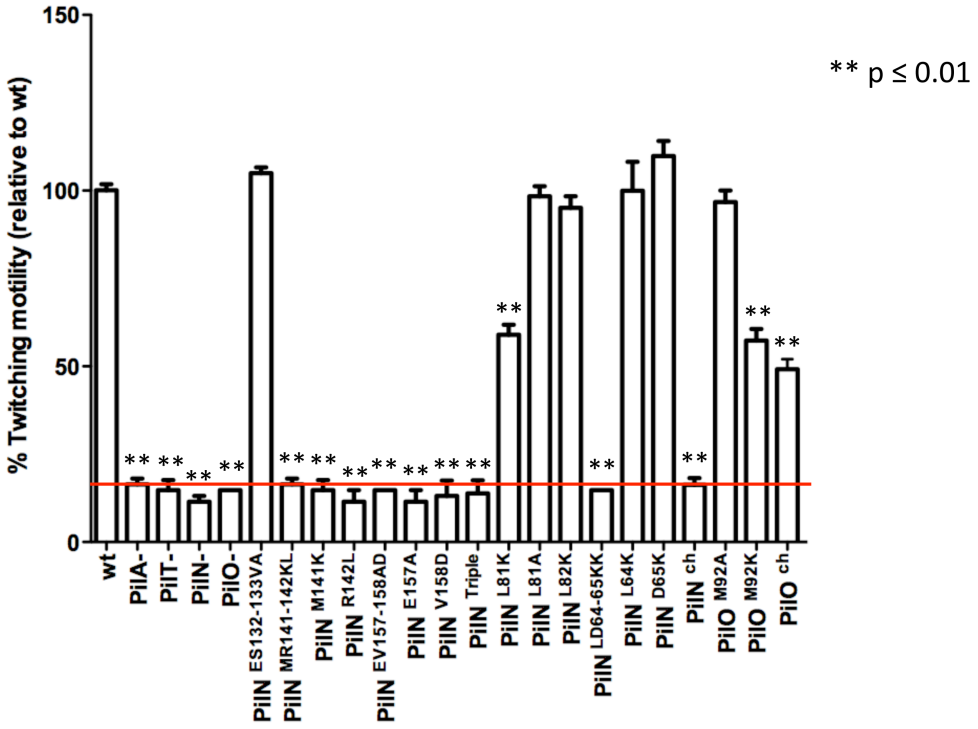

Figure S2.4. Twitching motility of PilN and PilO mutants compared to wild-type. Single colonies of each mutant were stab inoculated on a 1% LB agar plate and incubated for 36 h at 37 °C. The agar was removed and the plates were stained with a 1% crystal violet solution to visualize. Twitching motility zones were repeated in triplicate and measured using ImageJ software, and reported as the percent relative to wild-type (wt). Experiments were preformed in triplicate (N=3). Bars represent the means ± standard error. ** p ≤ 0.01.

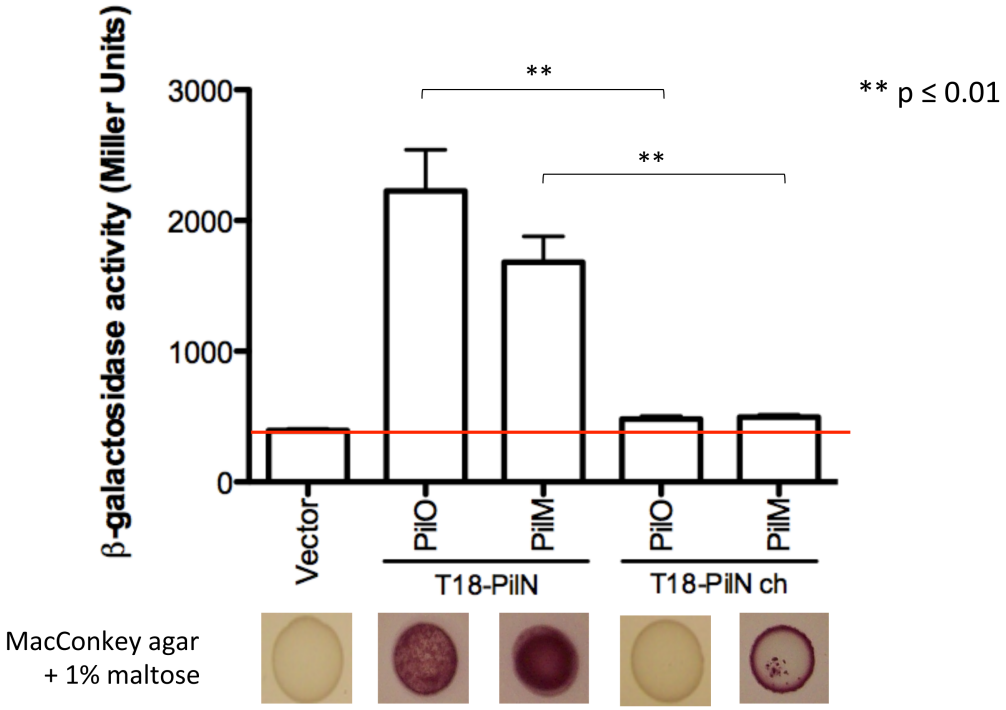

Figure S2.5. Interaction between PilM and PilN in the BTH system is altered when the TMS of PilN is replaced with that of PilO. Full-length PilN and PilN chimera (PilN ch) fused at the N termini to the T18 fragment, were tested for interaction with full-length PilM and PilO fused at the N termini to the T25 fragment of adenylate cyclase from *Bordetella pertussis* using the BTH assay. Experiments performed in triplicate (N=3). Bars represent the means ± standard error. ** p ≤ 0.01.

CHAPTER THREE

In vivo capture of type IV pilus system PilN and PilO homo- and heterodimers by Cys crosslinking

Preface

Chapter three consists of the following publication:

Leighton TL, Yong DH, Howell PL, and Burrows LL. 2016. *In vivo* capture of the type IV pilus system PilN and PilO homo- and heterodimers by Cys crosslinking. Journal of Biological Chemistry – DOI: 10.1074/jbc.M116.738377.

Attributions: DHY was an undergraduate thesis student mentored by TLL. TLL, DHY, LLB, and PLH designed the study and developed the methodology. TLL and DHY created all Cys mutant strain variants. Experiments were performed by TLL. TLL, LLB and PLH wrote and edited the manuscript.

Title page and author list

In vivo capture of type IV pilus system PilN and PilO homo- and heterodimers by Cys crosslinking

Leighton TL[1], Yong DH[1], Howell PL[2,3] and Burrows LL[1]*

[1] From the Department of Biochemistry and Biomedical Sciences and the Michael G. DeGroote Institute for Infectious Disease Research, McMaster University, ON, CAN.

[2] Program in Molecular Structure & Function, The Hospital for Sick Children and

[3] From the department of Biochemistry, University of Toronto, ON, CAN.

*To whom correspondence should be addressed:

Dr. Lori L. Burrows, 4H18 Health Sciences Centre, 1200 Main St. West, Hamilton, ON, L8N 3Z5 CANADA, Tel: (905)-525-9140 ext: 22029, Fax: (905) 522-9033, E-mail: burrowl@mcmaster.ca

Dr. P. Lynne Howell, 20-9-715 Peter Gilgan Centre for Research and Learning, 686 Bay St., Toronto, ON M5G 0A4 CANADA, Tel: (416) 813-5378, Fax: (416) 813-5022, E-mail: howell@sickkids.ca

Running Title: *In vivo* PilN and PilO dimerization

Abstract

Pseudomonas aeruginosa is a leading cause of hospital-acquired infections and resistant to many antibiotics. Type IV Pili (T4P) are among the key virulence factors used by *P. aeruginosa* for host cell attachment, biofilm formation, and twitching motility, making this system a promising target for novel therapeutics. Point mutations in the conserved PilMNOP alignment subcomplex were previously shown to have distinct effects on assembly and disassembly of T4P, suggesting that it may function in a dynamic manner. We introduced mutations encoding Cys substitutions into *pilN* and/or *pilO* on the chromosome to maintain normal stoichiometry and expression levels and captured covalent PilNO heterodimers as well as PilN and PilO homodimers *in vivo*. Most covalent PilN or PilO homodimers had minimal functional impact in *P. aeruginosa*, suggesting that homodimers are a physiologically relevant state. However, certain covalent homo- or heterodimers eliminated twitching motility, suggesting that specific PilNO configurations are essential for T4P function. These data were verified using soluble, N-terminal truncated fragments of PilN and PilO Cys mutants, which purified as a mixture of homo- and heterodimers at volumes consistent with a tetramer. Deletion of the genes encoding alignment subcomplex components, PilM or PilP – but not other T4P components, including motor ATPases PilB or PilT – blocked *in vivo* formation of disulfide-bonded PilNO heterodimers, suggesting that both PilM and PilP influence formation of the

heterodimer interface. Combined, our data suggest that T4P function depends on dynamic rearrangements at PilN and PilO interfaces.

Introduction

Many bacteria, including *Pseudomonas aeruginosa,* use type IV pili (T4P) for surface attachment/adhesion, biofilm formation and twitching motility (2-5,14,41). T4P are divided into T4aP and T4bP subgroups, based on differences in pilin size and organization of the assembly machinery (2,75). Here we focus on T4aP, henceforth referred to as T4P. T4P are long, thin, fibrous appendages, which extend from the bacteria, attach to a surface, and are retracted back into the cell, winching the cell forward. This flagellum-independent form of locomotion is called twitching motility. Four subcomplexes make up a T4P machine in *P. aeruginosa*; the outer membrane (OM) secretin (PilQ) and its pilotin (PilF) (42-46); the inner membrane (IM) platform protein (PilC) and cytoplasmic motor proteins (ATPases PilBTU) (48,49); the helical pilus fibre, composed mainly of the major pilin subunit (PilA) plus minor pilins (PilVWXE and FimU) and adhesin PilY1 (5,56,58); and the alignment subcomplex proteins (PilMNOP) which span from the cytoplasm to the OM secretin (50,51,54,55). PilN and PilO are bitopic IM proteins with similar predicted secondary structures. These proteins are essential for T4P function, and connect the cytoplasmic alignment subcomplex component, PilM, with the IM-associated lipoprotein PilP that interacts with the N0 domain of the secretin monomer, PilQ (54,65). Proposed functions of the PilMNOP

subcomplex include aligning the IM motor with the OM secretin, concentrating pilin subunits at the site of extension and retraction, and possibly transducing signals via conformational changes from the cytoplasmic ATPases to generate ‘open’ or ’closed’ states of the gated secretin (54,55).

The T4P and type II secretion (T2S) systems have analogous components and similar architecture (23,153). Whereas the T4P system extends and retracts an elongated pilus, the T2S system specializes in secreting protein substrates from the periplasm into the environment, via a short piston-like ‘pseudopilus’ (23,170,171). While the systems have different outputs, their underlying functional mechanism – which remains to be uncovered – are thought to be comparable. Orthologous components of the alignment subcomplexes in the two systems (PilMN/GspL, PilO/GspM, and PilP/GspC) have limited sequence identity, but atomic resolution structures revealed a high degree of structural similarity, and all three components form equimolar complexes with a ratio of 1:1:1 (51,55,113,114,116,124,126). PilN- and PilO-like proteins in the T2S system (GspL and GspM, respectively) form both homo- and heterodimers, though it is not yet clear if this is consistent in the T4P system (101,113,116,118,122,172). Previous work in *P. aeruginosa* showed that PilP fails to interact with a PilO homodimer and requires both PilN and PilO for stability (50,55). Although PilO crystallized as a homodimer (51), complementation of a *pilO* mutant with a plasmid-borne copy of the gene led to formation of predominantly PilO homodimers at the cost of PilN stability, and thus

T4P function (50). In *Thermus thermophilus,* purified T4P alignment subcomplex components were estimated by transmission cryoelectron microscopy imaging to be in a ratio of 2:2:2 for PilM:PilN:PilO, where initial PilN homodimers in complex with PilM were disrupted by the addition of PilO, ultimately forming PilNO heterodimers (124). These observations, coupled with data from the *P. aeruginosa* system, suggested that the PilNO heterodimer was the relevant functional state *in vivo,* while PilN and PilO homodimers might represent early intermediates during formation of the assembly system, or in complementation experiments, artifacts of overexpression (55).

Cysteine disulfide-bonding analysis is useful for clarifying protein tertiary and quaternary structure, and for investigating dynamic interactions among components of cellular machineries (173,174). The ability of two Cys residues to form a disulfide bond depends on proximity of their side chains, with bond formation occurring in an oxidizing environment at a Cβ-Cβ distance of 4-8 Å (175). Disulfide bonding imposes structural constraints, and analysis of its effects on function can reveal the importance of conformational changes. Using Cys substitution mutants, *in vivo* formation of both homo- and heterodimers of GspL and GspM was observed in the T2S system of *Dickeya dadantii* (122). The authors suggested that alternate interactions between homo- and heterodimers of GspL and GspM – i.e. GspLL and GspMM versus 2x GspLM –occurred *in vivo*. Formation of disulfide bonds between residues that were predicted to be outwardly facing suggested that these interactions might be controlled through

rotation of the proteins, including their transmembrane segments (TMSs) (122). This mechanism was proposed to propagate movement from the cytoplasmic to periplasmic regions of the T2S system machinery, when the ATPase GspE, equivalent to T4P extension ATPase PilB, interacted with the cytoplasmic domain of GspL, equivalent to PilM (122). The interaction itself, or the hydrolysis of ATP and resulting conformational changes in GspE, could induce a corresponding change in GspL, transduced to GspM through their interaction. Previous work in the T2S system and more recently, the T4P system, provided evidence for interactions between the equivalents of PilM and the cytoplasmic ATPase, PilB, either directly or in conjunction with the platform protein, PilC (111,119,176,177). These interactions might similarly transduce conformational changes that contribute to pilus assembly or disassembly.

We hypothesized that dynamic movement of the T4P alignment subcomplex proteins PilN and PilO may occur during (or because of) extension and retraction of pili, and that PilO's ability to interact with both itself and PilN may reflect a functionally relevant switch between homo- and heterodimers. We introduced Cys substitutions at predicted interfaces between PilNO and PilOO, and used non-reducing SDS-PAGE to observe dimer formation. Covalent PilN and PilO homodimers, as well as PilNO heterodimers, were captured *in vivo* under physiological conditions. Depending on the location, disulfide bonding disrupted the normal function of the T4P system, inhibiting motility. Deletion of the motor ATPases had no effect on the dimerization state of PilN and PilO –

arguing against a link between motor function and conformational switching – but loss of either PilM or PilP specifically blocked PilNO heterodimer formation. These data provide new insights into dynamics of the T4P system.

Results

Selection of residues for Cys substitution

Our PilO homodimer structure (PDB 2RJZ)(51) was used to identify candidate residues predicted to be within appropriate distances for disulfide-bond formation (Figure 3.1A - top). In the PilO model, two relevant interfaces were identified: the core, comprising mainly contacts between the α4-helix and β4-strand; and the coiled-coils, between the α1- and α2-helices (51). In the $PilO_{\Delta 68}$ model, the coiled-coils are truncated and folded back, since they are not anchored in the IM. Due to the potentially artificial nature of that particular interaction interface, we focused on residues in the core region previously shown to be important for function (178). Residues in the α4-helix and β4-strand of the PilO homodimer model with an estimated distance between β-carbons of less than 8 Å were selected for mutagenesis (175,179,180) (Figure 3.1A – bottom).

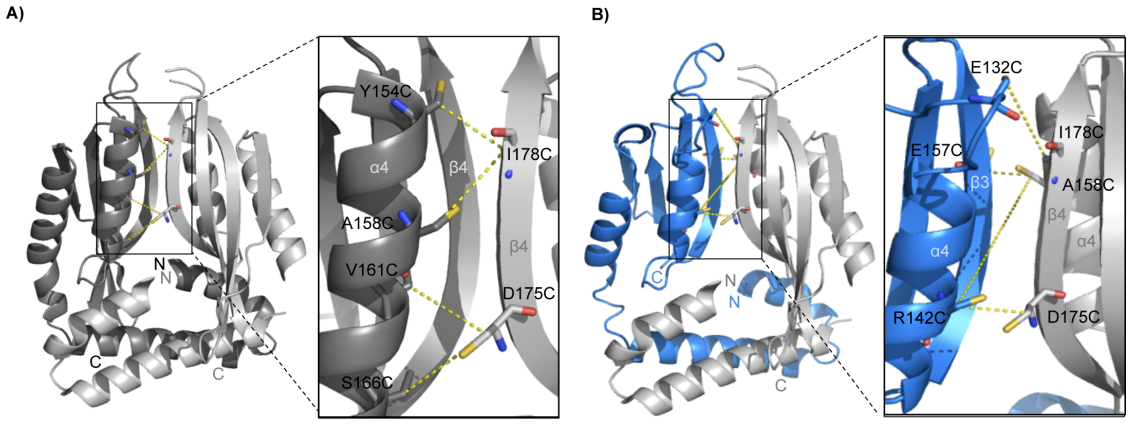

PilO (α4 helix)	PilO (β4 strand)	Distance (Å)
S166C	D175C	4.9
V161C	D175C	6.3
A158C	I178C	6.6
Y154C	I178C	7.2

PilN (blue)	PilO (grey)	Distance (Å)
R142C	D175C	5.1
E157C	A158C	3.8
E132C	I178C	7.7
R142C	A158C	18.7

Figure 3.1. Locations of residues chosen for Cys substitution mutagenesis in PilN and PilO. A cartoon diagram representation mapping the N and C termini, secondary structure elements and structural domains of **(A)** a $PilO_{\Delta 68}$ dimer (PDB 2RJZ (51)), or **(B)** a $PilN_{\Delta 57}$ (blue) and $PilO_{\Delta 68}$ (grey) heterodimer using a Phyre[2] model (125) of PilN generated using the $PilO_{\Delta 68}$ homodimer as template. The core-core domains consist of PilN α-helices 3-4 and β-strands 1-4, and PilO α-helices 3-4 and β-strands 1-5. Inset shows zoomed view of interaction interface with residue substitutions labeled accordingly. Bottom - Tables indicate the distance between the Cβ of the substituted Cys residues (in angstroms) and cartoon depiction of residue locations.

All attempts to purify soluble *P. aeruginosa* PilN for structural studies, or to solve an X-ray crystal structure of the PilNO heterodimer, have so far been unsuccessful. The structure of a periplasmic portion of PilN from *T. thermophilus* is available (124); however, due to the low primary sequence identity with PilN

from *P. aeruginosa*, as well as a different arrangement of secondary structure elements (*Thermus* PilN has an extra α-helix inserted in the first αββ motif), we were unable to generate a high confidence model using that structural template. *P. aeruginosa* PilN is predicted to have a structural organization similar to PilO, thus we used the truncated *P. aeruginosa* PilO homodimer structure (51) to generate a high confidence Phyre^2 (125) model of a PilN$_{\Delta 57}$ monomer, and used the PilO homodimer interface to model a PilNO heterodimer using the same core-core interface (178) (Figure 3.1B - top). This model was used to design a series of single Cys substitutions in the α4-helix and β4-strand of either PilN or PilO (Figure 3.1B - bottom). The PilNO model has been partially validated in previous work (178), but for this study, we included a negative control Cys pair (PilN^{R142C}/PilO^{A158C}) at a Cβ distance of over 12 Å, considered too far for disulfide-bond formation (175,180).

To avoid issues arising from to non-stoichiometric expression, the mutations encoding the Cys substitutions of interest were introduced at the native *pilMNOPQ* locus of *P. aeruginosa* PAK by homologous recombination. Screening of the sequence-verified mutants for effects on expression and stability of each of the inner membrane alignment subcomplex proteins revealed no effects of the Cys substitutions on PilMNOP levels relative to wild-type (Figure 3.2A).

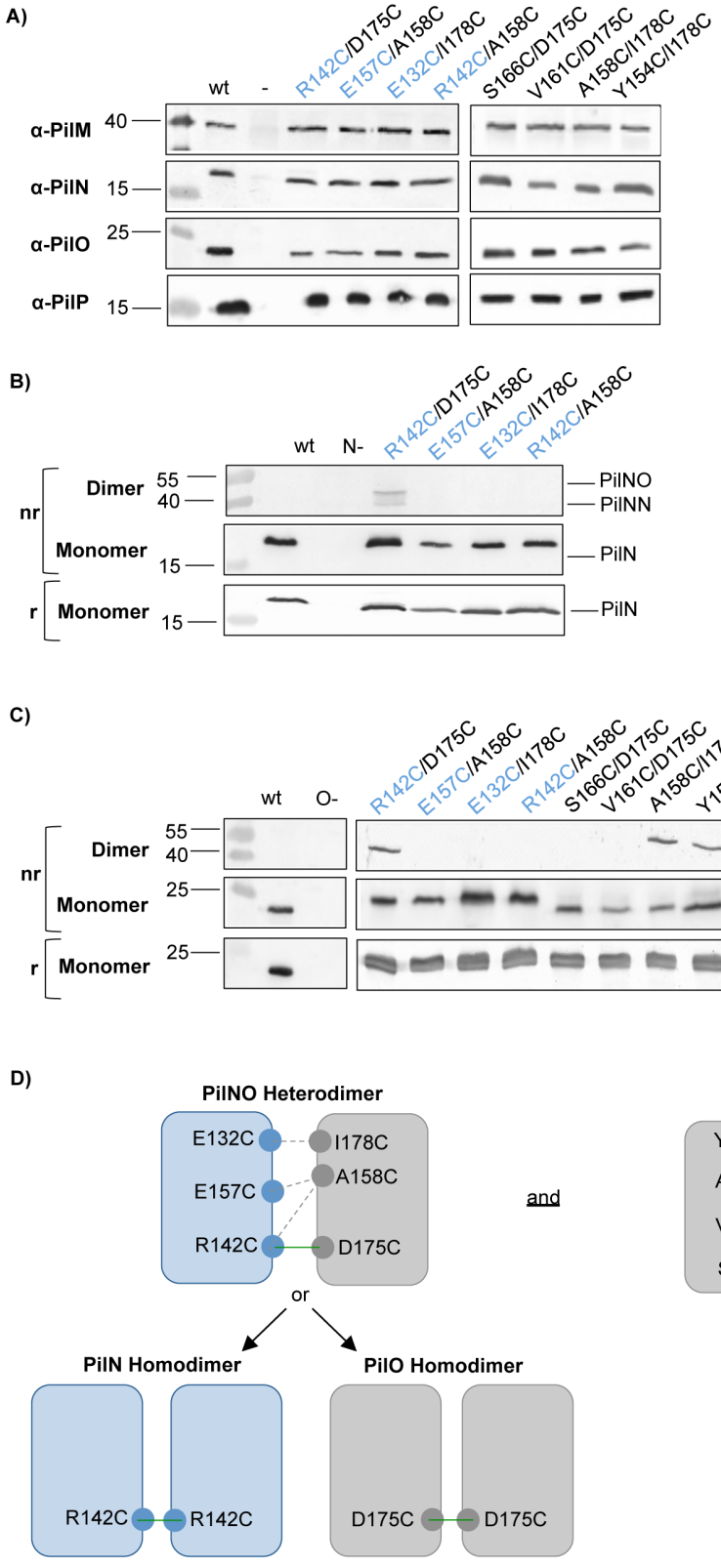
A)
wt
-
R142C/D175C
E157C/A158C
E132C/I178C
R142C/A158C
S166C/D175C
V161C/D175C
A158C/I178C
Y154C/I178C
α-PilM 40
α-PilN 15
α-PilO 25
α-PilP 15
B)
wt
N-
R142C/D175C
E157C/A158C
E132C/I178C
R142C/A158C
nr
Dimer 55 40
PilNO
PilNN
Monomer 15
PilN
r
Monomer 15
PilN
C)
wt
O-
R142C/D175C
E157C/A158C
E132C/I178C
R142C/A158C
S166C/D175C
V161C/D175C
A158C/I178C
Y154C/I178C
nr
Dimer 55 40
PilOO
Monomer 25
PilO
r
Monomer 25
PilO
D)
PilNO Heterodimer
E132C
E157C
R142C
I178C
A158C
D175C
and
PilO Homodimer
Y154C
A158C
V161C
S166C
I178C
D175C
or
PilN Homodimer
R142C
R142C
PilO Homodimer
D175C
D175C

Figure 3.2. Formation of disulfide-bonded homo- and heterodimers *in vivo.* Lysates for the wild-type (wt), negative controls (-) and the Cys mutants were subject to SDS-PAGE under non-reducing (nr) and reducing (r) conditions, then blotted with specific antibodies to **(A)** each alignment subcomplex component (α-PilM, α-PilN, α-PilO, α-PilP) to confirm stability of each protein in the Cys mutants, **(B)** PilN, and **(C)** PilO. PilN^{R142C}/PilO^{D175C} was able to form PilNO heterodimers (44.7 kDa) and PilN homodimers (43.8 kDa), whereas PilO$^{A158C/I178C}$ and PilO$^{Y154C/I178C}$ mutants were able to form disulfide bonds and form PilO homodimers (45.6 kDa) *in vivo*. **(D)** Cartoon schematic of the residues that were able to form disulfide bonds (green lines) in the crosslinking experiments, and their relative locations. Dashed lines indicate no dimer formation observed. The PilN^{R142C}/PilO^{D175C} Cys mutants formed PilNO heterodimers but also PilN^{R142C} and PilO^{D175C} homodimers. PilN residues indicated in blue text.

Formation of Cys cross-linked PilNO and PilOO dimers in vivo

Whole cell lysates of all mutants were analyzed in parallel in reducing and non-reducing conditions, followed by immunoblotting with anti-PilN or PilO antibodies. Of the PilNO Cys substitutions, only the PilN^{R142C}/PilO^{D175C} variant formed significant levels of cross-linked dimers *in vivo* (Figure 3.2B & C). Two bands appeared on the anti-PilN blot (Figure 3.2B) at the sizes consistent with *in vivo* formation of a PilNO heterodimer (44.7 kDa) and, unexpectedly, a PilN homodimer (43.8 kDa). Of the PilO double Cys mutants, both PilO$^{A158C/I178C}$ and PilO$^{Y154C/I178C}$ variants formed cross-linked dimers *in vivo* (Figure 3.2C) at a size consistent with that of PilO homodimers (45.6 kDa). These results further support the PilNO model, since at least one of each set of selected residue pairs formed

the predicted linkage (Figure 3.2D). This is the first evidence in any T4P system for PilN homodimerization under physiological conditions.

To further investigate PilN homodimerization, we leveraged a previously described $PilN_{\Delta44}/PilO_{\Delta51\_His}$ co-expression construct (55) that encodes truncated forms of both proteins. These proteins lack their short cytoplasmic N-termini and transmembrane segments, and encompass a larger portion of the periplasmic domains than the construct used for the afore-mentioned $PilO_{\Delta68}$ homodimer structure. A single PilN Cys mutant ($PilN_{\Delta44}^{R142C}/PilO_{\Delta51}$), a single PilO Cys mutant ($PilN_{\Delta44}/PilO_{\Delta51}^{D175C}$), or a double PilNO Cys pair ($PilN_{\Delta44}^{R142C}/PilO_{\Delta51}^{D175C}$) were expressed in *E. coli* Origami 2 DE3, which has a non-reducing cytoplasm to allow for the formation of disulfide bonds, and purified using Nickel-NTA affinity chromatography. Purified proteins were separated under reducing or non-reducing conditions, and probed with anti-PilN and PilO antibodies. The $PilN_{\Delta44}^{R142C}/PilO_{\Delta51}$ pair yielded disulfide-bonded PilN homodimers (~34.0 kDa) (Figure 3.3A). Interestingly, the same pair also formed apparent PilNO heterodimers, as PilN monomers were still visible in the non-reducing lane. Since PilN is unstable/insoluble in the absence of PilO (55), this result suggests that a proportion of PilN monomers did not participate in covalent self-interactions, but rather in non-covalent interactions with PilO. For $PilN_{\Delta44}/PilO_{\Delta51}^{D175C}$, PilO homodimers (~36.4 kDa) were clearly visible in the anti-PilO blot, showing that PilO occupies both homo- and heterodimer states (Figure 3.3B). When both PilN and PilO contained Cys substitutions

($PilN_{\Delta44}^{R142C}$/$PilO_{\Delta51}^{D175C}$), three subpopulations were identified: PilN homodimers, PilO homodimers, and PilNO heterodimers (~35.2 kDa; Figure 3.3A & B). In this case, nearly all PilN monomers were involved in covalent interactions in non-reducing conditions (Figure 3.3A & B) when compared to PilO. This suggests that PilO homodimers might occupy multiple orientations, some disulfide bonded and others not, implying in the latter case that the $PilO^{D175C}$ mutation was too far – or incorrectly oriented – for disulfide bond formation. These data confirm the observation that PilN and PilO form homodimers and heterodimers under physiological conditions in *P. aeruginosa*.

Since untagged covalent $PilN^{R142C}$ homodimers purified with C-terminally His tagged PilO, we realized that PilN homodimers must interact with PilO homodimers via an interface other than the one shown in Figure 3.1B; the most likely candidates for a second interface were the coiled coils below the core domains. Using size exclusion chromatography, we confirmed that $PilN_{\Delta44}^{R142C}$/$PilO_{\Delta51\_His}$ (as well as unmodified $PilN_{\Delta44}$/$PilO_{\Delta51\_His}$ and other Cys mutants) eluted from an S75 size exclusion column at a volume similar to the conalbumin standard (~75 kDa) (Figure 3.3C), consistent with a PilNO tetramer (70.4 kDa). Thus, PilNO can simultaneously form homo- and heterodimers via two distinct interfaces.

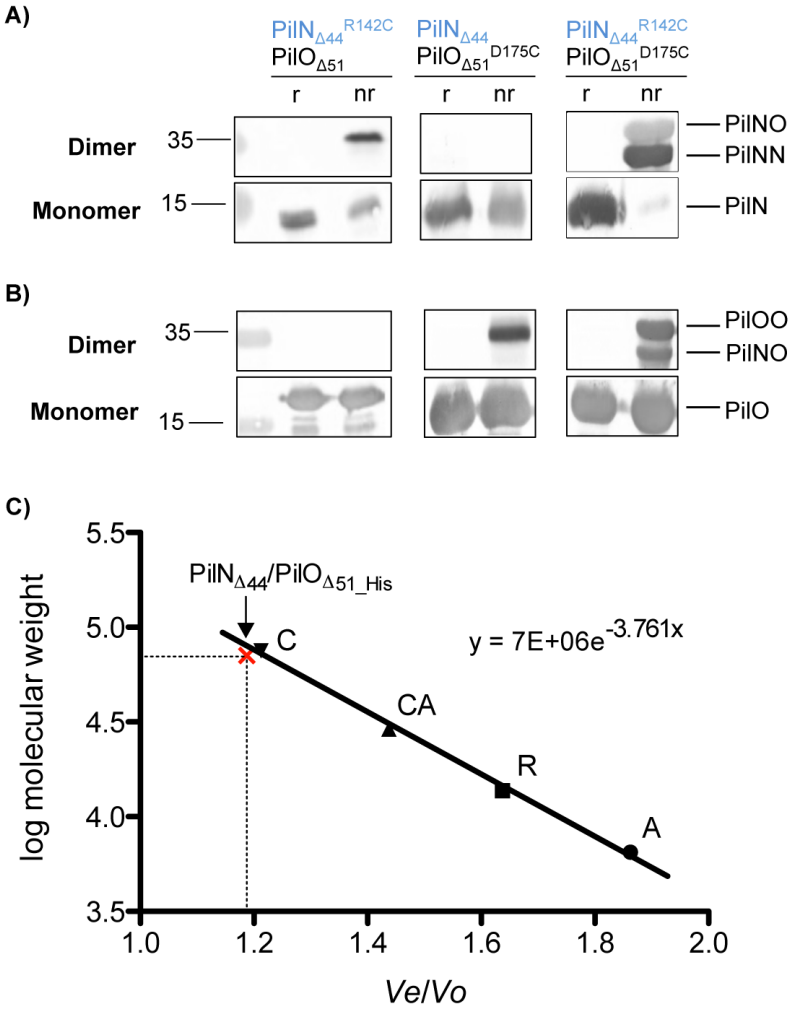

Figure 3.3. Confirmation of homo- and heterodimer formation of PilN and PilO using Cys crosslinking analysis *in vitro*. PilN$_{\Delta44}$ and PilO$_{\Delta51}$ were co-expressed with ether PilN^{R142C}, PilO^{D175C}, or both the PilN^{R142C}/PilO^{D175C} Cys mutations. After nickel affinity purification the proteins were subject to SDS-PAGE under either non-reducing (nr) or reducing (r) conditions and blotted with anti-sera specific for **(A)** PilN, or **(B)** PilO. We observed three disulfide-bonded subpopulations, PilN homodimers (34.0 kDa) in both the PilN^{R142C} and PilN^{R142C}/PilO^{D175C} samples (left and right panels), PilO homodimers (36.4 kDa) in both the PilO^{D175C} and PilN^{R142C}/PilO^{D175C} samples (center and right panels), and

PilNO heterodimers (35.2 kDa) in the double Cys mutant as well (right). **(C)** Gel filtration calibration curve for the protein standards on a Superdex 75 10/300 GL column; aprotinin (A; 6.5 kDa), RNAse A (R; 13.7 kDa), carbonic anhydrase (CA; 29.0 kDa), and conalbumin (C; 75.0 kDa). $PilN_{\Delta 44}$ and $PilO_{\Delta 51}$ co-eluted at a volume similar to conalbumin as indicated on graph with the red 'x'. The elution volumes (V_e) of the standards are divided by the void volume of the column (V_o) and plotted against the log of the standards' molecular weights to give the slope of the line which was used to solve for the molecular weight of the eluted $PilN_{\Delta 44}$ /$PilO_{\Delta 51\_His}$ complex (70.4 kDa).

Disulfide bond formation between PilN and/or PilO disrupts T4P function

To assess the functional consequences arising from formation of covalently linked dimers *in vivo*, the ability of the Cys mutant strains to assemble surface-exposed T4P was assessed (Figure 3.4A). The $PilN^{R142C}$/$PilO^{D175C}$ and $PilO^{A158C/I178C}$ mutants had very low levels of surface pili, and piliation of the $PilO^{Y154C/I178C}$ mutant was comparable to negative controls. Both the $PilO^{S166C/D175C}$ and $PilO^{V161C/D175C}$ mutants had a moderate reduction in surface pili, possibly related to their shared D175C mutation. These data suggest that pilus biogenesis requires specific PilN and PilO configurations that are perturbed by these mutations.

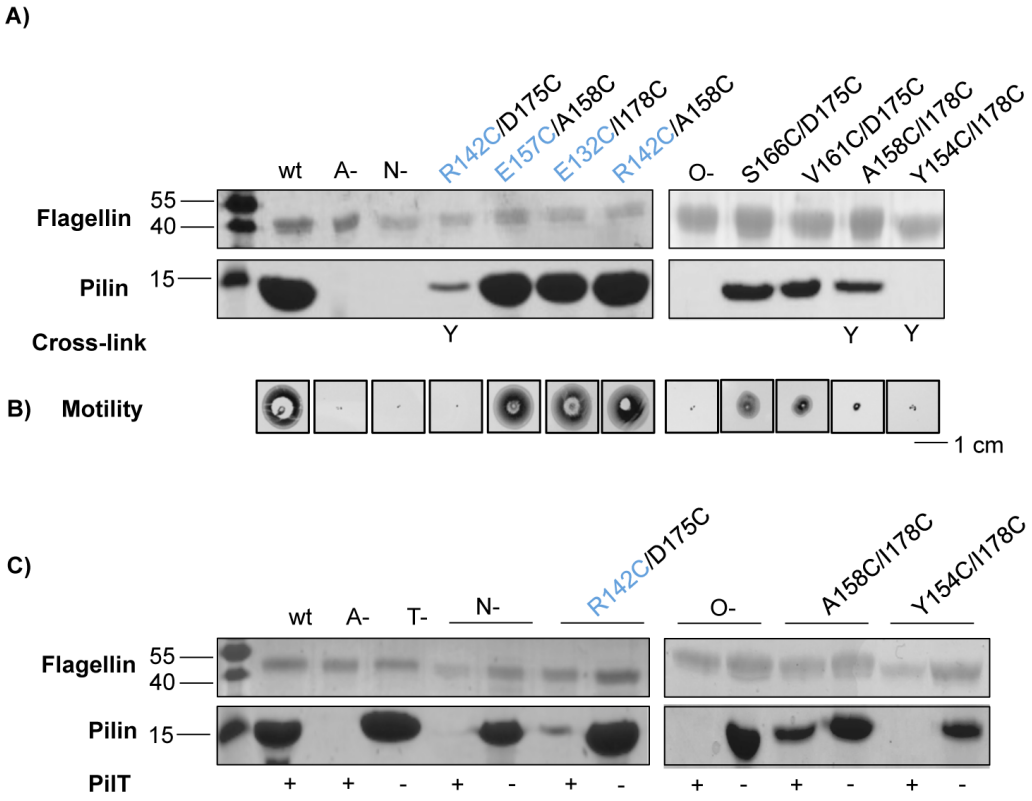

Figure 3.4. Functional consequences of covalent dimer formation in wild-type and retraction deficient backgrounds. PilN and PilO Cys mutants, plus wild-type (wt), non-piliated (A-), hyperpiliaited (T-) and negative controls (N- and O-) were tested for **(A)** sheared surface pili, and **(B)** twitching motility. Sheared surface preparations revealed that the PilN^{R142C}/PilO^{D175C} and PilO$^{A158C/I178C}$ mutants exhibited severely reduced levels of surface pili, while the PilO$^{Y154C/I178C}$ mutant exhibited no surface exposed pili and all were devoid of twitching motility similar to negative controls. Large disruptions in motility and piliation in the remaining PilNO Cys pairs was not observed. The ability of PilNO or PilOO Cys pairs to form Cys cross-links are indicated below (Y). **(C)** Select Cys mutants were introduced into a retraction deficient background, and revealed that all three double Cys mutants assemble more pili without the retraction ATPase, PilT. PilT presence (+) or absence (-) in each strain indicated below.

Since T4P function relies on dynamic assembly and disassembly of pili, it was important to assess motility as well as piliation levels (Figure 3.4B). Strains forming covalently cross-linked dimers (PilN^{R142C}/PilO^{D175C}, PilO$^{A158C/I178C}$, and PilO$^{Y154C/I178C}$) were incapable of twitching. PilO$^{S166C/D175C}$ and PilO$^{V161C/D175C}$ strains had approximately half of wild-type motility, consistent with their decrease in piliation levels, although no *in vivo* cross-linked dimers were observed for these mutants. The remaining Cys mutants twitched similarly to the wild-type.

Lack of piliation is caused by inefficient assembly

Any pili assembled in strains lacking the retraction ATPase, PilT, become trapped on the cell surface (157). Loss of pilus retraction in alignment subcomplex mutants was shown previously (49) to allow for capture of a few pili on the surface of the cells. Since three of the double Cys mutants had major reductions in the levels of surface pili (PilN^{R142C}/PilO^{D175C}, PilO$^{A158C/I178C}$, and PilO$^{Y154C/I178C}$), we hypothesized that they would assemble more pili in a retraction-deficient background, similar to *pilN* or *pilO* mutants. We disrupted *pilT* in these backgrounds and tested the resulting levels of surface piliation. As predicted, all mutants assembled more pili when retraction was disabled (Figure 3.4C). This result suggests that all mutants are capable of extending pili, but that assembly in those backgrounds is impaired, especially in the PilO$^{Y154C/I178C}$ mutant, resulting in net pilus retraction when PilT is active.

Specific single Cys mutations affect function of the T4P system

Since moderate reductions in twitching and piliation were observed in two PilO double Cys mutant strains ($PilO^{S166C/D175C}$ and $PilO^{V161C/D175C}$) that share a common substitution, we next investigated whether individual Cys substitutions disrupted T4P production and function. The stability of the alignment subcomplex components in strains with single Cys substitutions was tested using specific antibodies, and the levels of PilMNOP were found to be comparable to wild-type (Figure 3.5A). Each single Cys mutant produced pili at levels similar to wild-type, with the exception of $PilN^{R142C}$ that had a modest reduction in piliation (Figure 3.5B). Interestingly, neither $PilN^{R142C}$ and $PilO^{D175C}$ could twitch (Figure 3.5C), even though both produced pili; this phenotype is a hallmark of retraction defects. Motility of all other single Cys mutant strains was unaffected.

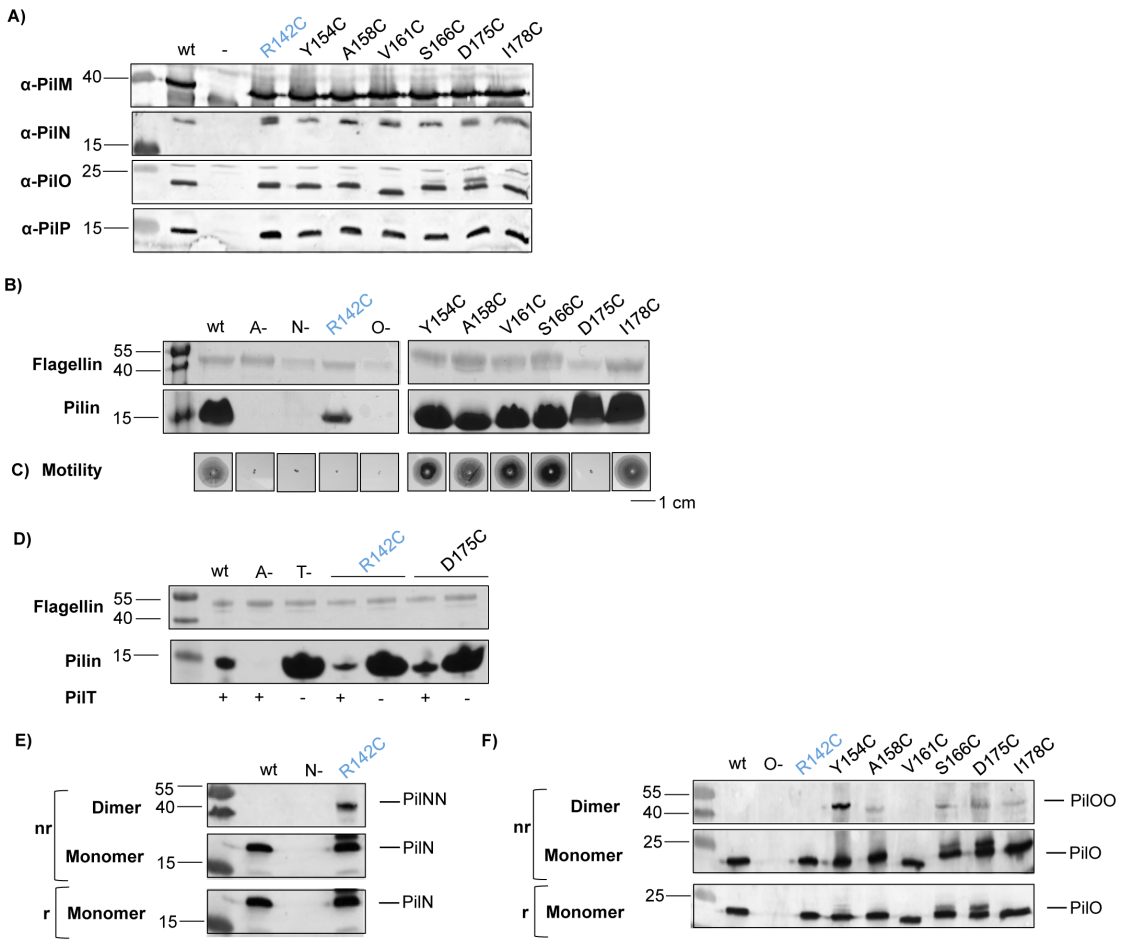

Figure 3.5. PilN^{R142C} and PilO^{D175C} single Cys substitutions cause T4P dysfunction in wild-type and retraction deficient backgrounds. Lysates for the wild-type (wt), negative controls (-) and the Cys mutants were subject to SDS-PAGE then blotted with specific antibodies to **(A)** each alignment subcomplex component (α-PilM, α-PilN, α-PilO, α-PilP) to confirm stability of each protein in the Cys mutants. Each mutant along with wt, non-piliated (A-), hyperpiliaited (T-) and negative controls (N- and O-) were tested for **(B)** sheared surface pili, and **(C)** twitching motility. PilN^{R142C} had less pili and motility than wt, whereas PilO^{D175C} had similar level of pili but no motility. **(D)** PilN^{R142C} and PilO^{D175C} were introduced into a retraction deficient background, and revealed that both Cys mutants can assemble more pili without the retraction ATPase, PilT. PilT

presence (+) or absence (-) in each strain indicated below. Whole cell lysates were then subject to SDS-PAGE under non-reducing (nr) and reducing (r) conditions, then blotted with specific antibodies to **(E)** PilN, and **(D)** PilO. All single Cys mutants were able to form homodimers to varying extents.

Single Cys substitutions allow for in vivo *homodimer formation but only a subset have functional consequences*

To better understand why PilN^{R142C} and PilO^{D175C} single mutants could extend pili but not twitch, we hypothesized that these residues might trap PilN or PilO in specific homodimer configurations, impairing function. Whole cell lysates of all single Cys mutants were analyzed in reducing and non-reducing conditions followed by immunoblotting with PilN and PilO antibodies. We were surprised to see that all single Cys mutants formed covalent homodimers *in vivo* to varying degrees, with PilN^{R142C} and PilO^{Y154C} forming the most, and fewer dimers captured for other Cys mutants such as PilO^{D175C} and PilO^{V161C}, where dimer formation is extremely weak (Figure 3.5E & F). These data suggest that with specific exceptions (PilN^{R142C} and PilO^{D175C}), covalent *in vivo* homodimerization of PilN and PilO can occur without functional consequences.

Heterodimer formation of PilN^{R142C} and PilO^{D175C} is abolished in a pilM *background*

As proposed for the T2S system (122), partner switching, or reorientation of PilN and PilO interfaces, might explain how PilN and PilO can form both homo- and heterodimers *in vivo*. We hypothesized that PilN might respond to

conformational changes in its cytoplasmic partner PilM, repositioning it relative to PilO. To test whether formation of covalent dimers requires PilM, the *pilM* gene was deleted in each of the PilN^{R142C}/PilO^{D175C}, PilO$^{A158C/I178C}$, and PilO$^{Y154C/I178C}$ strains. The absence of PilM was confirmed by Western blot (Figure 3.6A), and whole cell lysates of Cys mutant strains lacking PilM were analyzed in reducing and non-reducing conditions followed by immunoblot analysis with PilN or PilO antibodies. While both PilO$^{A158C/I178C}$ and PilO$^{Y154C/I178C}$ formed covalent homodimers in the absence of PilM, PilN^{R142C}/PilO^{D175C} no longer formed covalent heterodimers (Figure 3.6B & C).

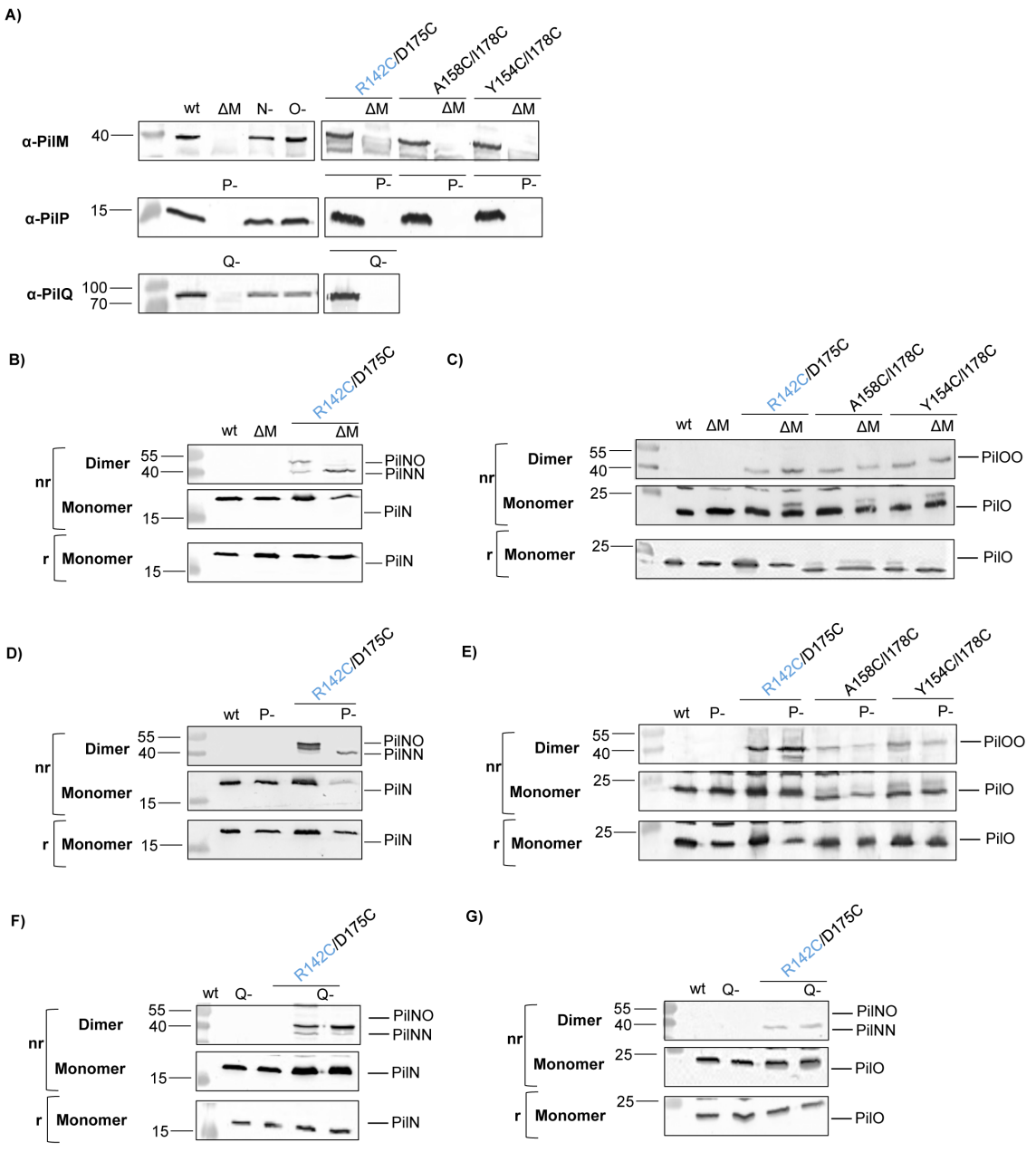

Figure 3.6. Heterodimer formation is abolished in *pilM* or *pilP* backgrounds. Lysates of PilN and PilO Cys mutants, wild-type (wt), PilM deletion (ΔM), PilP::FRT (P-) and the negative controls (N- and O-) were resolved using SDS-PAGE under non-reducing (nr) and reducing (r) conditions, and subject to Western blot detection using specific antibodies to **(A)** PilM, PilP and PilQ to

show the disruption of the proteins, **(B, D, & F)** PilN, and **(C, E, & G)** PilO. In the absence of PilM or PilP, Cys cross-linked homodimers ($PilO^{A158C/I178C}$ and $PilO^{Y154C/I178C}$) can still form, whereas the $PilN^{R142C}$/$PilO^{D175C}$ heterodimer cannot. The absence of PilQ does not alter the dimerization profile of the $PilN^{R142C}$/$PilO^{D175C}$ Cys pair.

Heterodimer formation of $PilN^{R142C}$ and $PilO^{D175C}$ is also abolished in a pilP *background*

To determine if the remaining member of the alignment subcomplex, PilP, had effects on PilNO dimer formation, we created a *pilP* strain expressing the Cys pairs of interest ($PilN^{R142C}$/$PilO^{D175C}$, $PilO^{A158C/I178C}$, and $PilO^{Y154C/I178C}$), confirmed the loss of PilP by Western blot (Figure 3.6A), and analyzed whole cell lysates as described above. The $PilN^{R142C}$/$PilO^{D175C}$ strain failed to form covalent PilNO heterodimers in the absence of PilP; however, PilN and PilO formed homodimers (Figure 3.6D & E), as in the *pilM* mutant. To investigate whether the absence of PilP alone affected the PilNO interface, or if the change in dimerization state was due to the lack of PilNO tethering via PilP to the N0 domain of PilQ (54), we created a *pilQ* strain expressing the $PilN^{R142C}$/$PilO^{D175C}$ Cys pair, confirmed loss of PilQ by Western blot (Figure 3.6A), and tested lysates as described above. Absence of PilQ had no effect on homo- or heterodimer formation (Figure 3.6F & G), suggesting that PilP specifically contributes to the formation of an interface conducive to the formation of a covalent bond between $PilN^{R142C}$/$PilO^{D175C}$.

Other T4P components do not modulate the PilNO interface

Recently, interactions between PilM and motor ATPases of the T4P system were identified for both *P. aeruginosa* and *M. xanthus* (111,119). Since PilM was important for formation of covalent PilN^{R142C}/PilO^{D175C} heterodimers, we hypothesized that conformational changes in PilM, driven by its interaction with other cytoplasmic components of the T4P system while bound to the N-terminus of PilN, might be propagated to periplasmic PilNO interfaces. Three AAA+ ATPases modulate extension (PilB) and retraction (PilTU) of the pilus fibre (5,96,97). We created *pilB*, *pilT*, and *pilU* mutants containing the Cys pairs of interest (PilN^{R142C}/PilO^{D175C}, PilO$^{A158C/I178C}$, and PilO$^{Y154C/I178C}$) and confirmed the absence of each ATPase by Western blot (Figure 3.7). Unexpectedly, all strains formed covalent homo- and heterodimers (Figure 3.8), suggesting that the ATPases do not influence the PilNO interface.

We further investigated whether other T4P components associated with PilM, PilN or PilO, including PilA, the major component of the pilus fibre and PilC, the IM platform protein, influenced the dimerization state of PilN and PilO. Strains with disruptions in *pilA* or *pilC* plus the above Cys substitutions (Figure 3.7) formed covalent homo- and heterodimers similar to the wild-type (Figure 3.8A & C). These data suggest that only interactions among members of the alignment subcomplex modulate the interface between PilN and PilO.

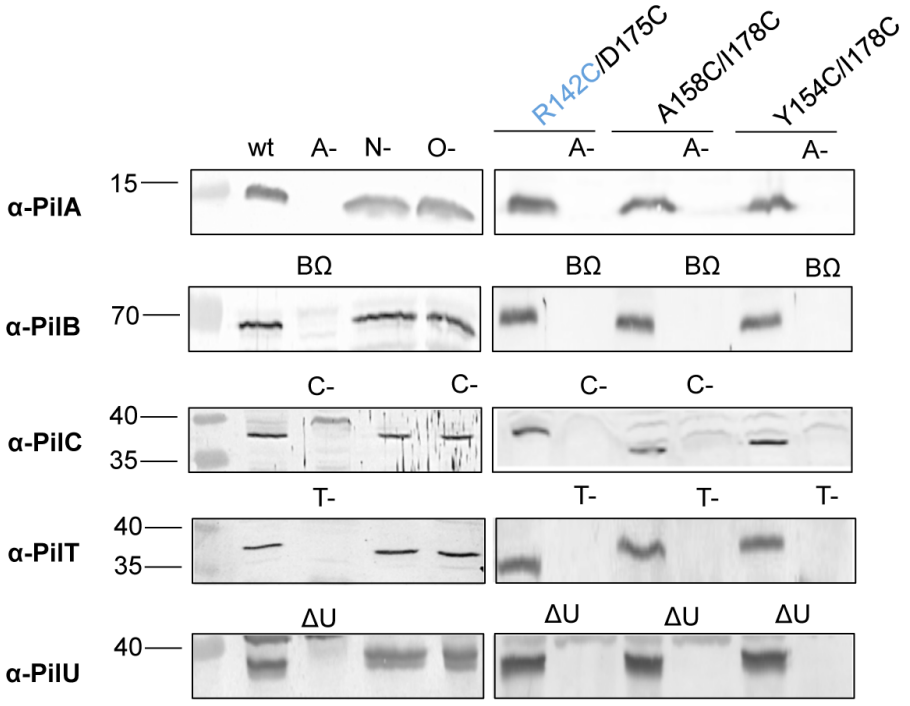

Figure 3.7. Disruption of *pilA, pilB, pilC, pilT,* and *pilU* in PilN^{R142C}/PilO^{D175C}, PilO$^{A158C/I178C}$, & PilO$^{Y154C/I178C}$ backgrounds. Lysates of wild-type (wt), negative control strains (A-, BΩ, C-, N-, O-, T-, and ΔU), and Cys mutants were tested for expression and stability of each protein using protein-specific antisera. Symbols: – indicates the gene was disrupted via an FRT insertion, Δ indicates the gene was produced by a deletion of the gene, and Ω indicates the gene was disrupted by an Ω cassette insertion.

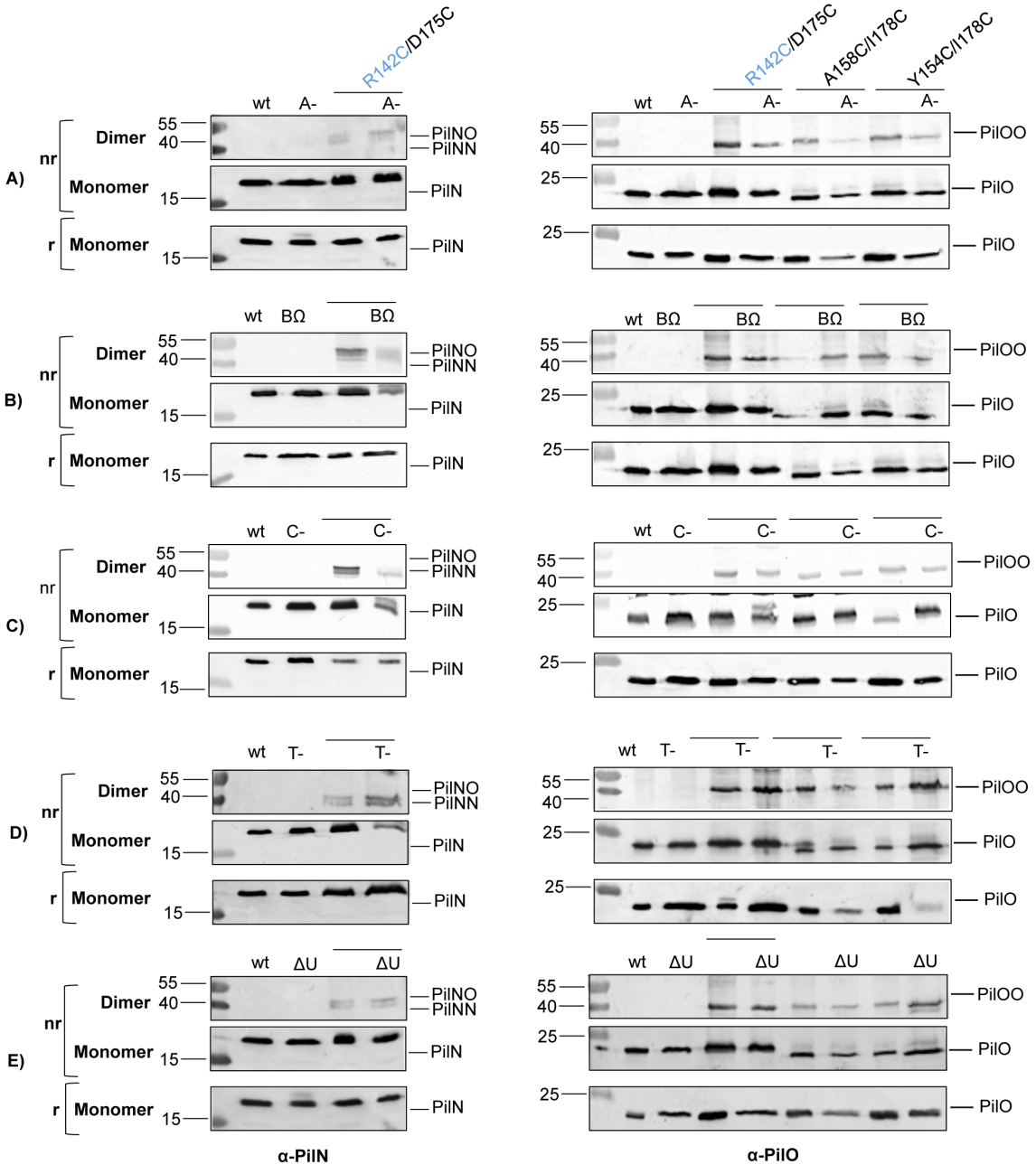

Figure 3.8. Dimerization of PilN^{R142C}/PilO^{D175C}, PilO$^{A158C/I178C}$, & PilO$^{Y154C/I178C}$ is unaffected by loss of non-alignment subcomplex components. Wild-type (wt), negative controls (A-, BΩ, C-, N-, O-, T-, and ΔU) and Cys mutant lysates were tested for the ability of PilN and PilO to form homo- or heterodimers on non-reducing SDS-PAGE. PilN (left) and PilO (right) were blotted for using protein-

specific antisera. Symbols: – indicates the gene was disrupted via an FRT insertion, Δ indicates the gene was produced by a deletion of the gene, and Ω indicates the gene was disrupted by an Ω cassette insertion.

Discussion

The PilMNOP alignment subcomplex is highly conserved among T4P-expressing bacteria (5). Previous studies demonstrated that PilN and PilO form stable heterodimers in a 1:1 stoichiometry (51), however, the precise interface(s) between PilN and PilO has not yet been elucidated. We used disulfide-bonding analysis to study the interactions between these components, and to assess the functional consequences of covalently crosslinking PilN and/or PilO. Our results revealed that PilN and PilO form both homo- and heterodimers *in vivo* under physiological conditions, and that conformational flexibility of these states is necessary for T4P function.

PilN and PilO may form dimers of dimers in vivo

Studies in the T2S system showed that PilN- and PilO-like proteins (GspL and GspM, respectively) form homo- and heterodimers, possibly via a process called “partner switching” involving large rotations in the TMS and core interfaces (122). Here we captured PilO homodimers – previously observed upon over-expression *in trans* (50,51) – when expressed at native levels and stoichiometry from the *Pseudomonas* chromosome, confirming that the PilO homodimer interface revealed by structural studies is physiological (Figure 3.2C).

Unexpectedly, while trying to understand if PilNO heterodimers share the same interface as PilO homodimers, we identified multiple species on an anti-PilN Western blot (Figure 3.2B), with masses corresponding to PilNO heterodimers and PilN homodimers. Although a PilN homodimer (bound to PilM) from the T4P system of *T. thermophilus* was observed *in vitro* (124), to our knowledge this is the first report of PilN and PilO homodimers in their native context.

When soluble periplasmic fragments of PilN and PilO ($PilN^{R142C}$ and $PilO^{D175C}$, Figure 3.3A & B) were expressed in *E. coli*, they formed covalent homodimers. Co-expression of $PilO^{D175C}$ with $PilN^{R142C}$ led to capture of three subpopulations: $PilN^{R142C}$ homodimers, $PilO^{D175C}$ homodimers, and $PilN^{R142C}$/$PilO^{D175C}$ heterodimers (Figure 3.3A & B), suggesting that there are (at least) two possible states for each protein. Interestingly, a large amount of PilO monomers remained in the non-reducing lanes, indicating that a substantial proportion of PilO was either present as a monomer, or participating in non-covalent dimers, possibly as a result of non-permissive positioning of a PilO interaction interface for disulfide bond formation.

P. aeruginosa PilN expressed *in vitro* without PilO is mostly insoluble (55), which has precluded studies of PilN alone. We hypothesized that formation of covalent PilN homodimers might stabilize it in the absence of PilO, and attempted to purify $PilN_{\Delta44\_His}{}^{R142C}$ under non-reducing conditions, but the protein remained mostly insoluble. However, untagged $PilN^{R142C}$ homodimers co-purified with tagged PilO, and the molecular mass of the complex was ~75 kDa (Figure 3.3C),

likely corresponding to a 2:2 $PilN_{\Delta 44}$:$PilO_{\Delta 51\_His}$ complex. This stoichiometry fits with our previous data, where PilNOP were shown by gel filtration to elute as either a trimer, or a dimer of trimers (55). A dimeric complex of PilMNO (2:2:2) was identified in *T. thermophilus* (124), consistent with our finding that *P. aeruginosa* PilN and PilO form a dimer of dimers (50,54,55,124).

Only two of four predicted PilO Cys mutant pairs, and one of three PilNO pairs, formed disulfide bonds, suggesting that the truncated $PilO_{\Delta 68}$ structure (Figure 3.1A)(51) and the $PilN_{\Delta 57}$/$PilO_{\Delta 68}$ heterodimer homology model derived from it (Figure 3.1B) do not exactly mirror the *in vivo* conformation of the proteins. However, the ability to cross-link both homo- and heterodimers of PilN and PilO *in vivo* confirms that select residues are close enough and in the appropriate orientation to allow for disulfide bond formation. The recent cryoelectron tomography study of the *M. xanthus* T4P system (71), with resolutions averaging 4 nm, now offers the exciting possibility that we could image the T4P systems of our *P. aeruginosa* Cys mutants *in situ*, to see how crosslinking of PilNO affects configuration of the machinery.

Interestingly, the relative position of the Cys residues able to crosslink PilO homodimers *in vivo* were at the “top” of the predicted interface in most cases, while they were at the “bottom” for the PilNO heterodimer (Figure 3.2D), suggesting that the homo- and heterodimer interfaces might be angled differently. Models of the core interaction interface between PilN and PilO in *T. thermophilus* (124) and *M. xanthus* (71) show them as tilted, possibly owing to longer predicted

coiled-coils in PilO (51). The persistence of PilN and PilO monomers (Figure 3.2B & C and Figure 3.3A & B) not involved in covalent interactions suggests the coexistence of multiple PilN and PilO interaction species. This scenario was reported for T2SS PilP- and PilQ-like proteins (GspC and GspD, respectively), where contacts were established at three distinct interfaces *in vivo* (181). These observations – combined with our results – suggest that homo- and heterodimers may occur simultaneously. The oppositely charged coiled-coils of PilNO (51) could serve as the primary interaction interface between heterodimers (Figure 3.9B) whereas the core could mediate homodimer interactions (Figure 3.9C). This models previous results, where up to six combined point mutations along the PilN core region failed to disrupt PilNO heterodimers in a bacterial two hybrid assay (178). Further, this model could explain why PilN^{R142C} and PilO^{D75C} residues at the “bottom” of the original model (Figure 3.1) participate in both homo- and heterodimers (Figure 3.2B & C and Figure 3.3A & B), as a tilted PilNO core interface could position these residues in close enough proximity to form a disulfide bond. Importantly, our data do not support large rotations in the core-core interface, as suggested previously in the T2S system (122).

PilN and PilO homodimers may represent a functional – rather than assembly intermediate – state of the T4P system

Our data show that covalent PilN or PilO homodimerization is not necessarily detrimental to function. With the exception of PilN^{R142C} and PilO^{D175C}, none of the single Cys mutants had obvious piliation or motility defects (Figure

3.5B & C), despite their capacity to form covalent homodimers *in vivo* (Figure 3.5E & F). The relative abundance of covalent homodimers formed by each mutant did not correlate with T4P dysfunction, as PilO^{Y154C} formed the most, but without functional consequences. This result suggests that crosslinking only of specific residues affects function, and supports the idea that PilN and PilO homodimers represent a normal state of the T4P system.

Three covalent pairs (PilN^{R142C}/PilO^{D175C}, PilO$^{A158C/I178C}$ and PilO$^{Y154C/I178C}$) resulted in significant loss of surface piliation and complete loss of motility (Figure 3.4A & B). This result suggests that dynamic PilNO interactions are required for correct pilus function. In a retraction deficient background, where aassembled pili are trapped on the surface (157), all three double Cys mutants extended more pili (Figure 3.4C) indicating that covalently linked dimers permit some pilus assembly. Thus, lack of motility in these strains more likely arises from extension-retraction imbalances. We showed previously (178) that substitution of specific residues at the PilN and PilO coiled-coil interface also confers an assembly-competent, yet retraction-deficient phenotype. Together, these data emphasize that precise but dynamic interfaces between PilNO contribute to function.

Previous work in *T. thermophilus* suggested that a dimeric complex of PilMN (two PilMs and two PilNs) form an intermediate transmembrane platform onto which other alignment subcomplex components dock (124). The addition of PilO to the PilMN subassembly was proposed to dissociate PilN homodimers, sequestering each monomer into a PilNO heterodimer. Our data support an

alternate model, in which PilN and PilO might homodimerize via their core domains (Figure 3.9C), while simultaneously heterodimerizing via their coiled-coils, and potentially their TMS (Figure 3.9B) (178). This scenario could explain how untagged, covalent PilN homodimers were co-purified with tagged PilO homodimers, as both constructs retain their coiled coils (Figure 3.3). Alternatively, tetrameric arrangement of PilN and PilO homodimers could suggest an alternative PilNO interface on the 'side' of the core homodimer interface (Figure 3.9B); however we have no evidence to support this idea. The PilN^{R142C} and PilO^{D175C} residues are located near the base of the modeled core interfaces and could be oriented more laterally (Figure 3.9B) than depicted by our static models (Figure 3.1), explaining why these particular residues were the only ones that successfully formed crosslinked heterodimers.

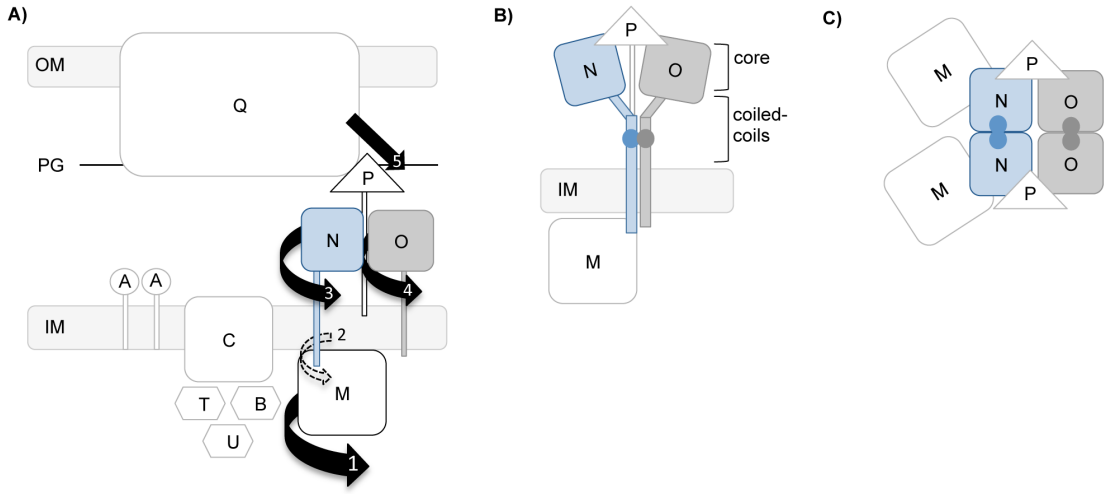

Figure 3.9. Model of the interaction between PilN and PilO with other T4P components. (A) Cartoon schematic of the T4P system in *P. aeruginosa* with the Pil nomenclature. Major cell compartments are labeled: inner membrane (IM), peptidoglycan (PG), and outer membrane (OM). Specific T4P components are highlighted: PilQ, the secretin; PilC, the IM platform protein; PilBTU, the 3 cytoplasmic ATPases; PilA, the major pilin subunit; and PilMNOP, the alignment subcomplex components. Numbered arrows indicate order of hypothesized movement generated from the cytoplasm outwards. **(B)** T4P system cartoon model showing PilN and PilO heterodimer formation mediated through the coiled-coils. **(C)** A top-down view of PilN and PilO homodimers mediated through their core domains. Movement in PilM could be transduced through PilN and PilO, ultimately leading to a movement of PilP – creating a signal transduction network between the inner and outer T4P components.

Modulation of the PilNO core interface by the other alignment subcomplex components

Crosslinking of Cys residues at select locations within the PilNO equivalents (GspLM) in the T2S system suggested rotation of the proteins through their TMSs and periplasmic cores (122). In the T2S system, PilM orthologs interact with the single cytoplasmic motor ATPase (115,117,156,162), and more recently, interactions between PilM and the T4P motor ATPases in *P. aeruginosa* and *M. xanthus* were confirmed (111,119). Thus we tested whether interactions with the cytoplasmic component of the alignment subcomplex, PilM, which is bound to the N-terminus of PilN, modulated PilNO interfaces.

$PilN^{R142C}$/$PilO^{D175C}$ heterodimers, but not homodimers, were lost in the

absence of PilM, (Figure 3.6B & C), suggesting that the PilNO interface no longer adopts an orientation permissive for disulfide bond formation. New crystal structures of a *P. aeruginosa* PilM homodimer and of monomeric PilM fused to its binding partner, $PilN_{1-12}$, revealed that in the absence of PilN, the 7 N-terminal residues of PilM ($PilM_{1-7}$) bind in the PilN binding cleft of a second PilM monomer (111). Thus, PilM dimerizes in the absence of PilN. In this scenario, the lack of PilM-PilN interaction may favor PilN and PilO homodimer formation, whereas when PilM becomes monomeric upon binding PilN's N-terminus, a corresponding shift in the position of the PilNO core interface could induce heterodimer formation. PilM's interactions with its cytoplasmic partners, PilB, PilT and/or PilC (111), differed depending on whether it was bound to PilN, potentially revealing a mechanism for switching between assembly and disassembly. These differential interactions might similarly modulate PilNO homo- versus heterodimer states in the periplasm. However, disruption of *pilB, pilT* or *pilU* had no effect on PilN and PilO dimerization (Figure 3.8B, D & E). The PilM ortholog in the T2S system (cyto-GspL) interacts with the PilC ortholog (GspF) (101); but disruption of *pilC* in our system similarly had no effect on dimerization (Figure 3.8C). These data argue against changes in motor state affecting PilNO interactions.

The major pilin interacts with PilNOPQ in *P. aeruginosa* (54), but its specific interaction partner(s) are unknown. TEM studies of *T. thermophilus* revealed a stable complex composed of PilMNO-PilA (124) and PilN was suggested to interact directly with PilA. One could envision that PilN and PilO

might help extract PilA from the IM during assembly, priming the base of the pilus fibre for incorporation of the next PilA subunit. However, loss of *pilA* had no effect on PilNO dimerization states (Figure 3.8A).

In *M. xanthus,* PilQ recruits PilP, which binds PilN and PilO, and PilN binds PilM, creating a transenvelope complex (74). In *P. aeruginosa*, a similar pathway has been proposed, where PilP binds PilQ as well as PilNO, but doesn't bind PilO homodimers (55). Here, loss of PilP prevented formation of $PilN^{R142C}$/$PilO^{D175C}$ heterodimers (Figure 3.6D & E), while loss of PilQ had no effect (Figure 3.6F & G). The unstructured N-terminus of PilP could interact with the core or coiled coil regions of the PilNO heterodimer, stabilizing the interface in an orientation that allowed for disulfide bond formation. The core regions of PilN or PilO may adopt homodimer orientations, while the large electrostatic difference predicted for the coiled-coils of PilN and PilO (51) could promote heterodimerization.

PilN and PilO rearrangement during 'active' and 'resting' states of the T4P system

Recently, elegant cryoelectron tomography studies of the *M. xanthus* T4P system allowed for derivation of a 'pseudo-atomic' model that suggests differences between the 'active' and 'resting' states of the machinery (71). The active state occurs during assembly or disassembly of the fibre, when a PilB or PilT ATPase is engaged at the base of the system, whereas the resting state was ATPase-free. PilM was proposed to form a ring surrounding a dimer of PilC, and

expansion of the ring upon binding of PilB or PilT during the active state, accompanied by conformational rearrangement of the density associated with PilN and PilO's coiled-coils, was observed (71). Without PilM, density corresponding to PilC and the ATPases was missing (71). In our work, only PilM or PilP could modulate the PilNO core interface; we speculate that subtle reorientation of PilN and PilO may only occur during the transition between states of the T4P system, consistent with the hypothesis that PilM disengages from PilN (111). Although a ratcheting mechanism – where PilNO dynamics contribute to stepwise addition or removal of pilin subunits – cannot be ruled out, our data do not support this idea.

Experimental Procedures

Strains, media and growth conditions

Bacterial strains used in this study are listed in Table 3.1. E*. coli* and *P. aeruginosa* were grown at 37 °C in Luria-Bertani (LB) media supplemented with antibiotics at the following final concentrations when necessary (μg mL^{-1}): ampicillin (Ap), 100; carbapenem (Cb), 200; kanamycin (Kn), 50; gentamicin (Gm), 15 for *E. coli* and 30 for *P. aeruginosa*, unless otherwise specified. Bacterial strains were stored at -80 °C in LB with 20% glycerol (v/v). Plasmids were transformed by heat shock into chemically competent cells. All constructs were verified by DNA sequencing (MOBIX – McMaster University).

Generation of Cys mutants

Sets of double Cys mutations in PilO, as well as single Cys mutations in PilN and PilO, were chosen with reference to the $PilO_{\Delta 68}$ homodimer crystal structure PDB 2RJZ (51) and a $PilN_{\Delta 57}/PilO_{\Delta 68}$ heterodimer homology model, created by substituting the Phyre[2] generated $PilN_{\Delta 57}$ monomer in place of a PilO subunit in the PilO homodimer structure (51,125). Distances were measured in Pymol and residues were selected to ensure that the distance between Cβ atoms was less than 8 Å (Figure 3.1). Codons for selected Cys substitutions were introduced into either a pEX18Gm::*pilMNOP* construct (for PilNO Cys pairs) or a pEX18Gm::*pilNOP* construct (for double PilO Cys mutants) using the QuikChange Site-Directed Mutagenesis Kit (Stratagene) following the manufacturer's protocol. Mutations were verified by DNA sequencing (MOBIX).

Generation of pilN and pilO Cys mutations onto the chromosome of P. aeruginosa PAK

Cys-encoding chromosomal mutants of *P. aeruginosa* were generated by biparental mating with *E.* coli SM10 using a Flp-FRT (FLP recombination target) system as previously described (18). Constructs containing the desired Cys substitutions, pEX18Gm::*pilMNOP* for PilNO Cys mutants and pEX18Gm::*pilNOP* for PilO Cys mutants, were introduced into *E. coli* SM10 cells for biparental mating with PAK *pilN::FRT* and PAK *pilO::FRT* respectively (12). The *E. coli* SM10 donor was counter selected by plating on Pseudomonas isolation agar (PIA; Difco) containing Gm (100 μg mL^{-1}). Gm-resistant *P. aeruginosa* isolates

were streaked on LB-no salt sucrose plates (1% w/v bacto-tryptone, 0.5% w/v bacto-yeast extract, 5% w/v sucrose) then incubated for 16 h at 30 °C. Select colonies were restreaked in parallel on LB and LB plates supplemented with Gm. Gm-sensitive colonies were screened by PCR using *pilN* or *pilO* primer pairs (Table 3.2) to confirm replacement of the original FRT-disrupted gene, and PCR products of the expected size were DNA-sequenced (MOBIX) to confirm incorporation of the desired mutations.

Preparation of whole cell lysates

P. aeruginosa strains were grown on LB agar plates overnight at 37 °C. Cells were scraped from the surface and resuspended in 1X PBS (phosphate buffered saline, pH 7.4) to an OD_{600} of 0.6. A 1 mL aliquot of cells was collected by centrifugation at 2292 x *g* for 3 min in a microcentrifuge. The cell pellet was resuspended in 100 µL of either 1X SDS-PAGE (sodium dodecyl sulfate-polyacrylamide gel electrophoresis) loading buffer (125mM Tris, pH 6.8, 2% (v/v) β-ME, 20% (v/v) glycerol, 4% (w/v) SDS and 0.001% (w/v) bromophenol blue) or 1X non-reducing SDS-PAGE loading buffer (no β-ME), and subject to Western blot analysis.

Western blot analysis

Samples were separated on 15% SDS-PAGE gels for 1.5 h at 160 V and transferred to nitrocellulose membranes for 1 h at 225 mA. Membranes were blocked using a 5% (w/v) low fat skim milk powder in 1x PBS for 1 h at room temperature on a shaking platform, followed by incubation with protein specific

antibodies at the following dilutions; α-PilM, α-PilN, α-PilO, and α-PilP at dilutions of 1/1000 (50), α-PilB, α-PilT, and α-PilU at 1/2000, 1/500, and 1/5000, respectively (98), α-PilA at 1/5000 (83) and α-PilC at 1/1000 (49). Blots were incubated in primary antibody ~16 h at 4°C on a rocking platform. The membranes were washed twice in 1x PBS for 5 min then incubated in goat-anti-rabbit IgG-alkaline phosphatase conjugated secondary antibody (Bio-Rad) at a dilution of 1/3000 for 1 h at room temperature. The membranes were washed twice in 1x PBS for 5 min, and visualized with alkaline phosphatase developing reagent (Bio-Rad) following the manufacturer's protocol.

Expression and purification of $PilN_{\Delta 44}$ and $PilO_{\Delta 51}$

N-terminally truncated versions of PilN and PilO were previously cloned into the EcoRI/HindIII and NdeI/XhoI cloning sites, respectively, of a pET28a vector, creating a vector that over expresses untagged $PilN_{\Delta 44}$ and C-terminal 6x-His tagged $PilO_{\Delta 51\_His}$ (51,55). Cys mutations were introduced into this construct using the QuikChange Site-Directed Mutagenesis Kit (Stratagene) following the manufacturer's instructions to create pET28a::$pilN_{\Delta 44}/pilO_{\Delta 51\_His}$ containing $pilN_{\Delta 44}^{R142C}$, $pilO_{\Delta 51}^{D175C}$, or a double $pilN_{\Delta 44}^{R142C}/pilO_{\Delta 51}^{D175C}$ construct. Constructs were transformed into *E. c*oli Origami2 (DE3) pLysS cells and plated on LB agar plates supplemented with 50 mg ml^{-1} kanamycin. A single colony was used to inoculate 20 ml of LB containing 50 mg ml^{-1} kanamycin, and incubated overnight at 37 °C, shaking. The overnight culture was used to inoculate 1 L of fresh LB (1:100 dilution) containing antibiotic and the cells were grown at 37 °C,

with shaking, to an OD_{600} of 0.6. Protein expression was induced by adding IPTG (isopropyl β-D-1 thiogalactopyranoside, Sigma Aldrich) to the culture at a final concentration of 1 mM. The cells were allowed to grow for 4 h at 37 °C, prior to being harvested by centrifugation (3,993 x *g*, 15 min, 4 °C) in an Avanti J-26 XPI centrifuge (Beckman Coulter). Bacterial pellets were frozen at -80 °C until further use.

Bacterial pellets were thawed and resuspended in 10 mL Nickel A buffer (20 mM Tris-HCl pH 7.2, 500 mM KCl, 10 mM imidazole, 10% (v/v) glycerol), then combined in a 50 mL screw cap tube with 1 complete EDTA-free protease inhibitor tablet (Roche). Cells were lysed via sonication on ice, on setting 4, for 2 min with cycles of 10 s on and 10 s off (Sonicator 3000; Misonix). The lysates were centrifuged (11,000 x *g*, 30 min, 4 °C) in an Avanti J-26 XPI centrifuge (Beckman Coulter) to remove intact cells and other cellular debris. Pelleted material was retained for analysis by SDS-PAGE, while supernatants were filtered through 0.22 µm Acrodisc syringe filter (Pall Corporation). The lysate was purified using Nickel-NTA affinity chromatography on an AKTA start FPLC (VWR). Protein lysate was flowed through a 1 mL His-Trap™ FF column (GE Healthcare) pre-equilibrated with buffer, and washed with Nickel A buffer, then increasing amounts of Nickel B buffer (20 mM Tris-HCl pH 7.2, 500 mM KCl, 300 mM imidizole, 10% (v/v) glycerol) in a linear gradient. The bound protein was eluted from the column in pure Nickel B buffer and collected in 1 mL fractions. An aliquot of each fraction was mixed 1:1 with 2X reducing or non-reducing SDS-

PAGE loading and electrophoresed on a 15% SDS-PAGE gel. The gel was stained using Coomassie Blue Staining solution (0.1% Coomassie Brilliant Blue R-250, 50% (v/v) methanol and 10% (v/v) glacial acetic acid), or developed by Western blot using protein-specific antibodies as described above.

Twitching motility assays

Twitching assays were performed as previously described (5,96,97,149). Briefly, single colonies were stab inoculated to the bottom of a 1% LB agar plate. The plates were incubated for 36 h at 37 °C. Post incubation, the agar was carefully removed and the adherent bacteria stained with 1% (w/v) crystal violet dye, followed by washing with tap water to remove unbound dye. Twitching zone areas were measured using ImageJ software (NIH). Statistical significance of differences compared to wild-type was determined using Student's *t*-test. All experiments were performed in triplicate with at least three independent replicates.

Sheared surface protein preparation

Surface pili and flagella were analyzed as described previously (149) with the following modifications. *P. aeruginosa* strains of interest were streaked in a grid-like pattern on large LB 1.5% agar plates and incubated at 37 °C for ~16 h. The cells were scraped from the plates with glass coverslips and resuspended in 4.5 mL of 1X PBS. Centrifugation of the cells were preformed in 1.5 mL Eppendorf tubes at 11,688 x *g*. Cell pellets were resuspended in 150 µL of 1X SDS sample buffer (125mM Tris, pH 6.8, 2% (v/v) β-ME, 20% (v/v) glycerol, 4%

(w/v) SDS and 0.001% (w/v) bromophenol blue) and visualized on a 15% SDS-PAGE gel by staining with Coomassie Blue Staining solution.

In vivo *disulfide crosslinking analysis*

Spontaneous disulfide bond formation between PilN and PilO Cys mutants was assessed in bacteria grown on solid media. Whole cell lysates of the various strains were resuspended in reducing or non-reducing SDS-PAGE buffer were boiled for 10 min to lyse cells, electrophoresed on a 15% SDS-PAGE gel and subject to Western blotting with protein specific antibodies for PilN and PilO as previously described.

Generation of PilN and PilO Cys pairs in various T4P component mutant backgrounds

To test the contributions of other T4P proteins to dimer formation, select Cys mutants were generated in previously generated T4P mutant backgrounds (Table 3.1). To create strains with Cys substitutions and devoid of PilM, a construct comprised of 700 bp up and downstream of the *pilM* gene (Δ*pilM*) was subcloned into pEX18Gm using XbaI/EcoRI. The resulting suicide construct was transformed into *E. coli* SM10 and transferred to *P. aeruginosa* PAK strains already containing *pilN*^{R142C}/*pilO*^{D175C}, *pilO*$^{A158C/I178C}$ or *pilO*$^{Y154C/I178C}$ by biparental mating, and mutants were selected as described above.

To make Cys mutant strains lacking PilA, PilC, PilQ, or PilT, we used previously engineered suicide constructs for *pilA::*FRT (166)*, pilC::*FRT (49)*, pilQ*::FRT (72), and *pilT:*:FRT (96) mutants. These constructs were introduced

into the *P. aeruginosa* PAK PilN^{R142C}/PilO^{D175C}, PilO$^{A158C/I178C}$ or PilO$^{Y154C/I178C}$ backgrounds, with the exception of *pilQ*::FRT which was only introduced into the PilN^{R142C}/PilO^{D175C} background. Briefly, a suicide vector containing the target gene (*pilA, pilC, pilQ,* or *pilT*) disrupted by a gentamicin resistance cassette flanked by FRT sites (pEX18Ap *pilA*::GmFRT, pEX18Ap *pilC*::GmFRT, pEX18Ap *pilQ*::GmFRT, or pEX18Ap *pilT*::GmFRT respectively) (22) were introduced into chemically competent *E. coli* SM10 cells. The constructs were transferred to *P. aeruginosa* PAK strains containing *pilN*^{R142C}/*pilO*^{D175C}, *pilO*$^{A158C/I178C}$ or *pilO*$^{Y154C/I178C}$ by biparental mating as described above. After overnight incubation on sucrose plates, select colonies were plated in parallel on LB plates supplemented with either Cb or Gm, and Gm-resistant, Cb-sensitive colonies were selected. The integrated Gm cassette was removed by conjugally transferring the Flp-expressing pFLP2 from *E. coli* SM10 into *P. aeruginosa* as previously described (18). *E. coli* SM10 was counter-selected by plating on *Pseudomonas* isolation agar (Difco) containing Cb. pFLP2 was cured by streaking Cb-resistant isolates on LB-no salt plates containing 5% (w/v) sucrose, and incubating for 16 h at 30 °C. Select colonies were streaked in parallel on LB plates, LB plus Cb and LB plus Gm plates. Cb- and Gm-sensitive colonies were selected and the *pilA*::FRT, *pilC*::FRT, *pilQ*::FRT and *pilT*::FRT mutations confirmed by PCR and DNA sequencing using the primers listed in Table 3.2.

In some cases, we started with various *P. aeruginosa* PAK mutant backgrounds; *pilB*Ω (107)*, pilP::*FRT (50), and Δ*pilU* (gift of Dr. Matthew

Wolfgang) and introduced suicide vectors containing the desired PilN and PilO Cys pairs (as described above). After selection for Gm-sensitive colonies, we screened for correct incorporation of PilN and PilO Cys pairs through PCR using *pilN* or *pilO* primer pairs (Table 3.2) and mutations were confirmed by DNA sequencing (MOBIX).

Table 3.1: Bacterial Strains

Strain	Description	Source/Reference
***E. coli* strains**		
DH5α	F-, φ80lacZ, M15, Δ(lacZYA-argF), U169, recA1, endA1, hsdR17(rk-,mk+), phoAsupE44, thi-1, gyrA96, relA1, λ-	Invitrogen
Origami2 (DE3)pLysS	Δ(ara-leu)7697 ΔlacX74 ΔphoA PvuII phoR araD139 ahpC galE galK rpsL F′[lac^+ $lacI^q$ pro] (DE3) gor522::Tn10 trxB pLysS (Cam^R, Str^R, Tet^R)	Novagen
SM10	thi-1, thr, leu, tonA, lacy, supE, recA, RP4-2-Tcr::Mu, Km^r; mobilizes plasmids into *P. aeruginosa* via conjugation	(182)
***P. aeruginosa* strains**		
PAK	Wild-type	J. Boyd
ΔpilM	Deletion of *pilM*	(50)
pilN::FRT	FRT scar at position 124 within *pilN*	(50)
pilO::FRT	FRT scar at position 328 within *pilO*	(50)
pilP::FRT	FRT scar at position 86 within *pilP*	(50)
pilQ::FRT	FRT scar at position at 571 within *pilQ*	(72)
pilT::FRT	FRT scar at position 540 within *pilT*	(96)
pilA::FRT	FRT scar at SphI site within *pilA*	(166)
*pilB*Ω	*pilB* with Ω cassette insertion	(107)
ΔpilU	Deletion of *pilU*	Dr. M. Wolfgang
pilC::FRT	FRT scar at position 365 within *pilC*	(49)
$PilN^{R142C}$/$PilO^{D175C}$	*pilN* R142C & *pilO* D175C	This study
$PilN^{E157C}$/$PilO^{A158C}$	*pilN* E157C & *pilO* A158C	This study
$PilN^{E132C}$/$PilO^{I178C}$	*pilN* E132C & *pilO* I178C	This study
$PilN^{R142C}$/$PilO^{A158C}$	*pilN* R142C & *pilO* A158C	This study
$PilO^{S166C/D175C}$	*pilO* S166C, D175C	This study
$PilO^{V161C/D175C}$	*pilO* V161C, D175C	This study
$PilO^{A158C/I178C}$	*pilO* A158C, I178C	This study
$PilO^{Y154C/I178C}$	*pilO* Y154C, I178C	This study
$PilN^{R142C}$	*pilN* R142C	This study
$PilO^{Y154C}$	*pilO* Y154C	This study
$PilO^{A158C}$	*pilO* A158C	This study
$PilO^{V161C}$	*pilO* V161C	This study
$PilO^{S166C}$	*pilO* S166C	This study
$PilO^{D175C}$	*pilO* D175C	This study
$PilO^{I178C}$	*pilO* I178C	This study

PilN^{R142C}/PilO^{D175C} *ΔpilM*	*pilN* R142C & *pilO* D175C with deletion of *pilM*	This study
PilO$^{A158C/I178C}$ *ΔpilM*	*pilO* A158C, I178C with deletion of *pilM*	This study
PilO$^{Y154C/I178C}$ *ΔpilM*	*pilO* V154C, I178C with deletion of *pilM*	This study
PilN^{R142C}/PilO^{D175C} *pilA::FRT*	*pilN* R142C & *pilO* D175C with FRT insertion at SphI site within *pilA*	This study
PilO$^{A158C/I178C}$ *pilA::FRT*	*pilO* A158C, I178C with FRT insertion at SphI site within *pilA*	This study
PilO$^{Y154C/I178C}$ *pilA::FRT*	*pilO* Y154C, I178C with FRT insertion at SphI site within *pilA*	This study
PilN^{R142C}/PilO^{D175C} *pilB*Ω	*pilN* R142C & *pilO* D175C with Ω cassette insertion *pilB*	This study
PilO$^{A158C/I178C}$ *pilB*Ω	*pilO* A158C, I178C with Ω cassette insertion *pilB*	This study
PilO$^{Y154C/I178C}$ *pilB*Ω	*pilO* V154C, I178C with Ω cassette insertion *pilB*	This study
PilN^{R142C}/PilO^{D175C} *pilC::FRT*	*pilN* R142C & *pilO* D175C with FRT insertion at position 365 within *pilC*	This study
PilO$^{A158C/I178C}$ *pilC::FRT*	*pilO* A158C, I178C with FRT insertion at position 365 within *pilC*	This study
PilO$^{Y154C/I178C}$ *pilC::FRT*	*pilO* V154C, I178C with FRT insertion at position 365 within *pilC*	This study
PilN^{R142C}/PilO^{D175C} *pilP::FRT*	*pilN* R142C & *pilO* D175C with FRT insertion at position 86 within *pilP*	This study
PilO$^{A158C/I178C}$ *pilP::FRT*	*pilO* A158C, I178C with FRT insertion at position 86 within *pilP*	This study
PilO$^{Y154C/I178C}$ *pilP::FRT*	*pilO* V154C, I178C with FRT insertion at position 86 within *pilP*	This study
PilN^{R142C}/PilO^{D175C} *pilQ::FRT*	*pilN* R142C & *pilO* D175C with FRT insertion at position 571 within *pilQ*	This study
PilN^{R142C}/PilO^{D175C} *pilT::FRT*	*pilN* R142C & *pilO* D175C with FRT insertion at position 540 within *pilT*	This study
PilO$^{A158C/I178C}$ *pilT::FRT*	*pilO* A158C, D178C with FRT insertion at position 540 within *pilT*	This study
PilO$^{Y154C/I178C}$ *pilT::FRT*	*pilO* V154C, D178C with FRT insertion at position 540 within *pilT*	This study
PilN^{R142C}/PilO^{D175C} *ΔpilU*	*pilN* R142C & *pilO* D175C with deletion of *pilU*	This study
PilO$^{A158C/I178C}$ *ΔpilU*	*pilO* A158C, I178C with deletion of *pilU*	This study
PilO$^{Y154C/I178C}$ *ΔpilU*	*pilO* Y154C, I178C with deletion of *pilU*	This study

Table 3.2: Oligonucleotide Primer Sequences

Primer Name	Oligonucleotide Sequence (5' – 3')
PilA Fwd	TATATAACTCTAGAGATGAAAGCTCAAAAAGGCTTT
PilA Rev	TATTATAAGAATTCGTTACTTAGAGCAACC
PilB Fwd	TATATAACTCTAGAGATGAACGACAGCAT
PilB Rev	TATTATAAGAATTCGTTAATCCTTGGTCAC
PilC Fwd	TATATAACTCTAGAGATGGCGGACAAAGCGTTAAAAACCAG
PilC Rev	TATATATGGAATTCGTTATCCGACGACGTTGCCGAG
PilM Fwd	TATATATATCTAGAGGTGCTAGGGCTCATAAAGAAGAAAG
PilM Rev	TATTATAAGAATTCGTCAGTCGAAACTCCTCAACGCC
PilN Fwd	TATATAACTCTAGAGATGGCACGGATCAACCTTCTACCCTGG
PilN Rev	TATATATGGAATTCGTCATTTCTTGGCTCCTTGCGCAACCCC
PilO Fwd	TATATATATCTAGAGATGAGTCTGGCCAGTTCCCTG
PilO Rev	TATATATAGAATTCGTCATTTCTTCAGCCCCTTGTCG
PilP Fwd	TATATATGGAATTCGATGAGAGCCCGC
PilP Rev	TATATATAGAATTCGTCAGGAGCGTTCCTTGAGAGTC
PilT Fwd	TATATAACTCTAGAGATGGATATTACCGAGCTG
PilT Rev	TATATATAGAATTCGTCAGAAGTTTTCCGG
PilU Fwd	TATATAACTCTAGAGATGGAATTCGAAAAGCTG
PilU Rev	TATATATAGAATTCGTCAGCGGAAGCGCCG
PilN E132C Fwd	CGCCGGCGCGGCCTGCTCCAACAACCGCG
PilN E132C Rev	CGCGGTTGTTGGAGCAGGCCGCGCCGGCG
PilN R142C Fwd	CGTTTCCAATCTCATGTGCAACATGGACGCGTC
PilN R142C Rev	GACGCGTCCATGTTGCACATGAGATTGGAAACG
PilN E157C Fwd	GCCCCGACCCTGAACTGCGTCAAGGCGGTGACC
PilN E157C Rev	GGTCACCGCCTTGACGCAGTTCAGGGTCGGGGC
PilO Y154C Fwd	GTGGTCGGCGGCTGCCACGACTTGG

PilO Y154C Rev	CCAAGTCGTGGCAGCCGCCGACCAC
PilO A158C Fwd	GGCTACCACGACTTGTGCACCTTCGTCAGCGGC
PilO A158C Rev	GCCGCTGACGAAGGTGCACAAGTCGTGGTAGCC
PilO V161C Fwd	GACTTGGCGACCTTCTGCAGCGGCGTGTCCAG
PilO V161C Rev	CTGGACACGCCGCTGCAGAAGGTCGCCAAGTC
PilO S166C Fwd	GCGGCGTGTCCTGCCTGCCGCGG
PilO S166C Rev	CCGCGGCAGGCAGGACACGCCGC
PilO D175C Fwd	GGATCGTCACCCTGCATTGCTTCGAGATCAAGCCGG
PilO D175C Rev	CCGGCTTGATCTCGAAGCAATGCAGGGTGACGATCC
PilO I178C Fwd	CTGCATGACTTCGAGTGCAAGCCGGTCGCGCC
PilO I178C Rev	GGCGCGACCGGCTTGCACTCGAAGTCATGCAG

Acknowledgements

This work was supported by an Operating Grant MOP-93585 from *the Canadian Institutes of Health Research* to L.L.B and P.L.H. P.L.H. is the recipient of a Tier I Canada Research Chair.

Conflict of Interest

The authors declare no conflict of interest.

CHAPTER FOUR

Analysis of *Pseudomonas aeruginosa* PilO based on a new high-resolution structure: conserved unstructured regions are important for type IV pilus function

Preface

Chapter 4 consists of the following manuscript for submission:

Leighton TL, Mok MC, Junop MS, Howell PL, and Burrows LL. 2016. Analysis of *Pseudomonas aeruginosa* PilO based on a new high-resolution structure: conserved, unstructured regions are important for type IV pilus function

Attributions: TLL cloned, expressed, purified and crystallized the proteins. MCM and MSJ collected diffraction data and solved the structure. Constructs for site-directed mutagenesis were designed, cloned and mated by TLL. TLL performed all the Western blots, twitching motility and pilin preparation assays. TLL and LLB designed the experiments. The manuscript was prepared by TLL, PLH and LLB.

Title page and author list

Analysis of *Pseudomonas aeruginosa* PilO based on a new high-resolution structure: conserved, unstructured regions are important for type IV pilus function

Leighton TL[1], Mok MC[1,2], Junop MS[2], Howell PL[3,4] and Burrows LL[1]*

[1] Department of Biochemistry and Biomedical Sciences and the Michael G. DeGroote Institute for Infectious Disease Research, McMaster University, ON.
[2]Department of Biochemistry, University of Western Ontario, ON, CANADA.
[3]Program in Molecular Structure & Function, The Hospital for Sick Children, ON.
[4]Department of Biochemistry, University of Toronto, ON, CANADA.

*To whom correspondence should be addressed:
Dr. Lori L. Burrows, 4H18 Health Sciences Centre, 1200 Main St. West, Hamilton, ON, L8N 3Z5 CANADA, Tel: (905)-525-9140 ext: 22029, Fax: (905) 522-9033, E-mail: burrowl@mcmaster.ca
Dr. P. Lynne Howell, 20-9-715 Peter Giligan Centre for Research and Learning, 686 Bay St., Toronto, ON M5G 0A4 CANADA, Tel: (416) 813-5378, Fax: (416) 813-5022, E-mail: howell@sickkids.ca

Running Title: PilO structure and mutational analysis

Abstract

Pseudomonas aeruginosa is a Gram-negative, opportunistic pathogen that uses long, thin fibres called type IV pili (T4P) for adherence to surfaces, biofilm formation, and twitching motility. A conserved subcomplex of PilMNOP is required for extension and retraction of the pilus fibres from the cell. To better understand the interactions within this subcomplex, we attempted to co-crystallize a stable complex of the soluble periplasmic portions of PilNOP, using reductive surface methylation to promote crystal formation. A single protein, $PilO_{\Delta 109}$, was crystallized and the structure determined to 1.7 Å resolution using molecular replacement. This new higher resolution structure revealed two novel features: a shorter N-terminal α1-helix followed by a longer unstructured loop, and a discontinuous β-strand in the second $\alpha\beta\beta$ motif, matching that in the first motif. PISA software identified a potential dimer interface that was very different from the previous structure, but had striking similarity to the PilO homolog from the type II secretion system of *Vibrio cholerae*, EpsM. Using bioinformatics, we identified highly conserved residues within largely unstructured regions in PilO proteins from various Pseudomonads and performed site-directed mutagenesis to assess their role in T4P function. Substitution of R169D and I170A, both located within a loop region of PilO, decreased the amount of surface piliation and twitching motility. These residues could be important protein-protein interactions with PilN or PilP, as perturbation of these interfaces have negative impacts on function of the system.

Keywords: Type IV pili, type II secretion, reductive methylation, site directed mutagenesis

Introduction

Type IV pili (T4P) are long, thin (5-8nm diameter) hair-like appendages which extend from the bacterial surface and promote attachment, cell-cell aggregation, biofilm formation, and twitching motility (2-5,10,14). T4P are produced by a wide variety of bacteria and archaea, including the opportunistic pathogen, *Pseudomonas aeruginosa*. This bacterium, which is also notorious for its resistance to several classes of antibiotics, infects immunocompromised individuals such as those with severe burns, cystic fibrosis, or acquired immune deficiency syndrome (AIDS) (8). Bacteria lacking T4P are impaired in host colonization and thus less infectious (7,9). Twitching motility is a form of flagellar-independent movement, caused by repeated rounds of T4P extension, adhesion, and retraction, moving the bacteria towards the point of attachment (14,30).

The T4aP (henceforth known as T4P) system in *P. aeruginosa* is composed of four subcomplexes which together form a transenvelope network that spans the inner and outer membranes (4). The outer membrane (OM) secretin is composed of an oligomer of 14 PilQ monomers and their pilotin protein, PilF, forming a gated pore through which the pilus extends (Koo *et al.*, in press)(46). The inner membrane (IM) motor subcomplex is composed of a platform protein PilC (49), and three associated cytoplasmic ATPases, PilBTU

(48). The secretin and motor subcomplexes are linked by the alignment subcomplex, PilMNOP. These proteins form a complex network of protein-protein interactions from the cytoplasm to the periplasm and connect with the PilQ secretin, potentially controlling secretin gating (54,55,178). The final subcomplex is the pilus fibre itself, composed primarily of PilA monomers, but also minor pilins (PilVWXE/FimU) and PilY1 (5,56,58,81), which together form a long, helical fibre which extends from the cell (5,13,56,183). Together with several regulatory proteins whose functions are not well understood (41,75,143,144), these subcomplexes form a fully functional T4P system.

Four proteins make up the highly conserved alignment subcomplex (5,184), which connects the inner and outer membrane components of the T4P system, and is critical for its function. Located in the cytoplasm, PilM has an actin-like fold and is structurally similar to the bacterial cytoskeletal protein, FtsA (23,111,114). In *P. aeruginosa* the crystal structure of a PilM-PilN$_{1\text{-}12}$ chimera was determined by X-ray crystallography and revealed a binding pocket on PilM which interacts with a highly-conserved motif in in the N-terminus of PilN (51,111,114), similar to observations in *Thermus thermophilus* (114). Interestingly the interaction between PilM and PilN might be able to modulate which ATPase is able to interact with the platform protein (111), and although no structure for PilN from *P. aeruginosa* exists, it is predicted to look similar to PilO. A crystal structure of an N-terminally truncated (Δ68) version of a PilO homodimer was previously determined (PDB 2RJZ (51)), and the dimer interface shown to be physiologically

relevant (185). PilN and PilO are also capable of heterodimerization (50,51,55,178), and predicted to have similar topologies; a short cytoplasmic N terminus preceding a single transmembrane segment (TMS), followed by a periplasmic segment consisting of a coiled-coiled domain connected by a loop to a folded core domain composed of two ferredoxin-like αββ motifs (51). Although both homo- and heterodimers of PilN and PilO were identified *in vivo* (185), the IM-associated lipoprotein PilP binds only the PilNO heterodimer through its long N-terminal region and is unable to interact with PilO homodimers *in vitro* (55). The C-terminal β-domain of PilP interacts with the secretin monomer PilQ via its N0 domain, based on co-purification experiments (54). This complex network of protein-protein interactions allows the alignment subcomplex to form a continuous network through the periplasmic space, best demonstrated by a nearly complete model of the T4P system in *Myxococcus xanthus* (71). Through these interactions the alignment subcomplex ensures the correct alignment of the cytoplasmic motor components and OM secretin for efficient cycles of pilus extension and retraction.

To better visualize the physical interactions between the alignment subcomplex components, we took a structural approach. Previously, we showed that N-terminal truncations of PilNOP allowed for the isolation of soluble fragments that formed a stable heterotrimeric complex *in vitro*, which co-eluted in size exclusion chromatography experiments (55). During a series of systematic attempts to crystallize this stable heterotrimer, we used reductive methylation to

decrease the surface entropy with the goal of promoting crystal formation (186). The resulting crystals diffracted well but contained only one member of this subcomplex. We solved the structure of a $PilO_{\Delta 109}$ monomer using our previous $PilO_{\Delta 68}$ structure (PDB 2RJZ) as a template for molecular replacement (51). Our new PilO structure was of higher resolution and revealed novel structural features including a more unstructured N terminal α1-helix and a second discontinuous β-strand motif. We identified highly conserved residues that mapped to largely unstructured regions on the PilO structure, and investigated their roles in T4P function through site direction mutagenesis. We identified two residues that cause T4P dysfunction resulting in reduced piliation and motility, likely by disruption of PilO interactions with itself or other partners in the T4P system. This work furthers our understanding of residues critical for T4P function, and gives new insight into interfaces that can be targeted for novel therapeutics.

Experimental procedures

Strains, media and growth conditions.

Bacterial strains, and plasmids, as well as primers used in this study are listed in Supplementary Table S4.1 and S4.2 respectively. E*. coli* and *P. aeruginosa* were grown at 37 °C in Luria-Bertani (LB) media supplemented with antibiotics at the following final concentrations when necessary (μg/mL): ampicillin (Ap), 100; kanamycin (Kn), 50; gentamicin (Gm), 15 for *E. coli* and 30 for *P. aeruginosa*, unless otherwise specified. Plasmids were transformed by heat

shock into chemically competent cells. All constructs were verified by DNA sequencing (MOBIX – McMaster University).

Expression and purification of $PilN_{\Delta 44}/PilO_{\Delta 51}/PilP_{\Delta 18}$

N-terminally truncated versions of PilN and PilO were previously cloned into the EcoRI/HindIII and NdeI/XhoI cloning sites, respectively, of a pET28a vector, creating untagged but co-expressed $PilN_{\Delta 44}/PilO_{\Delta 51}$ (51,55). TOPO cloning was used to introduce an N-terminally truncated form of PilP into a pET151 vector (Invitrogen), creating a $PilP_{\Delta 18}$ construct with an N-terminal 6-His tag ($PilP_{\Delta 18\_His}$). Based on previous optimization studies, we expressed the PilNO and PilP fragments separately, combining the bacterial pellets at the purification stage. Briefly, the constructs were transformed separately into *E. c*oli BL21 cells and plated on LB agar plates supplemented with either Km (for the pET28a vector) or Ap (for the pET151 vector). A single colony of each transformant was used to inoculate separate 20 mL aliquots of LB containing appropriate antibiotics, and incubated overnight at 37 °C, shaking at 200 rpm. Each overnight culture was used to inoculate 1 L of fresh LB (1:100 dilution) containing antibiotic and the cells were grown at 37 °C, with shaking, to an OD_{600} of approximately 0.6. Protein expression was induced by adding IPTG (isopropyl β-D-1 thiogalactopyranoside, Sigma Aldrich) to the cultures at a final concentration of 1 mM. The cells were incubated for 4 h at 37 °C, prior to being harvested by centrifugation (3,993 x *g*, 15 min, 4 °C) in an Avanti J-26 XPI centrifuge (Beckman Coulter). Bacterial pellets were frozen at -80 °C until further use.

Bacterial pellets were thawed, each resuspended in 10 mL Nickel A buffer (20 mM HEPES pH 7.5, 500 mM KCl, 10 mM imidazole, 10% (v/v) glycerol), then both pellets ($PilN_{\Delta 44}$/$PilO_{\Delta 51}$ and $PilP_{\Delta 18\_His}$) were combined into a single 50 mL screw cap tube with 1 complete EDTA-free protease inhibitor tablet (Roche). Cells were lysed via sonication on ice, on setting 4, for 2 min with cycles of 10 s on and 10 s off (Sonicator 3000; Misonix). The lysates were centrifuged (11,000 x *g*, 30 min, 4 ^{o}C) in an Avanti J-26 XPI centrifuge (Beckman Coulter) to remove intact cells and other cellular debris. Pelleted material was retained for analysis by SDS-PAGE, while supernatants were filtered through 0.22 µm Acrodisc syringe filter (Pall Corporation). The lysate was purified using Nickel-NTA affinity chromatography on an AKTA start FPLC (VWR). Protein lysate was flowed through a 1 mL His-Trap^{TM} FF column (GE Healthcare) pre-equilibrated with buffer, and washed with Nickel A buffer, then increasing amounts of Nickel B buffer (20 mM HEPES pH 7.5, 500 mM KCl, 300 mM imidizole, 10% (v/v) glycerol) in a linear gradient. The bound protein was eluted from the column in pure Nickel B buffer and collected in 1 mL fractions. An aliquot of each fraction was mixed 1:1 with 2X reducing or non-reducing SDS-PAGE loading and electrophoresed on a 15% SDS-PA gel. The gel was stained using Coomassie Blue Staining solution (0.1% (w/v) Coomassie Brilliant Blue R-250, 50% (v/v) methanol and 10% (v/v) glacial acetic acid), or developed by Western blot using protein-specific antisera as described below. His-tagged $PilP_{\Delta 18}$ was successfully able to pull out untagged $PilN_{\Delta 44}$ and $PilO_{\Delta 51}$ as previously described (55).

TEV Digestion

The $PilN_{\Delta 44}/PilO_{\Delta 51}/PilP_{\Delta 18\_His}$ protein complex elution fraction, plus 500 µL of 1 mg/mL of Tobacco Etch Virus (TEV) protease were added to a 12-30 mL Slide-A-Lyzer Dialysis Cassettes 10K MWCO (Thermo Scientific). The cassette and its contents were dialyzed into a new buffer (20 mM HEPES pH 7.5, 120 mM NaCl) overnight at 4°C, stirring. The sample was extracted from the cassette and run through a 1 mL His-Trap™ FF column (GE Healthcare) pre-equilibrated with the dialysis buffer to separate $PilN_{\Delta 44}/PilO_{\Delta 51}/PilP_{\Delta 18}$ complex from His-tag. Flow through from the column was collected and the protein complex was concentrated down using a Vivaspin-20 10 kDa centrifugal concentrator (GE Healthcare) in an Allegra X-14 (Beckman Coulter) benchtop centrifuge (3,000 x *g*, 30 min, 4 °C) to concentrate the protein complex. A Bradford assay was used to measure the final protein concentration of the complex at approximately 10 mg/mL.

Reductive Methylation

Modification of surface-exposed lysine residues on the $PilN_{\Delta 44}/PilO_{\Delta 51}/PilP_{\Delta 18}$ complex was carried out using the Hampton Research Reductive Alkylation kit protocol following manufacturer's instructions (Hampton Research). Briefly, 20 µL of 1 M dimethylamine borane complex (ABC) was added to 1 mL of 10 mg/mL protein, and inverted to mix. Then 40 µL of 1M formaldehyde was added to the tube, and incubated for 2 h at 4 °C rocking. After the 2 h incubation, another 20 µL of ABC was added to the tube followed by

another 40 µL of 1M formaldehyde. The tube was incubated again at 4 ^{o}C for 2 h. Finally 10 µL of ABC was added to the tube and the reaction incubated overnight at 4 ^{o}C with rocking. The reaction was stopped with the addition of 125 µL of 1 M glycine, and incubated for 2 h, rocking at 4 ^{o}C. The methylated protein complex was then separated from the reaction products through size exclusion chromatography.

Size exclusion chromatography of the PilN$_{\Delta 44}$/PilO$_{\Delta 51}$/PilP$_{\Delta 18}$ subcomplex

Analytical gel filtration of the methylated PilN$_{\Delta 44}$/PilO$_{\Delta 51}$/PilP$_{\Delta 18}$ protein complex was performed using an AKTA FPLC (GE Healthcare) equipped with a Superdex S75 10/300 GL (GE Healthcare) column. The column was pre-equilibrated with a 20 mM HEPES pH 7.5 and 120 mM NaCl buffer prior to injection of the protein sample. Typically, 500 µL of a 10 mg/mL protein solution was loaded onto the column. Gel filtrations were run at a flow rate of 0.6 mL/min onto the S75 column at 4 ^{o}C, and fractions were collected in a 96-well plate format, with the absorbance at 280 nm monitored over the course of the experiment. The purest PilN$_{\Delta 44}$/PilO$_{\Delta 51}$/PilP$_{\Delta 18}$ protein fractions, as determined by SDS-PAGE and staining with Coomassie blue (Supplementary Figure S3.1), were pooled and concentrated down using a Vivaspin 2 (10 kDa) centrifugal concentrator (GE Healthcare) in an Allegra X-14 (Beckman Coulter) benchtop centrifuge (3,000 x *g*, 30 min, 4 °C).

Crystallization and structural determination

Native $PilN_{\Delta 44}/PilO_{\Delta 51}/PilP_{\Delta 18}$ crystals were grown using the hanging drop/vapour diffusion method in a 1:1 ratio of protein (12 mg/mL in 20 mM HEPES pH 7.5 and 120 mM NaCl buffer) to precipitant (0.2 M NaCl, 0.1 M N-cyclohexyl-3-aminopropanesulfonic acid (CAPS) pH 10.5, 20% (v/v) polyethylene glycol (PEG) 8000) with the addition of 0.2 µL of 30% (v/v) dimethyl sulfoxide (DMSO)) over 1.5 M ammonium sulphate, and kept at 4 ^{o}C for approximately 6 months, with trays being checked each week for the first 2 months, then on a monthly basis. Data was collected at wavelength 0.979 Å on the 08ID-1 beamline at the Canadian Light Source (CLS) in Saskatchewan, Canada.

The HKL2000 program suite (187) was used to process the data which exhibited the symmetry of the hexagonal space group $P6_122$. The structure of PilO was determined by molecular replacement with Phaser from the CCP4 software package (188) using a truncated model of $PilO_{\Delta 68}$ (PDB 2RJZ (51)) as a template. At this point it became clear that only one protein (PilO) was present in the crystal. The protein could be modelled from residue 110 to the C terminus ($PilO_{\Delta 109}$). The data collection and model refinement statistics are presented in Table 4.1. Root-mean-square deviation (r.m.s.d) values between the superimposed structures, and graphical presentation were both performed in PyMOL (v 1.8; Schrodinger).

Mass Spectrometry of the $PilN_{\Delta 44}/PilO_{\Delta 51}/PilP_{\Delta 18}$ complex

Methylated and unmethylated samples of 1 mg/mL$PilN_{\Delta 44}/PilO_{\Delta 51}/PilP_{\Delta 18}$ in a 20 mM HEPES pH 7.5 and 120 mM NaCl buffer were sent to the Biointerfaces Institute (McMaster University) for analysis. Briefly, the sample was mixed in a 1:1 ratio with a saturated solution of sinapinic acid prepared in a 30:70 (v/v) Acetonitrile:TFA 0.1% in water. One µL of the samples was spotted on a MALDI pad and subject to matrix-assisted laser desorption/ionization time-of-flight/time-of-flight (MALDI-TOF/TOF) on a Bruker UltrafleXtreme linear detector in positive ion mode to determine the mass to charge ratio of the proteins.

For the analysis of the crystals by mass spectrometry, 2 crystals were washed in the initial buffer (20 mM HEPES pH 7.5 and 120 mM NaCl), then a 0.1% (v/v) acetonitrile solution. The crystals were dissolved in 15 µL of 20 mM HEPES pH 7.5 and 100 mM NaCl buffer and sent to the Biointerfaces Institute (McMaster University) for analysis.

PilO bioinformatics analysis

The *P. aeruginosa* PAK PilO sequence was retrieved from the *Pseudomonas* Genome Database (167) and was aligned using Jalview 2.8.2 (168,169) with a subset of Pseudomonads (*P. fluorescens*, *P. syringae* pv. phaseolicola 1448A, *P. savastanoi, P. syringae, P. protegens* CHA0*, P. avellanae, P. stutzeri* A1501*, P. resinovorans, P. chlororaphis*). The mapped secondary structure elements are based on the new $PilO_{\Delta 109}$ structure described herein.

Generation of PilO mutants

Sites for the introduction of single or double point mutations in PilO were chosen with reference to the new $PilO_{\Delta 109}$ structure (below). To maintain native stoichiometry and expression levels, mutations of interest were introduced onto the *P. aeruginosa* chromosome at the native *pilO* locus. First, codons for PilO residue substitutions were introduced into a pEX18Gm::*pilNOP* construct using the QuikChange Site-Directed Mutagenesis Kit (Stratagene) following the manufacturer's protocol with primers listed in Supplementary Table S4.2. Genes and mutations were sequenced (MOBIX) to verify their identity.

Next, *pilO* mutants were constructed using a Flp-FRT (FLP recombination target) system as previously described (147). Briefly, the suicide vectors containing the mutant *pilO* gene plus the flanking genes (*pilN* and *pilP*) to provide homologous regions for recombination were introduced into *E. coli* SM10 cells. The constructs were transferred by conjugation in a 1:9 ratio of *P. aeruginosa* to *E. coli*. The mixed culture was pelleted for 3 min at 2292 x *g* in a microcentrifuge, and the pellet was resuspended in 50 µL of LB, spot-plated on LB agar, and incubated overnight at 37 °C. A *P. aeruginosa* PAK strain which contained a *pilO::FRT* mutation (50) was used as a recipient for the pEX18Gm::*pilNOP* constructs in mating experiments. After mating, cells were scraped from the LB agar plate, resuspended in 1 mL of LB and the *E. coli* SM10 donor was counterselected by plating on *Pseudomonas* isolation agar (PIA; Difco) containing Gm (100 µg/mL). Gm-resistant *P. aeruginosa* isolates were streaked

on LB no salt plates with sucrose (1% (w/v) bacto-tryptone, 0.5% (w/v) bacto-yeast extract, 5% (w/v) sucrose) then incubated for 16 h at 30°C. Select colonies were cultured in parallel on LB and LB plates supplemented with Gm. Gm-sensitive colonies were screened by PCR using *pilO* primers to confirm replacement of the FRT-disrupted gene, and PCR products of the expected size were sequenced to confirm incorporation of the desired mutations.

Twitching motility assays

Twitching assays were performed as previously described (149). Briefly, single colonies were stab inoculated to the bottom of a 1% LB agar plate. The plates were incubated for 36 h at 37 °C. Post incubation, the agar was carefully removed and the adherent bacteria stained with 1% (w/v) crystal violet dye, followed by washing with tap water to remove unbound dye. Areas of the twitching zones were measured using ImageJ software (NIH). All experiments were performed in triplicate with at least three independent replicates.

Sheared surface protein preparation

Surface pili and flagella were analyzed as described previously (149). Briefly, the strains of interest were streaked in a grid-like pattern on LB agar plates and incubated at 37 °C for ~16 h. The cells were scraped from the plates with glass coverslips and resuspended in 4.5 mL of PBS. Surface proteins were sheared by vortexing the cell suspensions for 30 s. Cells were transferred to three separate 1.5 mL Eppendorf tubes and pelleted by centrifugation at 11,688 x *g* for 5 min. Supernatant was transferred to fresh tubes and centrifuged at 11,688

x *g* for 20 min to remove remaining cells. Supernatants were transferred to new tubes and surface proteins were precipitated by adding 1/10 volume of 5M NaCl and 30% (w/v) polyethylene glycol (PEG 8000, Sigma Aldrich) to each tube and incubating on ice for 90 min. Precipitated proteins were collected by centrifugation at 11,688 x *g*, resuspended in 150 µL of 1X SDS sample buffer (125mM Tris, pH 6.8, 2% β-mercaptoethanol, 20% glycerol, 4% SDS and 0.001% bromophenol blue). Samples were boiled for 10 min and separated on 15% SDS-PAGE gels. Proteins were visualized by staining with Coomassie brilliant blue.

Preparation of whole cell lysates

P. aeruginosa strains were grown on LB agar plates overnight at 37 °C. Cells were scraped from the surface and resuspended in 1X PBS to an OD_{600} of 0.6. A 1 mL aliquot of cells was collected by centrifugation at 2292 x *g* for 3 min in a microcentrifuge. The cell pellet was resuspended in 100 µL of 1X SDS sample buffer and boiled for 10 min. Whole cell lysate samples were separated on 15% SDS-PAGE gels and subject to Western blot analysis.

Western blot analysis

Whole cell lysate samples were separated on 15% SDS-PAGE gels and transferred to nitrocellulose membranes for 1 h at 225 mA. Membranes were blocked using a 5% (w/v) low fat skim milk powder in 1x PBS for 1 h at room temperature on a shaking platform, followed by incubation with the appropriate antisera for 2 h at room temperature, at a dilutions as follows: PilM 1/2500, and PilNOP 1/1000 each. The membranes were washed twice in 1x PBS for 5 min

then incubated in goat-anti-rabbit IgG-alkaline phosphatase conjugated secondary antibody (Bio-Rad) at a dilution of 1/3000 for 1 h at room temperature. The membranes were washed twice in 1x PBS for 5 min, and visualized with alkaline phosphatase developing reagent (Bio-Rad) following the manufacturer's protocol.

Results

A new 1.7 Å crystal structure of $PilO_{\Delta 109}$ reveals novel secondary structure characteristics

To better understand how PilN and PilO interact with one another and with PilP, we attempted to solve the structure of a stable, soluble heterotrimeric complex of $PilN_{\Delta 44}$/$PilO_{\Delta 51}$/$PilP_{\Delta 18}$ which elutes as a single peak from a size exclusion chromatography column. Although the protein complex was soluble, stable at various temperatures over long periods of time, and abundant, crystallization attempts were initially unsuccessful. We explored the use of reductive methylation, thought to promote crystal formation through chemical modification of surface-exposed lysines thereby decreasing surface entropy, in an attempt to crystallize the proteins (186). All three proteins were confirmed to be present after reductive methylation as determined by SDS-PAGE and Coomassie staining (Supplementary Figure S4.1) and methylation of the proteins was confirmed by matrix-assisted laser desorption/ionization time-of-flight/time-of-flight (MALDI-TOF/TOF) at the Biointerfaces Institute (McMaster

University)(Supplementary Figure S4.2). A small array of hexagonal pyramid shaped crystals were grown (Supplementary Figure S4.1 - inset) and data were collected at the Canadian Light Source (CLS) and processed using HKL2000 (187). During the preliminary analysis, it became clear that only one of the three proteins (PilO) used to set the drops was present in the crystal. Although the construct used encompassed residues 52-208, we were only able to model residues 110-206. Analysis of the crystals using MALDI-TOF/TOF at the Biointerfaces Institute (McMaster University) confirmed that proteolysis had occurred during the crystallization process, and revealed various PilO fragments present with the largest peak corresponding to a PilO fragment with a molecular weight of 10,522 Da, similar to the predicted weight of 10,560 Da for a PilO 110-206 fragment (Supplementary Figure S4.3). Using our previous 2.2 Å $PilO_{\Delta 68}$ structure (PDB 2RJZ) (51) as a template, a 1.7 Å structure of $PilO_{\Delta 109}$ was solved by molecular replacement and refined to an R_{work}/R_{free} value of 21.0/25.1% (Table 4.1 and Figure 4.1).

Table 4.1. Data collection and refinement statistics for $PilO_{\Delta 109}$

Data Collection	
Beamline	CLS 08ID-1
Wavelength (Å)	0.979
Space group	$P6_122$
a, b, c (Å)	40.8, 40.8, 250.5
α, β, γ (°)	90, 90, 120
Resolution range (Å)	35.34-1.7 (1.79-1.7)
Total reflections	263281
Unique reflections	14759
Redundancy	6.7 (6.9)
Completeness (%)	99.9 (100)
Mean $I/\sigma(I)$	10.8 (2.9)
R_{merge} (%)	7.8 (54.2)
Anisotropic deltaB	11.52
Mosaicity (°)	0.54
Structure Refinement	
$R_{work/free}$ (%) *	21.0/25.1
R.m.s.d. Bond lengths (Å)	0.005
R.m.s.d. Bond angles (°)	0.769
Ramachandran plot ‡	
Total favoured (%)	98
Total allowed (%)	2
Coordinate error (Å) §	0.14
Wilson B factor	23.7
Average B-factors (Å^2) §	
Protein	40.58
Water	47.70
Atoms	
No. protein atoms	849
No. water	97

Note: Values in parentheses correspond to the highest resolution shell.
*, $R_{work} = \sum | |F_{obs}| - k|F_{calc}| | / |F_{obs}|$ where F_{obs} and F_{calc} are the observed and calculated structure factors, respectively. R_{free} is the sum extended over a subset of reflections (5%) excluded from all stages of the refinement.
‡, As calculated using MolProbity (189)
§, Maximum-likelihood based Coordinate Error and Average B-factors, as determined by PHENIX (190)

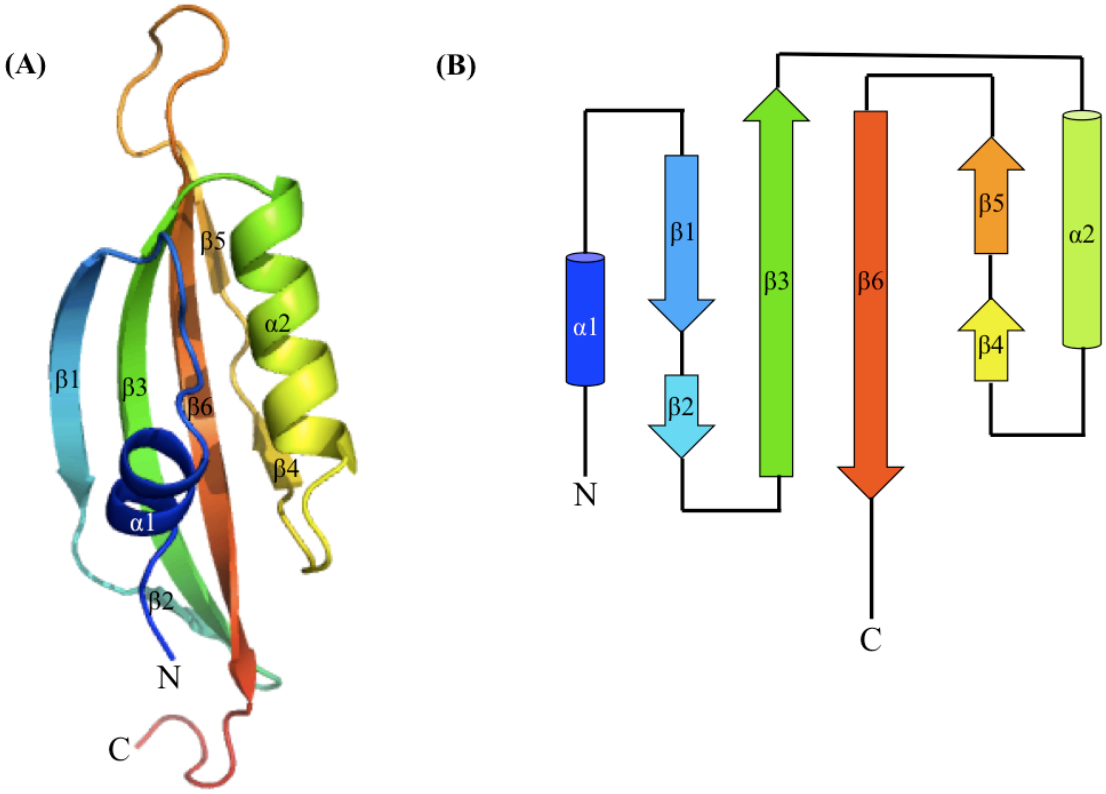

Figure 4.1. Structure and topology diagram of PilO$_{\Delta 109}$. (A) A cartoon representation mapping the N- and C-termini, and secondary structure elements of PilO$_{\Delta 109}$. **(B)** Topological diagram coloured according to rainbow colors from blue at the N-terminus to red at the C-terminus.

The new structure encompasses residues P110 to K206, 60% of the periplasmic region (just under 50% of the total protein). PilO$_{\Delta 109}$ contains two αββ motifs composed of α1-β1β2-β3 and α2-β4β5-β6, both of which have a discontinuous β-strand (β1β2 and β4β5) at the first β position in each of the motifs (Figure 4.1B). The αββ fold was first identified in EpsM from the type II secretion system (T2SS) of *Vibrio cholerae*, where it was considered to be a

simplified version of the ferredoxin fold (βαβ), and is typical of PilN and PilO homologues (51,116,126). The four β-strands form an antiparallel β-sheet on which the two α-helices pack. A pseudo 2-fold axis within the β-sheet relates the two compact αββ-subdomains with a r.m.s.d. value of 3.4 Å for 47 Cα atoms. Helices α1 and α2 are 8 and 13 residues in length, respectively, while β3 and β6 are 12 residues in length. Beta strands β1 and β2 are 8 and 3 residues in length, whereas β4 and β5 are 3 and 4 residues, respectively. The 2-residue linker between β1β2 includes P134 and E135, while the 2-residue linker between β4β5 contains D175 and F176; these residues are responsible for the observed strand discontinuity.

For comparison to the previous structure, we truncated the previous structure to include only residues 110-206 (known henceforth as $PilO^{2RJZ}_{\Delta 109}$), corresponding to the region defined in the new structure. The two structures were aligned using PyMOL with an r.m.s.d. of 1.2 Å over 97 Cα backbone atoms, highlighting their similarity (Figure 4.2A). When compared to the previous structure, the N-terminal α1-helix is more unstructured and tilted away from the β-sheet than observed in the $PilO^{2RJZ}_{\Delta 109}$ structure (Figure 4.2A – left). A second discontinuous β-strand (β4β5) not present in the $PilO^{2RJZ}_{\Delta 109}$ structure was identified in the new structure (Figure 4.2A – right). Examination of the hydrogen bonding between the β4β5- and β6-strands in the $PilO_{\Delta 109}$ structure using PyMOL revealed that main chain carbons of D175 and F176 do not participate, allowing for the formation of the discontinuous β-strand (Figure 4.2B). This unique feature

was not present in the previous PilO structure, as hydrogen bonding was complete through this segment (Figure 4.2C).

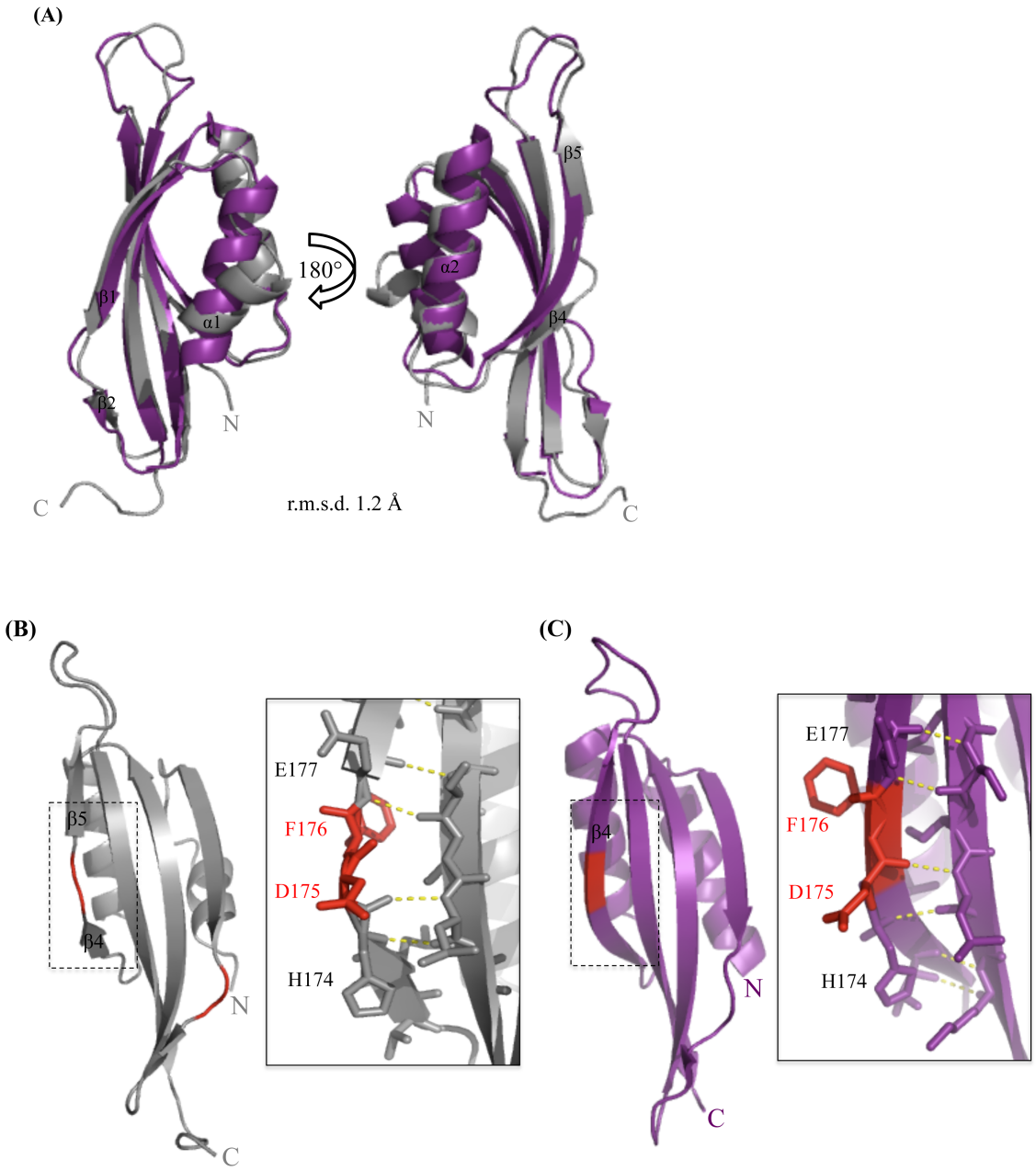

Figure 4.2. Comparison of the PilO structures. (A) Comparison of the $PilO_{\Delta 109}$ structure (grey) with the equivalent residues (110-206) of $PilO^{2RJZ}{}_{\Delta 109}$ (purple)

(PDB 2RJZ (51)). **(B)** Reverse view of the $PilO_{\Delta 109}$ structure (grey) highlighting the second discontinuous β4β5-strand (inset). **(C)** The equivalent region of the $PilO^{2RJZ}_{\Delta 109}$ structure (purple). Residues in red do not participating in hydrogen bonding (yellow dashed lines).

In the $PilO_{\Delta 109}$ structure, a dimethyl-Lys residue was located on the backside of the β6-strand. Prior to setting crystallization drops, the $PilN_{\Delta 44}/PilO_{\Delta 51}/PilP_{\Delta 18}$ complex was subject to reductive methylation and its complete modification confirmed by matrix-assisted laser desorption/ionization time-of-flight/time-of-flight (MALDI-TOF/TOF) at the Biointerfaces Institute (McMaster University) (Supplementary Figure S4.2). The $PilN_{\Delta 44}/PilO_{\Delta 51}/PilP_{\Delta 18}$ fragments each have 11 lysines residues able to be methylated. The difference in size for each protein after methylation (PilN 319 Da, PilO 313 Da, and PilP 324 Da) suggested the methylation of 10 lysine residues each (28 Da per lysine), plus an additional 28 Da for the N termini of each protein (Supplementary Figure S4.2). The high-resolution structure of $PilO_{\Delta 109}$ allowed for the visualization of a single Lys residue (K196), which was dimethylated (Figure 4.4B). The remaining lysine residues in the $PilO_{\Delta 109}$ fragment, K131, K179, K188, K203, and K206, were unable to be modelled in the structure due to missing electron density. Although we could not confirm whether any of these residues with dimethylated, the mass spectrometry results suggested that these residues likely were dimethylated.

The predicted dimer interface for PilO$_{\Delta 109}$ is more similar to the EspM from V. cholera, *than the previous PilO structure*

One molecule of PilO was found in the asymmetric unit. Using PISA software (191), two possible interaction interfaces with crystallographic symmetry mates were identified (Supplementary Figure S4.4). These interfaces bury 1,180 Å and 1,140 Å^2, respectively, compared with a total surface area of approximately 11,500 Å^2. The dimer with the largest buried surface area, considered to be more energetically favourable (-12 kcal/mol), was analyzed further (Figure 4.3A). The interface between the core domains of PilO$^{2RJZ}_{\Delta 109}$ was formed through interactions between the α2-helix of monomer 1 and the β4-strand of monomer 2 (Figure 4.3B)(51). These contacts are similar to the new structure of PilO$_{\Delta 109,}$ where the α2-helix and β4β5-strands are the main points of contact in the predicted dimerization interface. However due to the orientation of the individual monomers, the α2-helix of monomer 1 would interact with the α2-helix of monomer 2, and the same goes for the interaction of the broken β4β5 strand of each monomer. The monomer orientation in PilO$_{\Delta 109}$ places the β-sheets on the same side, forming a larger 8 stranded anti-parallel β-sheet (Figure 4.3A). This is in contrast to the PilO$^{2RJZ}_{\Delta 109}$ dimer where the β-sheets (and the α-helices) are on opposite sides (Figure 4.3B). The PilO$_{\Delta 109}$ interface resembles that reported for the 1.7 Å resolution structure of its T2SS homologue EpsM$_{\Delta 65}$ from *V. cholerae*, with the monomers arranged in the same antiparallel orientation (Figure 4.3C)(PDB 1UV7 (126)). EpsM$_{\Delta 65}$ has dimerization contacts between the α2-

helices of each monomer and between the β3-strands, equivalent to β4β5 in the $PilO_{\Delta 109}$ structure (Figure 4.3A) (126). This organization orients the N- and C-termini of the individual $PilO_{\Delta 109}$ and $EpsM_{\Delta 65}$ monomers in opposite directions, compared to the $PilO^{2RJZ}{}_{\Delta 109}$ structure where the N- and C-termini are oriented in the same direction (Figure 4.3B).

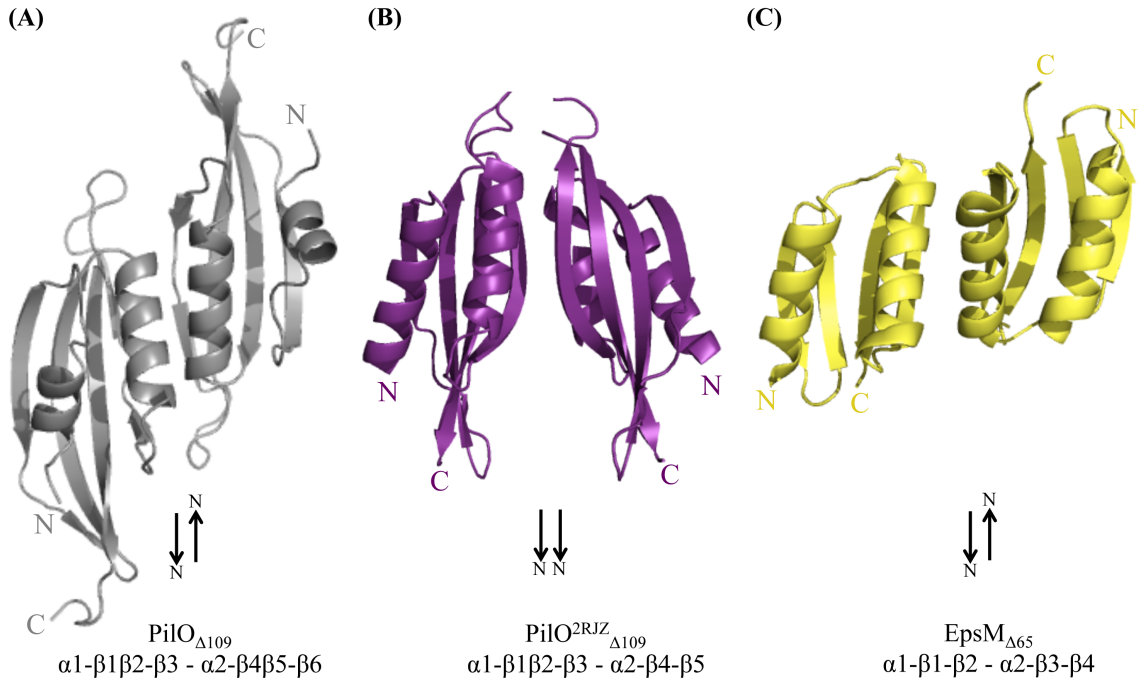

Figure 4.3. The predicted dimeric interface of the $PilO_{\Delta 109}$ structure is more similar to EpsM from *V. cholera*, than the previous PilO structure. (A) The most energetically favourable predicted interaction interface for the $PilO_{\Delta 109}$ structure (grey). **(B)** The dimer interface found in the $PilO^{2RJZ}{}_{\Delta 109}$ dimer (purple) (PDB 2RJZ (51)). **(C)** The $EpsM_{\Delta 65}$ crystal structure (yellow) from the T2SS of *V. cholera* (PDB 1UV7 (126)). Black arrows indicate direction of the N termini for each subunit.

Two highly conserved hydrophobic areas correspond to unstructured loop regions

The alignment subcomplex is highly conserved throughout Pseudomonads and other T4aP expressing bacteria (2). Alignment of *P. aeruginosa* PilO with homologues from various Pseudomonads revealed a number of notable features (Figure 4.4A). N-terminal residues (1-99) share a relatively low overall sequence conservation, whereas the core domain, consisting of the two αββ motifs, showed a much higher degree of sequence conservation, especially in regions of defined secondary structure as determined by our structure. The regions corresponding to the α-helices (α1 and α2) are highly conserved, as are the residues immediately following the α1-helix (109-116). These are formerly part of the longer α1-helix, but in our new $PilO_{\Delta 109}$ model are unstructured (Figure 4.1B). The β-strands are also relatively conserved, but interestingly there is a high degree of conservation in two largely hydrophobic regions, which correspond to the unstructured areas surrounding the discontinuous β2β3- and β4β5-strands.

Region 1 is defined as residues L132, L133, F140, Y141, and includes the two “β-strand breaker” residues P134 and E135 (Figure 4.4AB - left). Region 2, on the opposite side of the $PilO_{\Delta 109}$ model from Region 1, consists of residues L167, P168, R169, I170, V171, T172, L173, H174, and the “β-strand breaker” residues D175 and F176 (Figure 4.4B - right). Interestingly, the LPRIVTL residues (167-173) were previously identified as being the most highly conserved segment in PilO (51). Unstructured regions of proteins can often undergo

conformational changes to a more ordered state (folding into stable secondary or tertiary structures) upon interaction with their target substrates – including other proteins (192). With this information, we hypothesized that these highly conserved residues found in largely unstructured regions could play a potential role in protein-protein interactions with PilN and/or PilP. Each of the residues in this region (individually or in pairs)(Table 4.2) was successfully mutated with the exceptions of V171A and F176A, and those residues were not further analyzed.

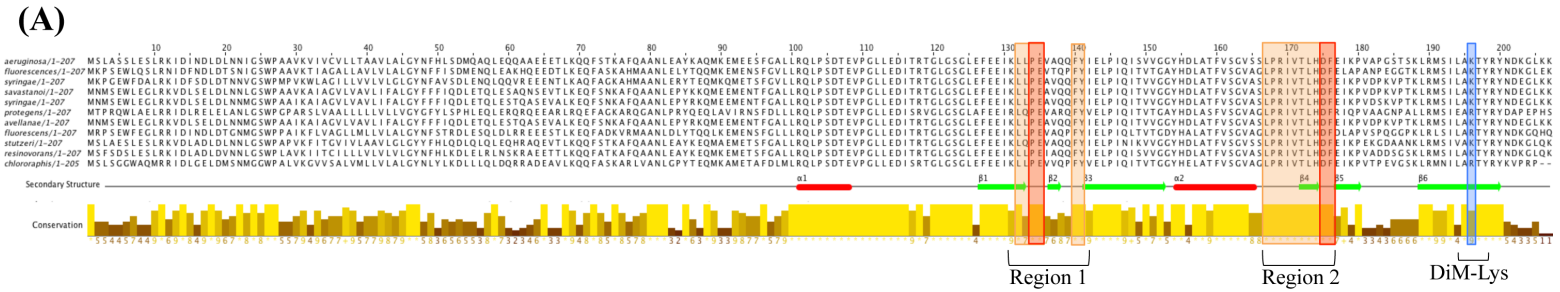
(A)
Secondary Structure
Conservation
Region 1
Region 2
DiM-Lys

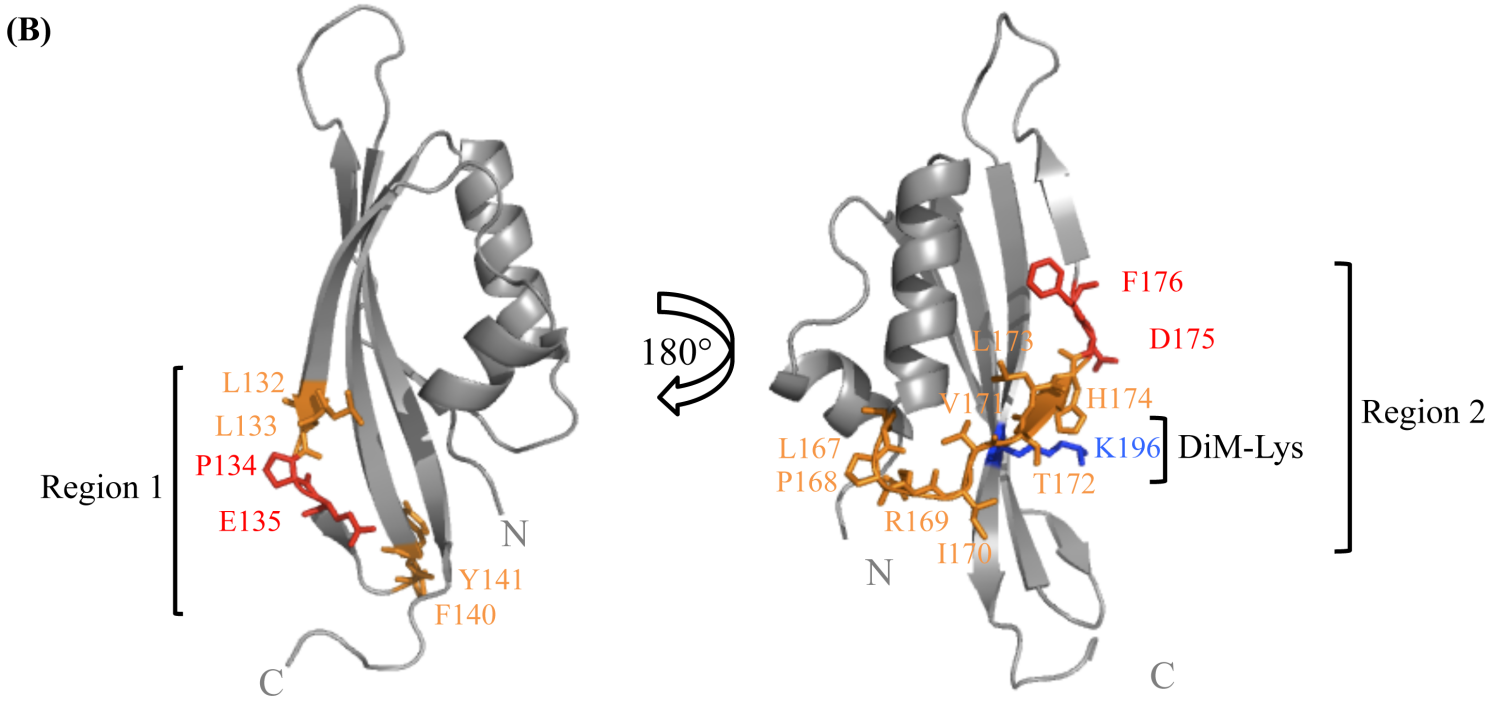
(B)
Region 1
L132
L133
P134
E135
Y141
F140
N
C
180°
F176
D175
L173
V171
H174
K196
DiM-Lys
L167
P168
T172
R169
I170
N
C
Region 2

Figure 4.4. Highly conserved residues in unstructured regions on the $PilO_{\Delta 109}$ structure chosen for site directed mutagenesis. (A) The sequence conservation of the PilO families from a subset of Pseudomonads (*P. fluorescens*, *P. syringae pv. phaseolicola* 1448A, *P. savastanoi, P. syringae, P. protegens* CHA0*, P. avellanae, P. stutzeri* A1501*, P. resinovorans, P. chlororaphis*) are indicated by the bars. The conservation of the residues is indicated by the bar and the intensity of the color (high conservation, high bar and bright yellow; low conservation, low bar and a dark brown color). The α-helices (red rectangles) and β-strands (green arrows) indicate secondary structure elements present in the $PilO_{\Delta 109}$ structure. **(B)** The structure of $PilO_{\Delta 109}$ indicating the position of the residues chosen for site directed mutagenesis. Conserved and unstructured residues (orange), B-strand breakers (red), and the position of the di-methyl Lys (blue), are indicated.

Two residues in the second PilO hydrophobic region are required for T4P function

Single or double point substitutions meant to disrupt hydrophobic or charged interactions were made in PilO (Table 4.2). PilMNOP stability is sensitive to perturbations in stoichiometry (50), thus all point substitutions were integrated into the *P. aeruginosa* chromosome at the native loci. After verifying the stable expression of all alignment subcomplex proteins using protein-specific antisera (Supplementary Figure S4.5), mutants were assessed for surface pilus expression and twitching motility. Of the mutants tested, only PilO R169D and I170A reduced twitching motility (approx. 40% and 50% relative to wild-type,

respectively) and consistent with this finding, had low levels of surface piliation (Figure 4.5).

Table 4.2. Summary of PilO mutants and their phenotypes.

PilO	Location	Twitching motility	Surface pili
LL132-133AA	Region 1 – β1	Yes	Yes
PE134-135AL	Region 1 – β1	Yes	Yes
F140A	Region 1 – β2–β3	Yes	Yes
Y141A	Region 1 – β2-β3	Yes	Yes
L167A	Region 2 – α2-β4	Yes	Yes
P168A	Region 2 – α2-β4	Yes	Yes
R169D	Region 2 – α2-β4	Reduced (≈ 40%)	Reduced (≈ 65%)
I170A	Region 2 – α2-β4	Reduced (≈ 50%)	Reduced (≈ 70%)
TL172-173AA	Region 2 – β4	Yes	Yes
H174A	Region 2 – β4	Yes	Yes
D175R	Region 2 – β4-β5	Yes	Yes

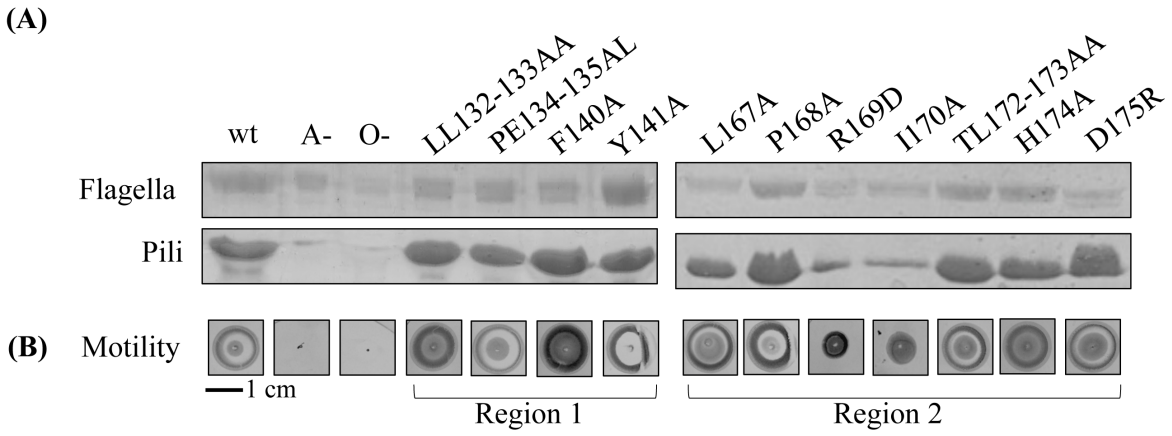

Figure 4.5. PilO R169D and I170A are able to disrupt T4P function. PilO mutants, along with wild-type (wt), non-piliated (A-), and negative controls (O-), were tested for **(A)** sheared surface pili, and **(B)** twitching motility. Sheared surface proteins were separated on 15% SDS-PA gel stained with Coomassie

brilliant blue to visualize. Twitching zones were stained with 1% (w/v) crystal violet.

Discussion

One of our goals was to visualize interfaces among components of the alignment subcomplex in three dimensions, through co-crystallization of a stable heterotrimeric PilNOP complex. Although trays were set with this purified complex, the resulting crystals contained only a truncated form of PilO ($PilO_{\Delta 109}$). We suspect that the high pH of CAPS in the crystallization drop may have led to dissociation of the PilNOP complex, leaving only the core αββ domain of PilO intact. Similarily, this phenomenon has been observed for other PilN and PilO homologs, where constructs that initially included the predicted coiled-coils and the αββ core, ultimately formed crystals containing only the core region, indicating that it is highly stable to proteolytic degradation (124,126).

Though shorter than our previously reported structure (PDB 2RJZ)(51), $PilO_{\Delta 109}$ is of higher resolution and details a number of structural differences. The N-terminal α-helix of $PilO_{\Delta 109}$ is shorter and tilted ~45^{o} away from the β-sheet, compared to the same helix in the previous structure (Figure 4.2A). Previously, only one discontinuous β-strand was identified in the first αββ motif (Figure 4.2C), but the new structure exhibits another β-strand break in the second αββ motif at the same position, resulting in secondary structure pattern of α1-β1β2-β3 and α2-β4β5-β6 (Figure 4.2B). Previous work mapped an extensive PilNO interface including the TMS, the coiled-coils (both missing this structure) as well as the

core regions (51,54,55,178). Whether the $PilO_{\Delta 109}$ fragment can form homodimers, or interact with PilN to form heterodimers, is currently under investigation.

Two potential interaction interfaces with crystallographic symmetry mates were investigated using PISA software (191) (Supplementary Figure S4.2). Interestingly, the more energetically favourable interface orients the N- and C-termini of each PilO monomer in opposite directions (Figure 4.3A). This interface is similar to the interface identified in the T2SS PilO orthologue, EpsM, which crystallized as a homodimer (Figure 4.3C) (PDB 1UV7 (126)). While it is possible that these head-to-tail oriented dimers could be biologically relevant, the PilO and EpsM proteins would have to interact horizontally (rather than vertically as portrayed in Figure 4.3), such that their N- and C-termini would be oriented out to the sides to accommodate the anchoring of the TMS into the membrane. However, it is more likely that the previously observed $PilO_{\Delta 68}$ dimer interface (Figure 4.3B), in which both N- and C-termini are oriented in the same direction, is biologically relevant.

Many of the highly conserved PilO residues were mapped to elements of defined secondary structure, but a large proportion were located in unstructured regions (Figure 4.4). Of these, only R169D and I170A mutations had effects on piliation and thus motility (Figure 4.5). These residues are found in the unstructured region between the α2-helix and the β4-strand (region 2), previously identified as the most highly conserved motif in PilO orthologues (51). This region

of PilO also participates in both homodimerization and formation of PilNO heterodimers (51,178,185). These residues are clustered very closely to the discontinuous β–strands, a feature not observed in the $PilO^{2RJZ}_{\Delta 109}$ structure (Figure 4.2BC) (51). The role of these discontinuous β-strands has yet to be determined, as other PilO or PilN homologs appear to have a single, continuous β-strand at the corresponding position (116,124,126). Split β-strands could afford these regions of PilO more flexibility to accommodate dynamic interactions with other periplasmic T4P components. Interestingly, replacing the "β-strand breaker" residues (P134 and E135 in region 1, or D175 in region 2) had no effect on T4P function.

In conclusion, we determined a higher-resolution structure of the PilO core domain, revealing new features including a second discontinuous β-strand. Two residues in close proximity to this feature are critical for normal T4P function. Although we were unable to obtain co-crystals of PilNOP, our structure provides potential evidence of conformational changes in PilO possibly due to the presence of PilN and PilP prior to crystallization, though this hypothesis has not yet been tested. High-resolution structures are useful tools when combined with other structural techniques, such as cyro-electron microscopy or small angle X-ray scattering. Recently, atomic structures from various bacterial species were used to model each of the T4P components in an electron cryotomographic envelope of the T4P system of *M. xanthus* (71). Through the study of piliated and non-piliated states of the T4P system, information regarding conformational

changes in T4P proteins can be modelled into these biologically relevant states, lending insights into the mechanism behind T4P function (71). These findings provide a stepping-stone for further investigation, with the aim of better understanding the interactions between the conserved alignment subcomplex proteins in *P. aeruginosa*.

Acknowledgments

This work was supported by an Operating Grant MOP-93585 from the Canadian Institutes of Health Research to L.L.B and P.L.H. P.L.H. is the recipient of a Tier I Canada Research Chair.

Supplementary data

Table S4.1: Bacterial Strains & Vectors

Strain	Description	Source/Reference
***E. coli* strains**		
DH5α	F– Φ80*lac*ZΔM15 Δ(*lac*ZYA-*arg*F) U169 *rec*A1 *end*A1 *hsd*R17 (rK–, mK+) *pho*A *sup*E44 λ– *thi*-1*gyr*A96 *rel*A1	ThermoFisher Scientific
BL21 (DE3)	F– *omp*T *hsd*SB(rB–, mB–) *gal dcm* (DE3)	ThermoFisher Scientific
SM10	thi-1, thr, leu, tonA, lacy, supE, recA, RP4-2-Tcr::Mu, Km^r; mobilizes plasmids into *P. aeruginosa* via conjugation	(165)
***P. aeruginosa* strains**		
PAK	Wild-type	J. Boyd
ΔpilM	Deletion of *pilM*	(50)
pilN::FRT	FRT scar at position 124 within *pilN*	(50)
pilO::FRT	FRT scar at position 328 within *pilO*	(50)
pilP::FRT	FRT scar at position 86 within *pilP*	(50)
PilO LL132-133AA	*pilO* with L132A and L133A double point substitutions	This study
PilO PE134-135AL	*pilO* with P134A and E135L double point substitutions	This study
PilO F140A	*pilO* with F140A point substitution	This study
PilO Y141A	*pilO* with Y141A point substitution	This study
PilO L167A	*pilO* with L167A point substitution	This study
PilO P168A	*pilO* with P168A point substitution	This study
PilO R169D	*pilO* with R169D point substitution	This study
PilO I170A	*pilO* with I170A point substitution	This study
PilO TL172-173AA	*pilO* with T172A and L173A double point substitutions	This study
PilO H174A	*pilO* with H174A point substitution	This study
PilO D175R	*pilO* with D175R point substitution	This study
Vectors	**Description**	**Source/Reference**
pEX18Gm	Suicide vector used for gene replacement, Gm^R	(147)
pEX18Gm::*pilNOP* PilO LL132-133AA	Suicide vector containing *pilNOP* with *pilO* LL132-133AA, Gm^R	This study

pEX18Gm::*pilNOP* PilO PE134-135AL	Suicide vector containing *pilNOP* with *pilO* PE134-135AL, Gm^R	This study
pEX18Gm::*pilNOP* PilO F140A	Suicide vector containing *pilNOP* with *pilO* F140A, Gm^R	This study
pEX18Gm::*pilNOP* PilO Y141A	Suicide vector containing *pilNOP* with *pilO* Y141A, Gm^R	This study
pEX18Gm::*pilNOP* PilO L167A	Suicide vector containing *pilNOP* with *pilO* L167A, Gm^R	This study
pEX18Gm::*pilNOP* PilO P168A	Suicide vector containing *pilNOP* with *pilO* P168A, Gm^R	This study
pEX18Gm::*pilNOP* PilO R169D	Suicide vector containing *pilNOP* with *pilO* R169D, Gm^R	This study
pEX18Gm::*pilNOP* PilO I170A	Suicide vector containing *pilNOP* with *pilO* I170A, Gm^R	This study
pEX18Gm::*pilNOP* PilO TL172-173AA	Suicide vector containing *pilNOP* with *pilO* TL172-173AA, Gm^R	This study
pEX18Gm::*pilNOP* PilO H174A	Suicide vector containing *pilNOP* with *pilO* H174A, Gm^R	This study
pEX18Gm::*pilNOP* PilO D175R	Suicide vector containing *pilNOP* with *pilO* D175R, Gm^R	This study

Table S4.2: Oligonucleotide Primer Sequences

Primer Name	Oligonucleotide Sequence (5' – 3')
PilM Fwd	TATATATATCTAGAGGTGCTAGGGCTCATAAAGAAGAAAG
PilP Rev	TATATATAGAATTCGTCAGGAGCGTTCCTTGAGAGTC
PilO Fwd	TATATATATCTAGAGATGAGTCTGGCCAGTTCCCTG
PilO LL132-133AA Fwd	AGGAAATCAAGGCGGCTCCCGAGGTTGCC
PilO LL132-133AA Rev	GGCAACCTCGGGAGCCGCCTTGATTTCCT
PilO PE134-135AL Fwd	ATCAAGCTGCTTGCCCTGGTTGCCCAGCAG
PilO PE134-135AL Rev	CTGCTGGGCAACCAGGGCAAGCAGCTTGAT
PilO F140A Fwd	GTTGCCCAGCAGGCCTACATCGAGCTG
PilO F140A Rev	CAGCTCGATGTAGGCCTGCTGGGCAAC
PilO Y141A Fwd	CCCAGCAGTTCGGCATCGAGCTGCC
PilO Y141A Rev	GGCAGCTCGATGCCGAACTGCTGGG
PilO L167A Fwd	CGTGTCCAGCGCGCCGCGGATCGTCA
PilO L167A Rev	TGACGATCCGCGGCGCGCTGGACACG
PilO P168A Fwd	GTGTCCAGCCTGGCGCGGATCGTCAC

PilO P168A Rev	GTCAGGATCCGCGCCAGGCTGGACAC
PilO R169D Fwd	TCCAGCCTGCCGGACATCGTCACCCTG
PilO R169D Rev	CAGGGTGACGATGTCCGGCAGGCTGGA
PilO I170A Fwd	CTGCCGCGGGCCGTCACCCTG
PilO I170A Rev	CAGGGTGACGGCCCGCGGCAG
PilO TL172-173AA Fwd	GCGGATCGTCGCCGCGCATGACTTCG
PilO TL172-173AA Rev	CGAAGTCATGCGCGGCGACGATCCGC
PilO H174A Fwd	ATCGTCACCCTGGCTGACTTCGAGATCAAGCCG
PilO H174A Rev	CGGCTTGATCTCGAAGTCAGCCAGGGTGACGAT
PilO D175R Fwd	ATCGTCACCCTGCATCGCTTCGAGATCAAGCC
PilO D175R Rev	GGCTTGATCTCGAAGCGATGCAGGGTGACGAT

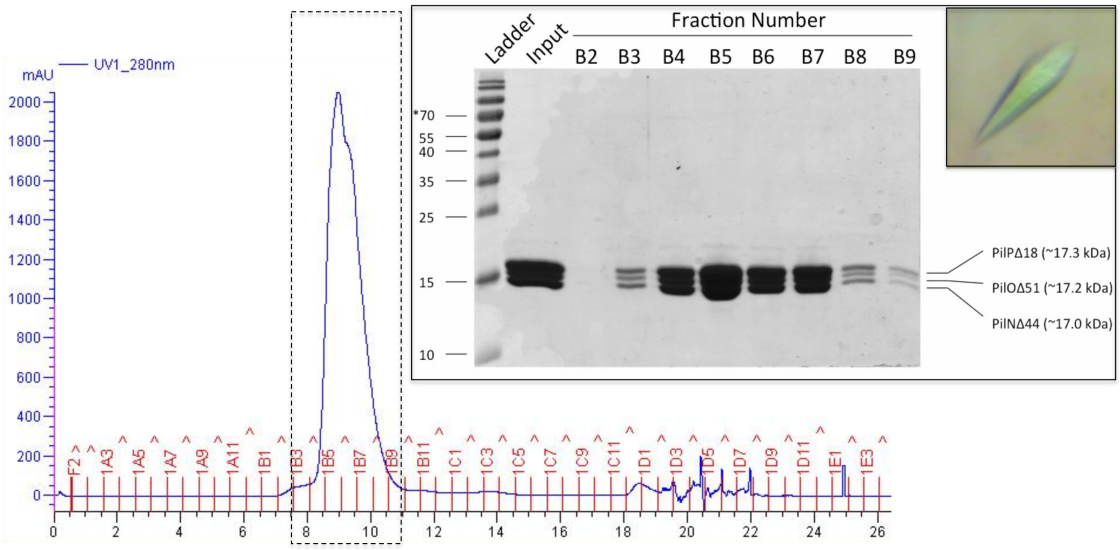

Figure S4.1. $PilN_{\Delta 44}/PilO_{\Delta 51}/PilP_{\Delta 18}$ co-purify from a gel filtration column as a stable heterotrimer following reductive methylation. Methylated $PilN_{\Delta 44}/PilO_{\Delta 51}/PilP_{\Delta 18}$ were co-purified and eluted as a single peak on a Superdex S75 10/300 GL (GE Healthcare) column. The proteins were separated on 15% SDS-PAGE and fractions B4-B8 were pooled, concentrated, and then used for crystallization experiments. Small hexagonal shaped crystals were produced (inset).

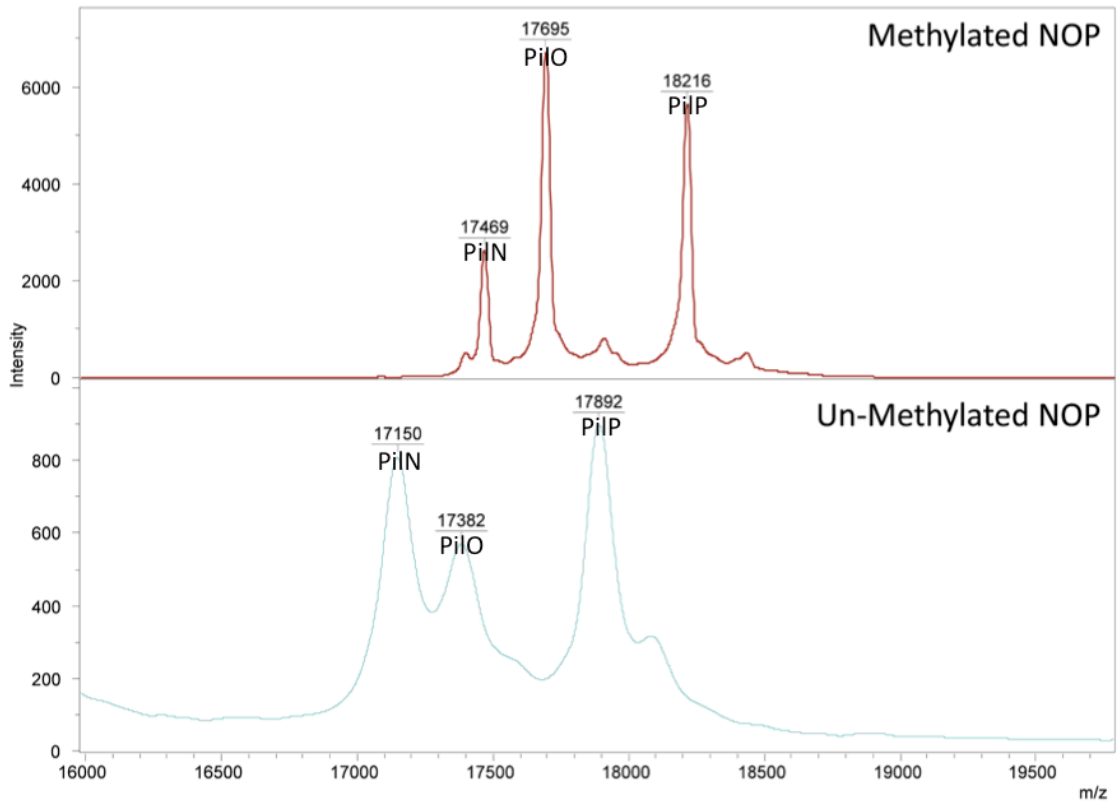

Figure S4.2. Mass spectrometry (MALDI-TOF/TOF) results indicate successful methylation of the PilN$_{\Delta 44}$/PilO$_{\Delta 51}$/PilP$_{\Delta 18}$ complex. Methylated (top) and unmethylated (bottom) samples of 1 mg/mL PilN$_{\Delta 44}$/PilO$_{\Delta 51}$/PilP$_{\Delta 18}$ was analyzed on a Bruker UltrafleXtreme linear detector in positive ion mode. Numbers above each peak are the molecular weight indicated in Da. The change in PilN was 319 Da, PilO 313 Da, and PilP 324 Da. All three protein fragments have 11 lysine residues, which could be methylated. A single dimethyl-Lys group adds 28 Da. The chromatogram shows the ion intensities according to mass-to-charge (m/z) ratio.

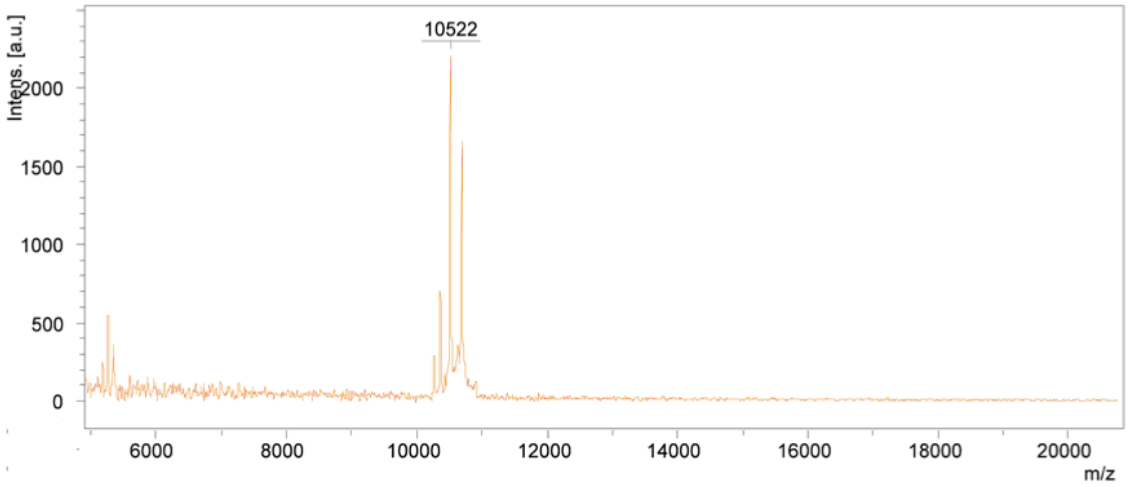

Figure S4.3. Mass spectrometry (MALDI-TOF/TOF) results indicate only PilO fragments were present in the crystals. Two crystals were washed and resuspended in buffer and was analyzed on a Bruker UltrafleXtreme linear detector in positive ion mode. The number above the peak is the molecular weight indicated in Da. This weight corresponds to a 110-206 fragment of PilO (approximate molecular weight of 10,560 Da). Remaining peaks were confirmed to be various PilO fragments. The chromatogram shows the ion intensities according to mass-to-charge (m/z) ratio

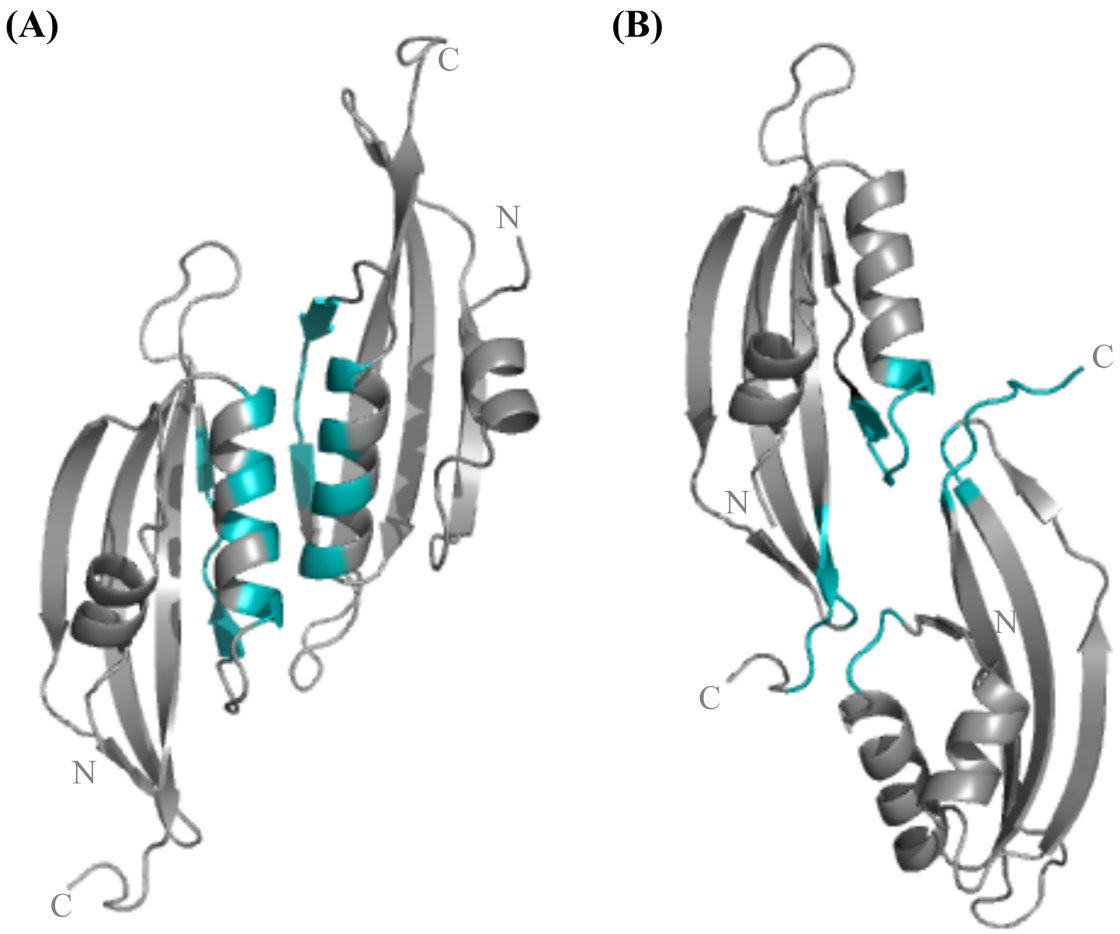

Figure S4.4. Predicted $PilO_{\Delta 109}$ structure dimerization interfaces. Coordinates for $PilO_{\Delta 109}$ were uploaded to the PISA (Proteins, Interfaces, Structures, and Assemblies) server (191), which calculates the probable quaternary structures/assemblies. Two potential $PilO_{\Delta 109}$ dimer interfaces were identified, **(A)** "side-by-side" arrangement (surface area = 11,520 $Å^2$, buried surface area = 1,180 $Å^2$, ΔG^{int} = -12.0 kcal/mol, and ΔG^{diss} = 4.4 kcal/mol) and, **(B)** "end-to-end" arrangement (surface area = 11,560 $Å^2$, buried surface area = 1,140 $Å^2$, ΔG^{int} = -11.0 kcal/mol, and ΔG^{diss} = 0.0 kcal/mol). Residues involved in interaction are indicated by teal color.

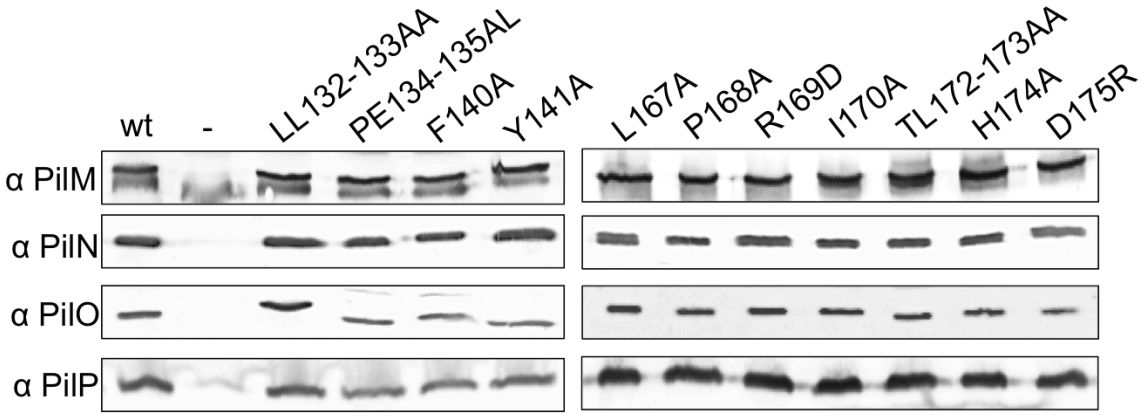

Figure S4.5. All alignment subcomplex proteins are stable when residues of interest in PilO are mutated. All PilO mutant strains, as well as wild-type (wt) and negative controls (-), were tested for expression and stability of alignment subcomplex proteins (PilMNOP) via Western blotting using protein specific antisera as indicated on left.

CHAPTER FIVE

Discussion, future directions, and conclusions

Discussion

PilNO interaction interfaces contribute to pilus extension/retraction

With their ability to extend and retract, T4P have been implicated in attachments to surfaces, biofilm formation, DNA uptake, and unique forms of locomotion including twitching motility (1-5,14). Extension of the pilus fibre from the cell involves the ATPase, PilB, which provides the power through ATP hydrolysis, and the IM platform protein, PilC, which together are proposed to drive the pilin subunits into the base of the growing fibre (4,48,49,98). Retraction – the reverse process – is governed by two retraction ATPases in *P. aeruginosa*, PilT and PilU (96,97). In this state, the pilus fibre is being pulled back into the cell, under tension if it is attached to a surface, and the pilin subunits are being redeposited into the IM. Our research supports a role for the alignment subcomplex proteins not only in assembly of the pilus fibre, but also its disassembly, a role which was previously unidentified (Chapter 2).

In the absence of any of the alignment subcomplex proteins, no surface-exposed pili are recovered, suggesting these components are essential. However, a small amount of surface piliation can be restored in these mutants through the disruption of PilT (49). This finding suggests that connection of the IM and OM components is important for the efficient extension of the pilus fibre from the cell, but conditionally essential for piliation. A mutation in the first coiled-coil region of PilN affected extension, while other mutations in the second coiled-coil region of either PilN or PilO disrupted both their interaction and pilus retraction,

indicating that PilNO interaction at their coiled coil interface is required for proper function of the T4P system. Similarly, a chimeric PilN construct with the TMS of PilO ($PilN_{chimera}$) had reduced pilus extension, possibly through altered interaction with PilM (Figure 2.5). Recent studies of PilMN interactions suggest that reversible association of PilN with PilM may govern the preferential binding of PilM to PilB, PilT, and/or PilC (111). The altered interaction between PilNO in the coiled-coils, and possibly changes in the PilMN interaction in the $PilN_{chimera}$, could explain the extension/retraction defects if a signal was not properly propagated to, or from, the cytoplasmic motor of the T4P system. These findings indicate that PilN and PilO interactions play a critical role in T4P dynamics and support the idea that these proteins are not simply static connectors of the inner and outer membrane parts of the machine.

A new model of PilNO interactions

Elegant electron cryotomography and mutational analyses recently allowed derivation of a model of the overall architecture of the T4P system in *M. xanthus* (PDB 3JC8 (71)). Because no high resolution structures of any *M. xanthus* proteins are available, hypothetical models of each component were generated using atomic structures from various bacterial species, and fitted into the tomographic maps at appropriate positions, assigned by changes in density in various mutant backgrounds (Figure 5.1). All components – with the exception of the pilus and PilC – form connected ring-like structures that create a

transenvelope conduit (71). The rings of PilQ span the OM (not pictured in Figure 5.1) and the periplasm, through the N0, N1, and three AMIN domains that interact directly with peptidoglycan. PilP forms a ring in the periplasm connected to the PilQ N0 domain above, and to the ring formed by PilN and PilO below (Figure 5.2A). The coiled-coils of PilN and PilO form a cage-like structure in the periplasm that extends down through the IM, and they are attached to the PilM ring through PilMN interactions. Based on the size of a PilM ring, only a single hexameric ATPase could be modelled, indicating that the extension and retraction ATPases occupy the same, and therefore mutually exclusive, location at the base of the apparatus. The final component PilC, located in the IM, lies between the cytoplasmic ATPase and the stem of the pilus, where it is hypothesized to rotate as it assembles the pilus fibre (71). Encouragingly, this model strongly resembled the cartoon schematic of the *P. aeruginosa* T4P system proposed in Chapter 1, which was based on information gleaned from the study of individual components or subcomplexes over the last decade (Figure 1.2). The structures used to fill out the component map were leveraged from various T4P or T2SS expressing bacteria, and although each system may have slightly different components, this model emphasizes that at a very basic level all T4P/T2S systems are similar.

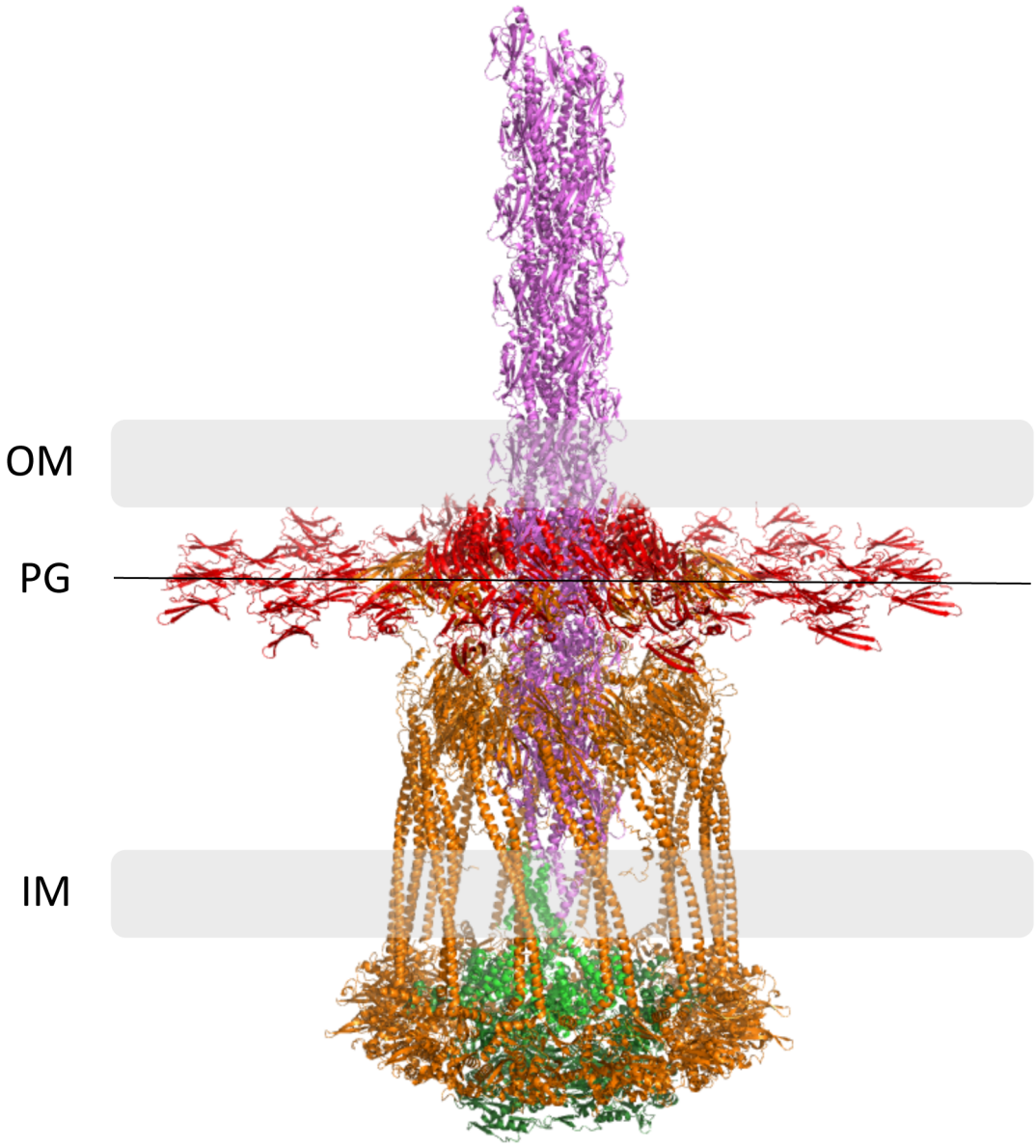

Figure 5.1. Architectural model of the type IV pilus system (PDB 3JC8; adapted from (71)). Components include the outer membrane (OM) secretin PilQ AMIN, N0 and N1 domains (red), the inner membrane (IM) motor subcomplex: PilC and PilB (green), the IM alignment subcomplex: PilM, PilN, PilO, and PilP (orange), and the pilins and pilus fibre: PilA (purple). PilQ AMIN domains interact with peptidoglycan (PG) as represented by the black line.

Proteins not shown: PilQ barrel domain, PilF, PilT, PilU, minor pilins, PilY1 and FimV.

Our previous work suggested that interaction between PilN and PilO was mediated through the TMS, the coiled-coils, and the core regions (Chapter 2). We hypothesized that PilN and PilO interacted throughout the length of the proteins, initiated by the TMS, similar to a zipper. However, at the time it was unclear why multiple PilN core region mutations failed to disrupt the interaction of PilN and PilO in a BTH system, but many of the same mutations had dramatic effects on T4P function when introduced individually into the chromosome (Chapter 2). A clue to resolving this conundrum came with the observation that PilN and PilO co-purified as a tetramer, and participated simultaneously in both homo- and heterodimer interactions (Chapter 3).

Cys substitutions were introduced within the core region of PilN and PilO with the goal of trapping these proteins as covalently linked heterodimers and/or homodimers *in vivo*. Two Cys pairs capable of forming covalent PilO homodimers were located at the “top” of the modelled PilO dimer interface. A single set of Cys residues were able to cross-link PilNO heterodimers located at the “bottom” of the predicted interface, but more interestingly, these residues were also involved in formation of covalent PilN and PilO homodimers. These data led to a new model of PilNO interaction, where the core domains of PilN and PilO participate in homodimer interactions, while the coiled-coils and transmembrane segments simultaneously mediate the heterodimeric interactions (Figure 5.2B). This model

explains why up to six combined point mutations in the core of PilN were unable to disrupt PilNO interaction in BTH assays, but individually abolished motility and surface piliation in *P. aeruginosa* (Chapter 2). It is likely that PilN homodimerization was disrupted *in vivo,* leading to the observed phenotypes. These findings have furthered our understanding of the PilNO interaction interfaces, and provided a more accurate model of how the machine is organized.

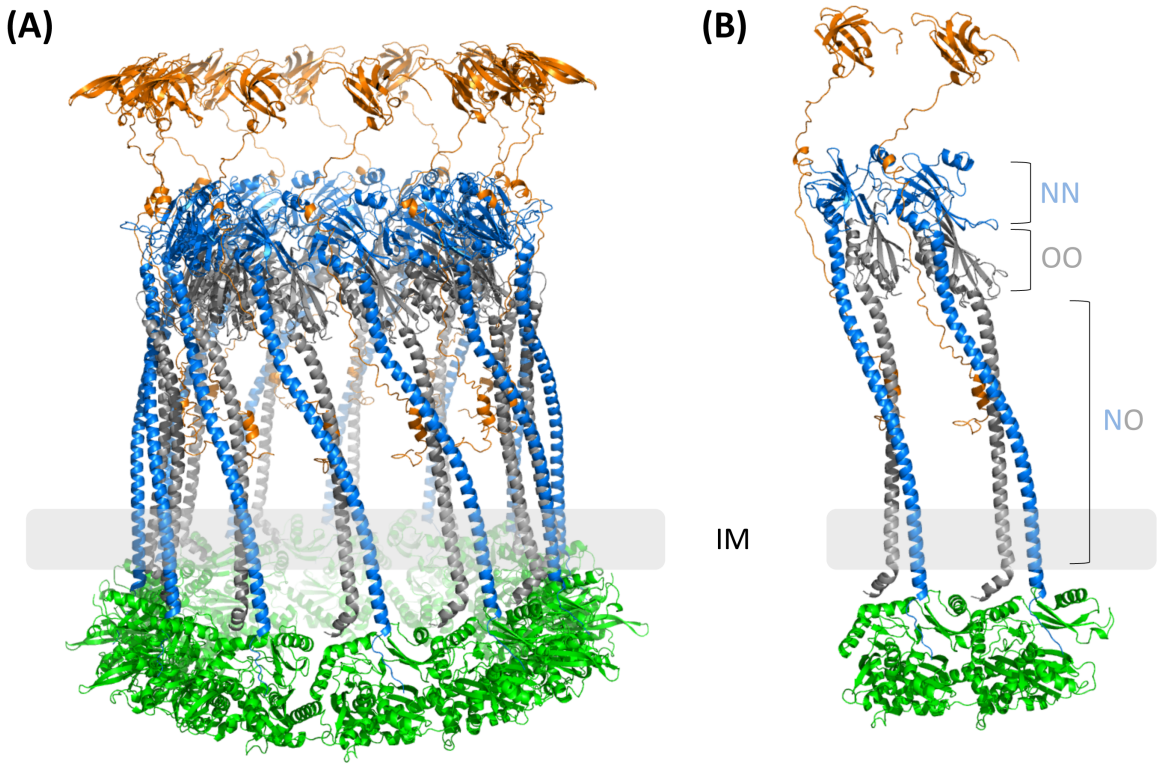

Figure 5.2. Model of the alignment subcomplex proteins (PDB 3JC8; adapted from (71)). (A) PilM (green) forms a ring in the cytoplasm and is connected to the N-terminus of PilN (blue). The coiled-coils of PilN and PilO (grey) form a cage-like structure in the periplasm, with the core domains stacked

on top of each other. The intrinsically disordered N-terminal segment of PilP (orange) interacts with a PilNO heterodimer and forms a ring-like structure in the periplasm where its structured beta sandwich domain would connect with the periplasmic N_0 domain of PilQ (not shown). Twelve subunits are modelled forming the ring-like structures. **(B)** Pairs of alignment subcomplex components (emphasizing the tetrameric arrangement of PilN and PilO), specifically indicating the regions of PilN homodimerization (NN), PilO homodimerization (OO) in the core, and the PilNO heterodimerization regions (NO) formed by the coiled-coils and the transmembrane segments. PilP binds to PilNO and not PilO homodimers *in vitro*, suggesting that it stabilizes the heterotetrameric configuration.

Seven PilNO tetramers likely surround a 14-membered secretin with 7-fold symmetry

Recent single particle cryo-EM analysis of the *P. aeruginosa* PilQ secretin at 7.4 Å resolution revealed that it has C7 symmetry with pseudo C14 symmetry (Koo et al., 2016 – in press). This structure resembles the general shape of other T4P system secretins, but with significantly more detail, highlighting 14-fold internal symmetry that is reduced to C7 symmetry through a repeating pattern of large and small features (spokes) at its edge. These data suggest that the T4P secretin from *P. aeruginosa* is likely composed of 14 PilQ subunits forming the pore in the OM and extending downwards into the periplasm.

The genes encoding PilMNOP are found in a polycistronic operon with the gene encoding PilQ. Previous studies support a 1:1 connectivity between PilQ-PilP, PilN-PilO-PilP, and PilM-PilN, suggesting an equivalent number of proteins

between the alignment subcomplex components and the secretin (55,67,111,114,128). Our data suggest that the functional stochiometry of PilNO (and thus likely PilMNOP) is a tetramer, formed by a heterodimer of PilNO homodimers (Figure 3.3). Seven alignment subcomplex pairs (totalling 14 subunits) nicely fits the C7 symmetry reported for the outer edge of the secretin. This arrangement would also satisfy the homo- and heterodimerization observed for PilN and PilO, while maintaining a continuous periplasmic ring (Figure 5.3A). Alternatively, it is possible that the C7 symmetry could translate to a 1:2 interaction between PilP and PilQ, resulting in only 7 alignment subcomplexes surrounding the fibre (Figure 5.3B). However, given the recent T4P system model, the size of the well-characterized PilO structure, and the ability of PilN and PilO to form homodimers *in vivo*, that arrangement seems less likely.

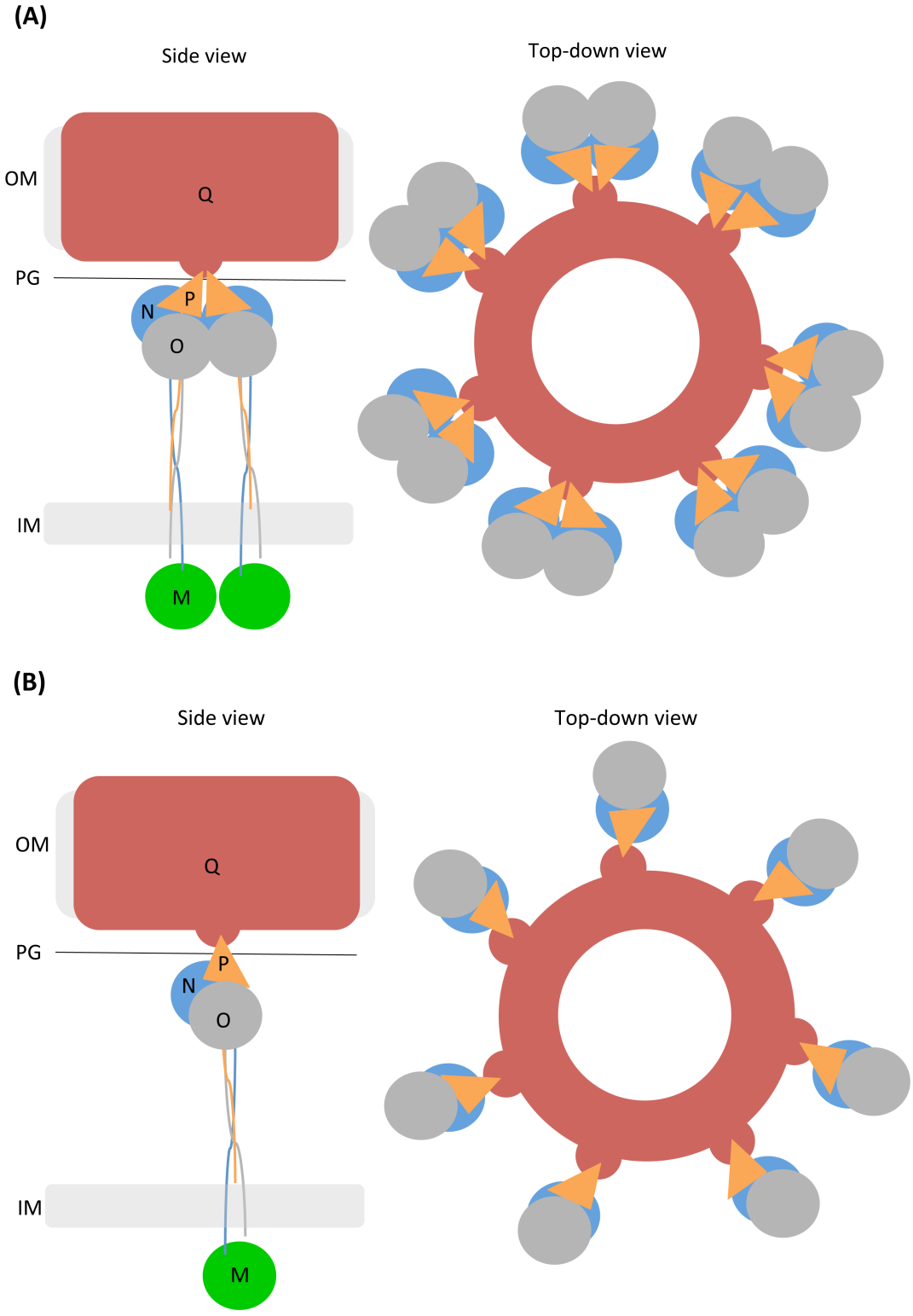
(A)
Side view
Top-down view
OM
Q
PG
P
N
O
IM
M
(B)
Side view
Top-down view
OM
Q
PG
P
N
O
IM
M

Figure 5.3. Cartoon models of the possible PilMNOP transenvelope complex conformations. The PilQ secretin (red) is composed of 14 subunits, with C7 symmetry at the edges as represented by the protrusions. **(A)** A 1:1:1:1:1 ratio of PilMNOPQ, where 14 alignment subcomplex subunits, PilM (green), PilN (blue), PilO (grey) and PilP (orange), surround the secretin. Homodimerization by PilN and PilO is possible in this model. **(B)** A 1:1:1:1:2 ratio of PilMNOPQ where 7 alignment subcomplex components surround the secretin. PilN and PilO homodimerization cannot occur. Outer membrane (OM). Peptidoglycan (PG). Inner membrane (IM).

Future directions

PilNO core interactions

To test our hypothesis that the coiled-coils of PilN and PilO mediate their heterodimerization, while the core of each protein participates in homodimerization, soluble PilN and PilO protein fragments lacking the coiled-coils will be tested for interaction. The boundaries of the core region as identified in the $PilO_{\Delta 109}$ fragment that was serendipitously crystallized (Chapter 4) were used to design a corresponding PilN core construct ($PilN_{\Delta 97}$). In preliminary trials, this construct is less prone to insolubility than previously tested PilN constructs containing the coiled coils. $PilN_{\Delta 97}$ and $PilO_{\Delta 109}$ fragments will be expressed in *E. coli*, purified separately, and the N-terminal His-tag on one of the proteins removed. A pull-down assay whereby the proteins will be incubated together and subsequently subject to nickel affinity chromatography can be used to detect potential interactions.

The N-terminus of PilP (specifically residues 18-93) was previously shown to interact with a PilNO heterodimer (54,55). Using the $PilN_{\Delta 97}$ and $PilO_{\Delta 109}$ core constructs, interaction with a full-length version of PilP less its signal sequence ($PilP_{\Delta 18}$) or the N-terminal fragment alone ($PilP_{19\text{-}93}$) will be tested. These experiments will clarify whether the core regions alone of PilN and PilO can interact, and whether the core regions of PilN and PilO are sufficient to bind PilP. This work would further our understanding of the minimal regions required for PilNO and/or PilNOP interactions, which will inform future structural efforts.

Crosslinking of the PilN and PilO coiled-coils

A large electrostatic difference between the PilN and PilO coiled-coils was thought to be a driving force behind their dimerization (51). In Chapter 2, specific residues in the coiled-coils of PilN and PilO were identified as important for T4P function. Building upon the model in Chapter 3, the PilNO coiled-coils will be tested for their ability to cross-link via disulfide bonds. We will introduce Cys substitutions at the $PilN^{L81}$ residue and the corresponding $PilO^{M92}$ residue that was critical for interaction in BTH assays, and determine the ability of these proteins to cross-link using non-reducing SDS-PAGE and Western blot analysis with our protein specific antibodies. If these residues can be cross-linked, we can determine if dimerization is disrupted in the absence of PilM or PilP, which could indicate that movement in the coiled-coils has occurred. These experiments will identify the relative proximity of these residues to one another *in vivo*, whether

PilN and PilO are also capable of forming homodimers in the coiled-coils (via single Cys substitutions), if there are any differences in structure of the extension- or retraction-deficient mutants, and what effect these mutations might have on T4P function.

Small molecule inhibitors of PilNO interactions

The ability to disrupt PilNO interactions by single residue substitutions is promising, as it suggests that small molecule inhibitors of PilNO interactions can be discovered, ultimately leading to T4P dysfunction in *P. aeruginosa*. The liquid BTH assay used to measure PilN and PilO interactions in Chapter 2 was adapted to fit a 96-well plate, and high Z'-scores (a measure of how well an assay can distinguish true hits from background noise) indicated that it was amenable to high-throughput screening (HTS). At the time, we thought that PilNO heterodimers interacted via their core regions as well as through other interfaces. However, in the BTH assay, mutations made in the core were unable to disrupt PilNO heterodimers. We concluded that the large core interaction interfaces were probably hard to disrupt with single mutations, and decided that this assay would not be suitable for the detection of small molecule inhibitors that block PilNO interactions. Now, given our revised model of PilNO interactions as proposed in Chapter 3, use of the high throughput BTH assay to detect inhibitors of PilNO interactions can be revisited.

A limitation of the BTH assay described in Chapter 2 was the lack of

apparent homodimerization of full length PilN or PilO, which led us to believe that these proteins did not participate in self-associations (Figure 2.2A). With the revised model of PilNO interaction as described in Chapter 3, the core regions of PilN and PilO are responsible for homodimerization, while the coiled-coils and TMS mediate heterodimerization. In the HTS facility at McMaster University, small molecule libraries can be screened using the 96-well plate format BTH assay, and the disruption of PilNO interactions can be monitored colourimetrically. Compounds able to disrupt PilNO heterodimer formation can be subsequently validated in secondary screens, including well-established phenotypic assays. By identifying small molecules capable of disrupting non-essential bacterial processes (such as the T4PS), we can effectively disarm the bacteria while decreasing the likelihood of mutation-based resistance to occur.

Additional roles of PilN and PilO in signalling

The alignment subcomplex proteins were identified as playing a role in the PilY1/SadC/c-di-GMP signalling cascade, as in their absence, PilY1 was unable to signal to SadC, which in turn caused low levels of c-di-GMP (87). Using Cys crosslinking, T4P functional and dysfunctional PilN and PilO homodimers were trapped *in vivo* (Chapter 3). When cross-linked at specific residues ($PilN^{R142C}$ and $PilO^{D175C}$) T4P dysfunction was observed, but this was not the case for the other PilN and PilO disulfide-bonded homodimers tested. If these Cys mutants are capable of disrupting the signalling between the external PilY1 and the internal

SadC proteins, swarming motility will continue when PilY1 is overexpressed. Additionally, the signalling between the alignment subcomplex proteins and SadC can be directly tested using a BTH system as described in Chapter 2. These data will provide further insights into the mechanisms behind the role of PilMNOP in controlling surface behaviours through a PilY1/SadC/c-di-GMP signalling cascade.

PilNOP structural studies

Although previous attempts have been made to crystallize all or portions of the highly soluble PilNOP periplasmic fragments (Chapter 4), new information regarding boundaries and single point substitutions will be used to generate a series of PilN and PilO constructs for structural determination. Although this section primarily describes the use of X-ray crystallography, other structural techniques (ex. small angle X-ray scattering, single particle cryo-EM) could also be attempted.

In *P. aeruginosa,* attempts to purify soluble PilN have been discouraging as in the absence of PilO, a $PilN_{\Delta 44}$ fragment is found in the insoluble fraction after nickel affinity chromatography. Interestingly, the $PilN_{\Delta 97}$ core fragment expressed alone yielded some soluble PilN protein capable of being purified, and it will be used to set up crystallization trials. Also, by generating the $PilN^{R142C}$ substitution in the $PilN_{\Delta 97}$ core fragment, covalent PilN homodimers will also be investigated. Currently, no experimentally determined structural information is

available for PilN from *P. aeruginosa*, which represents an important gap, especially since we now have PilM, PilO, and PilP structures from this species.

The conditions for PilO crystallization have been determined (51) (Chapter 4). PilO can be "locked" as a homodimer using Cys disulfide bonding, however only a subset of these residue substitutions caused T4P dysfunction (Chapter 3). The $PilO^{D175C}$ (which caused T4P disruption) and the $PilO^{I178C}$ (with wild-type T4P function) substitutions will be introduced into existing $PilO_{\Delta 68}$ and $PilO_{\Delta 109}$ constructs. The mutant PilO constructs will be purified using nickel affinity chromatography and gel filtration, and confirmed by Western blot analysis with PilO-specific antibodies. Crystallization trials of mutant PilO will proceed using the previously identified conditions. If crystals form and are of diffraction quality, the structure of the mutant PilOs will be solved using molecular replacement. These structural models will provide insights into the differences in the PilO mutant core interfaces capable of producing such dramatic effects on T4P function.

With the capacity for intact T4P systems to be visualized *in vivo* using cryotomography (as previously described for the T4P system in *M. xanthus* (71)), extension or retraction-deficient mutants as described in Chapters 2 and 3 can now be examined. Functional and non-functional variants, which can be locked into an extension deficient state (e.g. $PilN^{R142C}$) or a retraction deficient state (e.g. $PilN^{L81K}$ or $PilO^{M92K}$), could be visualized using cryotomography to identify what changes have occurred in T4P dysfunctional mutants. This information can help provide insight into what the mutations in these regions are doing to PilN and

PilO that disrupts the function of the T4P system.

In addition to trying different structural techniques, orthologous proteins from other bacterial species can be explored. Previously, purification of PilN and PilO from *P. syringae pv. phaseolicola* was attempted, but unfortunately these protein constructs (the equivalent of $PilN_{\Delta 44}$ and $PilO_{\Delta 51}$) were largely insoluble. With the core region of PilO clearly defined (Chapter 4), we will express and purify shorter constructs which only encompass the core domain, in an attempt to improve solubility of PilN and PilO from *P. syringae*.

In some Pseudomonads, the alignment subcomplex proteins have a slightly different arrangement, which could indicate a difference of function for these regions. The plant growth-promoting species *P. putida* undergoes a pili-dependent form of locomotion on surfaces (slightly different than twitching motility) and while PilM and PilN are predicted to look structurally similar to those of *P. aeruginosa*, this species encodes a single polypeptide with PilO and PilP domains (PilOP) (193). Why this strain has a natural fusion protein of PilO and PilP is unclear, but this unique component may provide functional and structural insights into T4P function.

Finally, branching out even further, as demonstrated by the work on the T4P system from *M. xanthus,* many of the T4P components between various bacterial species display a similar architectures, despite limited sequence conservation (71). Recently the structure of the extension ATPase, PilB, from *Geobacter sulfureducans* was solved (McCallum et al., – in preparation). This

structure proved useful by providing important mechanistic insights about the potential interactions of the ATPase and the IM platform protein, PilC, in the T4P system of *P. aeruginosa*.

Significance and conclusions

T4P are key virulence factors used by many bacteria, including the opportunistic pathogen *P. aeruginosa.* The alignment subcomplex proteins, PilMNOP, are highly conserved and are required for T4P function; therefore, a complete understanding of how these components interact and the mechanisms through which they contribute to T4P system function is required. This thesis explored the interaction interfaces and the dynamics of the PilN and PilO proteins from the T4P system of *P. aeruginosa*. The ability of point substitutions in PilN and PilO to cause subtle or drastic effects on T4P system function, depending on their specific locations, suggests that precise PilNO interactions are key to normal extension and retraction of the pilus fibre. The ability to simultaneously form both homo- and heterodimers of PilN and PilO might be important for propagating a signal for the “active” and/or “resting” states of the system, or may be involved in mediating other protein interactions which promote assembly or disassembly. Together, these data provide a more thorough understanding of alignment subcomplex dynamics and the mechanics behind T4P function. This information may be broadly applicable to other bacterial T4P systems, and to other bacterial machines such as the T2S system. The structural and functional data presented

in this work will add to the deeper understanding of the system that is necessary for the development of T4P-inhibitory compounds for *P. aeruginosa.*

REFERENCES

1. Bradley, D. E. (1973) Basic characterization of a *Pseudomonas aeruginosa* pilus-dependent bacteriophage with a long noncontractile tail. *Journal of virology* **12**, 1139-1148
2. Pelicic, V. (2008) Type IV pili: e pluribus unum? *Molecular microbiology* **68**, 827-837
3. Burrows, L. L. (2005) Weapons of mass retraction. *Molecular microbiology* **57**, 878-888
4. Burrows, L. L. (2012) *Pseudomonas aeruginosa* twitching motility: type IV pili in action. *Annual review of microbiology* **66**, 493-520
5. Mattick, J. S. (2002) Type IV pili and twitching motility. *Annual review of microbiology* **56**, 289-314
6. Farinha, M. A., Conway, B. D., Glasier, L. M., Ellert, N. W., Irvin, R. T., Sherburne, R., and Paranchych, W. (1994) Alteration of the pilin adhesin of *Pseudomonas aeruginosa* PAO results in normal pilus biogenesis but a loss of adherence to human pneumocyte cells and decreased virulence in mice. *Infection and immunity* **62**, 4118-4123
7. Hahn, H. P. (1997) The type-4 pilus is the major virulence-associated adhesin of *Pseudomonas aeruginosa*--a review. *Gene* **192**, 99-108
8. Govan, J. R., and Deretic, V. (1996) Microbial pathogenesis in cystic fibrosis: mucoid *Pseudomonas aeruginosa* and *Burkholderia cepacia*. *Microbiological reviews* **60**, 539-574
9. Heiniger, R. W., Winther-Larsen, H. C., Pickles, R. J., Koomey, M., and Wolfgang, M. C. (2010) Infection of human mucosal tissue by *Pseudomonas aeruginosa* requires sequential and mutually dependent virulence factors and a novel pilus-associated adhesin. *Cellular microbiology* **12**, 1158-1173
10. O'Toole, G. A., and Kolter, R. (1998) Flagellar and twitching motility are necessary for *Pseudomonas aeruginosa* biofilm development. *Molecular microbiology* **30**, 295-304
11. Chi, E., Mehl, T., Nunn, D., and Lory, S. (1991) Interaction of *Pseudomonas aeruginosa* with A549 pneumocyte cells. *Infection and immunity* **59**, 822-828
12. Giltner, C. L., Habash, M., and Burrows, L. L. (2010) *Pseudomonas aeruginosa* minor pilins are incorporated into type IV pili. *Journal of molecular biology* **398**, 444-461
13. Craig, L., Pique, M. E., and Tainer, J. A. (2004) Type IV pilus structure and bacterial pathogenicity. *Nature reviews. Microbiology* **2**, 363-378
14. Bradley, D. E. (1980) A function of *Pseudomonas aeruginosa* PAO polar pili: twitching motility. *Canadian journal of microbiology* **26**, 146-154

15. Woods, D. E., Straus, D. C., Johanson, W. G., Jr., Berry, V. K., and Bass, J. A. (1980) Role of pili in adherence of *Pseudomonas aeruginosa* to mammalian buccal epithelial cells. *Infection and immunity* **29**, 1146-1151
16. Wu, S. S., and Kaiser, D. (1995) Genetic and functional evidence that Type IV pili are required for social gliding motility in *Myxococcus xanthus*. *Molecular microbiology* **18**, 547-558
17. Meyer, T. F., Billyard, E., Haas, R., Storzbach, S., and So, M. (1984) Pilus genes of *Neisseria gonorrheae*: chromosomal organization and DNA sequence. *Proceedings of the National Academy of Sciences of the United States of America* **81**, 6110-6114
18. Swanson, J. (1973) Studies on gonococcus infection. IV. Pili: their role in attachment of gonococci to tissue culture cells. *The Journal of experimental medicine* **137**, 571-589
19. Donnenberg, M. S., Giron, J. A., Nataro, J. P., and Kaper, J. B. (1992) A plasmid-encoded type IV fimbrial gene of enteropathogenic *Escherichia coli* associated with localized adherence. *Molecular microbiology* **6**, 3427-3437
20. Giron, J. A., Levine, M. M., and Kaper, J. B. (1994) Longus: a long pilus ultrastructure produced by human enterotoxigenic *Escherichia coli*. *Molecular microbiology* **12**, 71-82
21. Taniguchi, T., Fujino, Y., Yamamoto, K., Miwatani, T., and Honda, T. (1995) Sequencing of the gene encoding the major pilin of pilus colonization factor antigen III (CFA/III) of human enterotoxigenic *Escherichia coli* and evidence that CFA/III is related to type IV pili. *Infection and immunity* **63**, 724-728
22. Melville, S., and Craig, L. (2013) Type IV pili in Gram-positive bacteria. *Microbiology and molecular biology reviews : MMBR* **77**, 323-341
23. Ayers, M., Howell, P. L., and Burrows, L. L. (2010) Architecture of the type II secretion and type IV pilus machineries. *Future microbiology* **5**, 1203-1218
24. Korotkov, K. V., Sandkvist, M., and Hol, W. G. (2012) The type II secretion system: biogenesis, molecular architecture and mechanism. *Nature reviews. Microbiology* **10**, 336-351
25. Nivaskumar, M., and Francetic, O. (2014) Type II secretion system: a magic beanstalk or a protein escalator. *Biochimica et biophysica acta* **1843**, 1568-1577
26. Filloux, A. (2004) The underlying mechanisms of type II protein secretion. *Biochimica et biophysica acta* **1694**, 163-179
27. Bleves, S., Viarre, V., Salacha, R., Michel, G. P., Filloux, A., and Voulhoux, R. (2010) Protein secretion systems in *Pseudomonas aeruginosa*: A wealth of pathogenic weapons. *International journal of medical microbiology : IJMM* **300**, 534-543
28. Pugsley, A. P. (1993) The complete general secretory pathway in gram-negative bacteria. *Microbiological reviews* **57**, 50-108

29. Novotny, C. P., and Fives-Taylor, P. (1974) Retraction of F pili. *Journal of bacteriology* **117**, 1306-1311
30. Skerker, J. M., and Berg, H. C. (2001) Direct observation of extension and retraction of type IV pili. *Proceedings of the National Academy of Sciences of the United States of America* **98**, 6901-6904
31. Gibiansky, M. L., Conrad, J. C., Jin, F., Gordon, V. D., Motto, D. A., Mathewson, M. A., Stopka, W. G., Zelasko, D. C., Shrout, J. D., and Wong, G. C. (2010) Bacteria use type IV pili to walk upright and detach from surfaces. *Science* **330**, 197
32. Jin, F., Conrad, J. C., Gibiansky, M. L., and Wong, G. C. (2011) Bacteria use type-IV pili to slingshot on surfaces. *Proceedings of the National Academy of Sciences of the United States of America* **108**, 12617-12622
33. Yeung, A. T., Torfs, E. C., Jamshidi, F., Bains, M., Wiegand, I., Hancock, R. E., and Overhage, J. (2009) Swarming of *Pseudomonas aeruginosa* is controlled by a broad spectrum of transcriptional regulators, including MetR. *Journal of bacteriology* **191**, 5592-5602
34. Maier, B., Potter, L., So, M., Long, C. D., Seifert, H. S., and Sheetz, M. P. (2002) Single pilus motor forces exceed 100 pN. *Proceedings of the National Academy of Sciences of the United States of America* **99**, 16012-16017
35. Merz, A. J., So, M., and Sheetz, M. P. (2000) Pilus retraction powers bacterial twitching motility. *Nature* **407**, 98-102
36. Hu, W., Yang, Z., Lux, R., Zhao, M., Wang, J., He, X., and Shi, W. (2012) Direct visualization of the interaction between pilin and exopolysaccharides of *Myxococcus xanthus* with eGFP-fused PilA protein. *FEMS microbiology letters* **326**, 23-30
37. Wang, S., Parsek, M. R., Wozniak, D. J., and Ma, L. Z. (2013) A spider web strategy of type IV pili-mediated migration to build a fibre-like Psl polysaccharide matrix in *Pseudomonas aeruginosa* biofilms. *Environmental microbiology* **15**, 2238-2253
38. Semmler, A. B., Whitchurch, C. B., and Mattick, J. S. (1999) A re-examination of twitching motility in *Pseudomonas aeruginosa*. *Microbiology* **145 (Pt 10)**, 2863-2873
39. Gloag, E. S., Turnbull, L., Javed, M. A., Wang, H., Gee, M. L., Wade, S. A., and Whitchurch, C. B. (2016) Stigmergy co-ordinates multicellular collective behaviours during *Myxococcus xanthus* surface migration. *Scientific reports* **6**, 26005
40. van Schaik, E. J., Giltner, C. L., Audette, G. F., Keizer, D. W., Bautista, D. L., Slupsky, C. M., Sykes, B. D., and Irvin, R. T. (2005) DNA binding: a novel function of *Pseudomonas aeruginosa* type IV pili. *Journal of bacteriology* **187**, 1455-1464
41. Leighton, T. L., Buensuceso, R., Howell, P. L., and Burrows, L. L. (2015) Biogenesis of *Pseudomonas aeruginosa* type IV pili and regulation of their function. *Environmental microbiology*

42. Collins, R. F., Davidsen, L., Derrick, J. P., Ford, R. C., and Tonjum, T. (2001) Analysis of the PilQ secretin from *Neisseria meningitidis* by transmission electron microscopy reveals a dodecameric quaternary structure. *Journal of bacteriology* **183**, 3825-3832
43. Collins, R. F., Ford, R. C., Kitmitto, A., Olsen, R. O., Tonjum, T., and Derrick, J. P. (2003) Three-dimensional structure of the *Neisseria meningitidis* secretin PilQ determined from negative-stain transmission electron microscopy. *Journal of bacteriology* **185**, 2611-2617
44. Burkhardt, J., Vonck, J., and Averhoff, B. (2011) Structure and function of PilQ, a secretin of the DNA transporter from the thermophilic bacterium *Thermus thermophilus* HB27. *The Journal of biological chemistry* **286**, 9977-9984
45. Koo, J., Burrows, L. L., and Howell, P. L. (2012) Decoding the roles of pilotins and accessory proteins in secretin escort services. *FEMS microbiology letters* **328**, 1-12
46. Koo, J., Tammam, S., Ku, S. Y., Sampaleanu, L. M., Burrows, L. L., and Howell, P. L. (2008) PilF is an outer membrane lipoprotein required for multimerization and localization of the *Pseudomonas aeruginosa* Type IV pilus secretin. *Journal of bacteriology* **190**, 6961-6969
47. Siewering, K., Jain, S., Friedrich, C., Webber-Birungi, M. T., Semchonok, D. A., Binzen, I., Wagner, A., Huntley, S., Kahnt, J., Klingl, A., Boekema, E. J., Sogaard-Andersen, L., and van der Does, C. (2014) Peptidoglycan-binding protein TsaP functions in surface assembly of type IV pili. *Proceedings of the National Academy of Sciences of the United States of America* **111**, E953-961
48. Chiang, P., Habash, M., and Burrows, L. L. (2005) Disparate subcellular localization patterns of *Pseudomonas aeruginosa* Type IV pilus ATPases involved in twitching motility. *Journal of bacteriology* **187**, 829-839
49. Takhar, H. K., Kemp, K., Kim, M., Howell, P. L., and Burrows, L. L. (2013) The platform protein is essential for type IV pilus biogenesis. *The Journal of biological chemistry* **288**, 9721-9728
50. Ayers, M., Sampaleanu, L. M., Tammam, S., Koo, J., Harvey, H., Howell, P. L., and Burrows, L. L. (2009) PilM/N/O/P proteins form an inner membrane complex that affects the stability of the *Pseudomonas aeruginosa* type IV pilus secretin. *Journal of molecular biology* **394**, 128-142
51. Sampaleanu, L. M., Bonanno, J. B., Ayers, M., Koo, J., Tammam, S., Burley, S. K., Almo, S. C., Burrows, L. L., and Howell, P. L. (2009) Periplasmic domains of *Pseudomonas aeruginosa* PilN and PilO form a stable heterodimeric complex. *Journal of molecular biology* **394**, 143-159
52. Wehbi, H., Portillo, E., Harvey, H., Shimkoff, A. E., Scheurwater, E. M., Howell, P. L., and Burrows, L. L. (2011) The peptidoglycan-binding protein FimV promotes assembly of the *Pseudomonas aeruginosa t*ype IV pilus secretin. *Journal of bacteriology* **193**, 540-550

53. Fulcher, N. B., Holliday, P. M., Klem, E., Cann, M. J., and Wolfgang, M. C. (2010) The *Pseudomonas aeruginosa* Chp chemosensory system regulates intracellular cAMP levels by modulating adenylate cyclase activity. *Molecular microbiology* **76**, 889-904
54. Tammam, S., Sampaleanu, L. M., Koo, J., Manoharan, K., Daubaras, M., Burrows, L. L., and Howell, P. L. (2013) PilMNOPQ from the *Pseudomonas aeruginosa* type IV pilus system form a transenvelope protein interaction network that interacts with PilA. *Journal of bacteriology* **195**, 2126-2135
55. Tammam, S., Sampaleanu, L. M., Koo, J., Sundaram, P., Ayers, M., Chong, P. A., Forman-Kay, J. D., Burrows, L. L., and Howell, P. L. (2011) Characterization of the PilN, PilO and PilP type IVa pilus subcomplex. *Molecular microbiology* **82**, 1496-1514
56. Nguyen, Y., Jackson, S. G., Aidoo, F., Junop, M., and Burrows, L. L. (2010) Structural characterization of novel *Pseudomonas aeruginosa* type IV pilins. *Journal of molecular biology* **395**, 491-503
57. Rudel, T., Scheurerpflug, I., and Meyer, T. F. (1995) *Neisseria* PilC protein identified as type-4 pilus tip-located adhesin. *Nature* **373**, 357-359
58. Nguyen, Y., Sugiman-Marangos, S., Harvey, H., Bell, S. D., Charlton, C. L., Junop, M. S., and Burrows, L. L. (2015) *Pseudomonas aeruginosa* minor pilins prime type IVa pilus assembly and promote surface display of the PilY1 adhesin. *The Journal of biological chemistry* **290**, 601-611
59. Crago, A. M., and Koronakis, V. (1998) *Salmonella* InvG forms a ring-like multimer that requires the InvH lipoprotein for outer membrane localization. *Molecular microbiology* **30**, 47-56
60. Opalka, N., Beckmann, R., Boisset, N., Simon, M. N., Russel, M., and Darst, S. A. (2003) Structure of the filamentous phage pIV multimer by cryo-electron microscopy. *Journal of molecular biology* **325**, 461-470
61. Tosi, T., Estrozi, L. F., Job, V., Guilvout, I., Pugsley, A. P., Schoehn, G., and Dessen, A. (2014) Structural similarity of secretins from type II and type III secretion systems. *Structure* **22**, 1348-1355
62. Korotkov, K. V., Gonen, T., and Hol, W. G. (2011) Secretins: dynamic channels for protein transport across membranes. *Trends in biochemical sciences* **36**, 433-443
63. Disconzi, E., Guilvout, I., Chami, M., Masi, M., Huysmans, G. H., Pugsley, A. P., and Bayan, N. (2014) Bacterial secretins form constitutively open pores akin to general porins. *Journal of bacteriology* **196**, 121-128
64. Bouley, J., Condemine, G., and Shevchik, V. E. (2001) The PDZ domain of OutC and the N-terminal region of OutD determine the secretion specificity of the type II out pathway of *Erwinia chrysanthemi*. *Journal of molecular biology* **308**, 205-219
65. Balasingham, S. V., Collins, R. F., Assalkhou, R., Homberset, H., Frye, S. A., Derrick, J. P., and Tonjum, T. (2007) Interactions between the

lipoprotein PilP and the secretin PilQ in *Neisseria meningitidis*. *Journal of bacteriology* **189**, 5716-5727

66. de Souza, R. F., Anantharaman, V., de Souza, S. J., Aravind, L., and Gueiros-Filho, F. J. (2008) AMIN domains have a predicted role in localization of diverse periplasmic protein complexes. *Bioinformatics* **24**, 2423-2426
67. Berry, J. L., Phelan, M. M., Collins, R. F., Adomavicius, T., Tonjum, T., Frye, S. A., Bird, L., Owens, R., Ford, R. C., Lian, L. Y., and Derrick, J. P. (2012) Structure and assembly of a trans-periplasmic channel for type IV pili in *Neisseria meningitidis*. *PLoS pathogens* **8**, e1002923
68. Rocaboy, M., Herman, R., Sauvage, E., Remaut, H., Moonens, K., Terrak, M., Charlier, P., and Kerff, F. (2013) The crystal structure of the cell division amidase AmiC reveals the fold of the AMIN domain, a new peptidoglycan binding domain. *Molecular microbiology* **90**, 267-277
69. Scheurwater, E. M., and Burrows, L. L. (2011) Maintaining network security: how macromolecular structures cross the peptidoglycan layer. *FEMS microbiology letters* **318**, 1-9
70. Burrows, L. L. (2013) A new route for polar navigation. *Molecular microbiology* **90**, 919-922
71. Chang, Y. W., Rettberg, L. A., Treuner-Lange, A., Iwasa, J., Sogaard-Andersen, L., and Jensen, G. J. (2016) Architecture of the type IVa pilus machine. *Science* **351**, aad2001
72. Koo, J., Tang, T., Harvey, H., Tammam, S., Sampaleanu, L., Burrows, L. L., and Howell, P. L. (2013) Functional mapping of PilF and PilQ in the *Pseudomonas aeruginosa* type IV pilus system. *Biochemistry* **52**, 2914-2923
73. Nickerson, N. N., Abby, S. S., Rocha, E. P., Chami, M., and Pugsley, A. P. (2012) A Single Amino Acid Substitution Changes the Self-Assembly Status of a Type IV Piliation Secretin. *Journal of bacteriology* **194**, 4951-4958
74. Friedrich, C., Bulyha, I., and Sogaard-Andersen, L. (2014) Outside-in assembly pathway of the type IV pilus system in *Myxococcus xanthus*. *Journal of bacteriology* **196**, 378-390
75. Strom, M. S., and Lory, S. (1993) Structure-function and biogenesis of the type IV pili. *Annual review of microbiology* **47**, 565-596
76. Belete, B., Lu, H., and Wozniak, D. J. (2008) *Pseudomonas aeruginosa* AlgR regulates type IV pilus biosynthesis by activating transcription of the *fimU-pilVWXY1Y2E* operon. *Journal of bacteriology* **190**, 2023-2030
77. Winther-Larsen, H. C., Wolfgang, M., Dunham, S., van Putten, J. P., Dorward, D., Lovold, C., Aas, F. E., and Koomey, M. (2005) A conserved set of pilin-like molecules controls type IV pilus dynamics and organelle-associated functions in *Neisseria gonorrhoeae*. *Molecular microbiology* **56**, 903-917

78. Winther-Larsen, H. C., Wolfgang, M. C., van Putten, J. P., Roos, N., Aas, F. E., Egge-Jacobsen, W. M., Maier, B., and Koomey, M. (2007) *Pseudomonas aeruginosa* Type IV pilus expression in *Neisseria gonorrhoeae:* effects of pilin subunit composition on function and organelle dynamics. *Journal of bacteriology* **189**, 6676-6685
79. Douzi, B., Durand, E., Bernard, C., Alphonse, S., Cambillau, C., Filloux, A., Tegoni, M., and Voulhoux, R. (2009) The XcpV/GspI pseudopilin has a central role in the assembly of a quaternary complex within the T2SS pseudopilus. *The Journal of biological chemistry* **284**, 34580-34589
80. Craig, L., Taylor, R. K., Pique, M. E., Adair, B. D., Arvai, A. S., Singh, M., Lloyd, S. J., Shin, D. S., Getzoff, E. D., Yeager, M., Forest, K. T., and Tainer, J. A. (2003) Type IV pilin structure and assembly: X-ray and EM analyses of *Vibrio cholerae* toxin-coregulated pilus and *Pseudomonas aeruginosa* PAK pilin. *Molecular cell* **11**, 1139-1150
81. Nguyen, Y., Harvey, H., Sugiman-Marangos, S., Bell, S. D., Buensuceso, R. N., Junop, M. S., and Burrows, L. L. (2015) Structural and functional studies of the *Pseudomonas aeruginosa* minor pilin, PilE. *The Journal of biological chemistry* **290**, 26856-26865
82. Giltner, C. L., Nguyen, Y., and Burrows, L. L. (2012) Type IV pilin proteins: versatile molecular modules. *Microbiology and molecular biology reviews : MMBR* **76**, 740-772
83. Harvey, H., Habash, M., Aidoo, F., and Burrows, L. L. (2009) Single-residue changes in the C-terminal disulfide-bonded loop of the P*seudomonas aeruginosa* type IV pilin influence pilus assembly and twitching motility. *Journal of bacteriology* **191**, 6513-6524
84. Li, J., Egelman, E. H., and Craig, L. (2012) Structure of the *Vibrio cholerae* Type IVb Pilus and stability comparison with the *Neisseria gonorrhoeae* type IVa pilus. *Journal of molecular biology* **418**, 47-64
85. Alm, R. A., Hallinan, J. P., Watson, A. A., and Mattick, J. S. (1996) Fimbrial biogenesis genes of *Pseudomonas aeruginosa: pilW* and *pilX* increase the similarity of type 4 fimbriae to the GSP protein-secretion systems and *pilY1* encodes a gonococcal PilC homologue. *Molecular microbiology* **22**, 161-173
86. Beaussart, A., Baker, A. E., Kuchma, S. L., El-Kirat-Chatel, S., O'Toole, G. A., and Dufrene, Y. F. (2014) Nanoscale Adhesion Forces of *Pseudomonas aeruginosa* Type IV Pili. *ACS nano* **8**, 10723-10733
87. Luo, Y., Zhao, K., Baker, A. E., Kuchma, S. L., Coggan, K. A., Wolfgang, M. C., Wong, G. C., and O'Toole, G. A. (2015) A Hierarchical Cascade of Second Messengers Regulates *Pseudomonas aeruginosa* Surface Behaviors. *mBio* **6**
88. Orans, J., Johnson, M. D., Coggan, K. A., Sperlazza, J. R., Heiniger, R. W., Wolfgang, M. C., and Redinbo, M. R. (2010) Crystal structure analysis reveals *Pseudomonas* PilY1 as an essential calcium-dependent regulator

of bacterial surface motility. *Proceedings of the National Academy of Sciences of the United States of America* **107**, 1065-1070

89. Johnson, M. D., Garrett, C. K., Bond, J. E., Coggan, K. A., Wolfgang, M. C., and Redinbo, M. R. (2011) *Pseudomonas aeruginosa* PilY1 binds integrin in an RGD- and calcium-dependent manner. *PloS one* **6**, e29629
90. Julio, S. M., Inatsuka, C. S., Mazar, J., Dieterich, C., Relman, D. A., and Cotter, P. A. (2009) Natural-host animal models indicate functional interchangeability between the filamentous haemagglutinins of *Bordetella pertussis* and *Bordetella bronchiseptica* and reveal a role for the mature C-terminal domain, but not the RGD motif, during infection. *Molecular microbiology* **71**, 1574-1590
91. Huang, Y. J., Wu, C. C., Chen, M. C., Fung, C. P., and Peng, H. L. (2006) Characterization of the type 3 fimbriae with different MrkD adhesins: possible role of the MrkD containing an RGD motif. *Biochemical and biophysical research communications* **350**, 537-542
92. Siryaporn, A., Kuchma, S. L., O'Toole, G. A., and Gitai, Z. (2014) Surface attachment induces *Pseudomonas aeruginosa* virulence. *Proceedings of the National Academy of Sciences of the United States of America*
93. Ha, D. G., Richman, M. E., and O'Toole, G. A. (2014) Deletion mutant library for investigation of functional outputs of cyclic diguanylate metabolism in *Pseudomonas aeruginosa* PA14. *Applied and environmental microbiology* **80**, 3384-3393
94. Kuchma, S. L., Ballok, A. E., Merritt, J. H., Hammond, J. H., Lu, W., Rabinowitz, J. D., and O'Toole, G. A. (2010) Cyclic-di-GMP-mediated repression of swarming motility by *Pseudomonas aeruginosa*: the *pilY1* gene and its impact on surface-associated behaviors. *Journal of bacteriology* **192**, 2950-2964
95. Bohn, Y. S., Brandes, G., Rakhimova, E., Horatzek, S., Salunkhe, P., Munder, A., van Barneveld, A., Jordan, D., Bredenbruch, F., Haussler, S., Riedel, K., Eberl, L., Jensen, P. O., Bjarnsholt, T., Moser, C., Hoiby, N., Tummler, B., and Wiehlmann, L. (2009) Multiple roles of *Pseudomonas aeruginosa* TBCF10839 PilY1 in motility, transport and infection. *Molecular microbiology* **71**, 730-747
96. Whitchurch, C. B., Hobbs, M., Livingston, S. P., Krishnapillai, V., and Mattick, J. S. (1991) Characterisation of a *Pseudomonas aeruginosa* twitching motility gene and evidence for a specialised protein export system widespread in eubacteria. *Gene* **101**, 33-44
97. Whitchurch, C. B., and Mattick, J. S. (1994) Characterization of a gene, *pilU*, required for twitching motility but not phage sensitivity in *Pseudomonas aeruginosa*. *Molecular microbiology* **13**, 1079-1091
98. Chiang, P., Sampaleanu, L. M., Ayers, M., Pahuta, M., Howell, P. L., and Burrows, L. L. (2008) Functional role of conserved residues in the characteristic secretion NTPase motifs of the *Pseudomonas aeruginosa* type IV pilus motor proteins PilB, PilT and PilU. *Microbiology* **154**, 114-126

99. Misic, A. M., Satyshur, K. A., and Forest, K. T. (2010) *P. aeruginosa* PilT structures with and without nucleotide reveal a dynamic type IV pilus retraction motor. *Journal of molecular biology* **400**, 1011-1021
100. Herdendorf, T. J., McCaslin, D. R., and Forest, K. T. (2002) *Aquifex aeolicus* PilT, homologue of a surface motility protein, is a thermostable oligomeric NTPase. *Journal of bacteriology* **184**, 6465-6471
101. Py, B., Loiseau, L., and Barras, F. (2001) An inner membrane platform in the type II secretion machinery of Gram-negative bacteria. *EMBO reports* **2**, 244-248
102. Satyshur, K. A., Worzalla, G. A., Meyer, L. S., Heiniger, E. K., Aukema, K. G., Misic, A. M., and Forest, K. T. (2007) Crystal structures of the pilus retraction motor PilT suggest large domain movements and subunit cooperation drive motility. *Structure* **15**, 363-376
103. Hare, S., Bayliss, R., Baron, C., and Waksman, G. (2006) A large domain swap in the VirB11 ATPase of *Brucella suis* leaves the hexameric assembly intact. *Journal of molecular biology* **360**, 56-66
104. Yeo, H. J., Savvides, S. N., Herr, A. B., Lanka, E., and Waksman, G. (2000) Crystal structure of the hexameric traffic ATPase of the *Helicobacter pylori* type IV secretion system. *Molecular cell* **6**, 1461-1472
105. Robien, M. A., Krumm, B. E., Sandkvist, M., and Hol, W. G. (2003) Crystal structure of the extracellular protein secretion NTPase EpsE of *Vibrio cholerae*. *Journal of molecular biology* **333**, 657-674
106. Chung, I. Y., Jang, H. J., Bae, H. W., and Cho, Y. H. (2014) A phage protein that inhibits the bacterial ATPase required for type IV pilus assembly. *Proceedings of the National Academy of Sciences of the United States of America* **111**, 11503-11508
107. Nunn, D., Bergman, S., and Lory, S. (1990) Products of three accessory genes, *pilB*, *pilC*, and *pilD*, are required for biogenesis of *Pseudomonas aeruginosa* pili. *Journal of bacteriology* **172**, 2911-2919
108. Kurre, R., Hone, A., Clausen, M., Meel, C., and Maier, B. (2012) PilT2 enhances the speed of gonococcal type IV pilus retraction and of twitching motility. *Molecular microbiology* **86**, 857-865
109. Bulyha, I., Schmidt, C., Lenz, P., Jakovljevic, V., Hone, A., Maier, B., Hoppert, M., and Sogaard-Andersen, L. (2009) Regulation of the type IV pili molecular machine by dynamic localization of two motor proteins. *Molecular microbiology* **74**, 691-706
110. Keilberg, D., Wuichet, K., Drescher, F., and Sogaard-Andersen, L. (2012) A response regulator interfaces between the Frz chemosensory system and the MglA/MglB GTPase/GAP module to regulate polarity in *Myxococcus xanthus*. *PLoS genetics* **8**, e1002951
111. McCallum, M., Tammam, S., Little, D. J., Robinson, H., Koo, J., Shah, M., Calmettes, C., Moraes, T. F., Burrows, L. L., and Howell, P. L. (2016) PilN binding modulates the structure and binding partners of the *Pseudomonas*

aeruginosa Type IVa Pilus protein PilM. *The Journal of biological chemistry*

112. Szwedziak, P., Wang, Q., Freund, S. M., and Lowe, J. (2012) FtsA forms actin-like protofilaments. *The EMBO journal* **31**, 2249-2260
113. Abendroth, J., Bagdasarian, M., Sandkvist, M., and Hol, W. G. (2004) The structure of the cytoplasmic domain of EpsL, an inner membrane component of the type II secretion system of *Vibrio cholerae*: an unusual member of the actin-like ATPase superfamily. *Journal of molecular biology* **344**, 619-633
114. Karuppiah, V., and Derrick, J. P. (2011) Structure of the PilM-PilN inner membrane type IV pilus biogenesis complex from *Thermus thermophilus*. *The Journal of biological chemistry* **286**, 24434-24442
115. Yamagata, A., Milgotina, E., Scanlon, K., Craig, L., Tainer, J. A., and Donnenberg, M. S. (2012) Structure of an essential type IV pilus biogenesis protein provides insights into pilus and type II secretion systems. *Journal of molecular biology* **419**, 110-124
116. Abendroth, J., Kreger, A. C., and Hol, W. G. (2009) The dimer formed by the periplasmic domain of EpsL from the Type 2 Secretion System of *Vibrio parahaemolyticus*. *Journal of structural biology* **168**, 313-322
117. Sandkvist, M., Bagdasarian, M., Howard, S. P., and DiRita, V. J. (1995) Interaction between the autokinase EpsE and EpsL in the cytoplasmic membrane is required for extracellular secretion in *Vibrio cholerae. The EMBO journal* **14**, 1664-1673
118. Sandkvist, M., Hough, L. P., Bagdasarian, M. M., and Bagdasarian, M. (1999) Direct interaction of the EpsL and EpsM proteins of the general secretion apparatus in *Vibrio cholerae*. *Journal of bacteriology* **181**, 3129-3135
119. Bischof, L. F., Friedrich, C., Harms, A., Sogaard-Andersen, L., and van der Does, C. (2016) The Type IV Pilus Assembly ATPase PilB of *Myxococcus xanthus* interacts with the Inner Membrane Platform Protein PilC and the Nucleotide Binding Protein PilM. *The Journal of biological chemistry*
120. Abendroth, J., Murphy, P., Sandkvist, M., Bagdasarian, M., and Hol, W. G. (2005) The X-ray structure of the type II secretion system complex formed by the N-terminal domain of EpsE and the cytoplasmic domain of EpsL of *Vibrio cholerae*. *Journal of molecular biology* **348**, 845-855
121. Crowther, L. J., Yamagata, A., Craig, L., Tainer, J. A., and Donnenberg, M. S. (2005) The ATPase activity of BfpD is greatly enhanced by zinc and allosteric interactions with other Bfp proteins. *The Journal of biological chemistry* **280**, 24839-24848
122. Lallemand, M., Login, F. H., Guschinskaya, N., Pineau, C., Effantin, G., Robert, X., and Shevchik, V. E. (2013) Dynamic interplay between the periplasmic and transmembrane domains of GspL and GspM in the type II secretion system. *PloS one* **8**, e79562

123. Sandkvist, M., Keith, J. M., Bagdasarian, M., and Howard, S. P. (2000) Two regions of EpsL involved in species-specific protein-protein interactions with EpsE and EpsM of the general secretion pathway in *Vibrio cholerae*. *Journal of bacteriology* **182**, 742-748
124. Karuppiah, V., Collins, R. F., Thistlethwaite, A., Gao, Y., and Derrick, J. P. (2013) Structure and assembly of an inner membrane platform for initiation of type IV pilus biogenesis. *Proceedings of the National Academy of Sciences of the United States of America* **110**, E4638-4647
125. Kelley, L. A., and Sternberg, M. J. (2009) Protein structure prediction on the Web: a case study using the Phyre server. *Nature protocols* **4**, 363-371
126. Abendroth, J., Rice, A. E., McLuskey, K., Bagdasarian, M., and Hol, W. G. (2004) The crystal structure of the periplasmic domain of the type II secretion system protein EpsM from *Vibrio cholerae*: the simplest version of the ferredoxin fold. *Journal of molecular biology* **338**, 585-596
127. Golovanov, A. P., Balasingham, S., Tzitzilonis, C., Goult, B. T., Lian, L. Y., Homberset, H., Tonjum, T., and Derrick, J. P. (2006) The solution structure of a domain from the *Neisseria meningitidis* lipoprotein PilP reveals a new beta-sandwich fold. *Journal of molecular biology* **364**, 186-195
128. Korotkov, K. V., Johnson, T. L., Jobling, M. G., Pruneda, J., Pardon, E., Heroux, A., Turley, S., Steyaert, J., Holmes, R. K., Sandkvist, M., and Hol, W. G. (2011) Structural and functional studies on the interaction of GspC and GspD in the type II secretion system. *PLoS pathogens* **7**, e1002228
129. Rumszauer, J., Schwarzenlander, C., and Averhoff, B. (2006) Identification, subcellular localization and functional interactions of PilMNOWQ and PilA4 involved in transformation competency and pilus biogenesis in the thermophilic bacterium *Thermus thermophilus* HB27. *The FEBS journal* **273**, 3261-3272
130. Korotkov, K. V., Krumm, B., Bagdasarian, M., and Hol, W. G. (2006) Structural and functional studies of EpsC, a crucial component of the type 2 secretion system from *Vibrio cholerae*. *Journal of molecular biology* **363**, 311-321
131. Lory, S., Merighi, M., and Hyodo, M. (2009) Multiple activities of c-di-GMP in *Pseudomonas aeruginosa*. *Nucleic acids symposium series*, 51-52
132. Merritt, J. H., Ha, D. G., Cowles, K. N., Lu, W., Morales, D. K., Rabinowitz, J., Gitai, Z., and O'Toole, G. A. (2010) Specific control of *Pseudomonas aeruginosa* surface-associated behaviors by two c-di-GMP diguanylate cyclases. *mBio* **1**
133. Baraquet, C., and Harwood, C. S. (2013) Cyclic diguanosine monophosphate represses bacterial flagella synthesis by interacting with the Walker A motif of the enhancer-binding protein FleQ. *Proceedings of the National Academy of Sciences of the United States of America* **110**, 18478-18483

134. Kuchma, S. L., Brothers, K. M., Merritt, J. H., Liberati, N. T., Ausubel, F. M., and O'Toole, G. A. (2007) BifA, a cyclic-Di-GMP phosphodiesterase, inversely regulates biofilm formation and swarming motility by *Pseudomonas aeruginosa* PA14. *Journal of bacteriology* **189**, 8165-8178
135. Georgiadou, M., Castagnini, M., Karimova, G., Ladant, D., and Pelicic, V. (2012) Large-scale study of the interactions between proteins involved in type IV pilus biology in *Neisseria meningitidis:* characterization of a subcomplex involved in pilus assembly. *Molecular microbiology* **84**, 857-873
136. Levy, S. B., and Marshall, B. (2004) Antibacterial resistance worldwide: causes, challenges and responses. *Nature medicine* **10**, S122-129
137. Coates, A. R., and Hu, Y. (2007) Novel approaches to developing new antibiotics for bacterial infections. *British journal of pharmacology* **152**, 1147-1154
138. Clatworthy, A. E., Pierson, E., and Hung, D. T. (2007) Targeting virulence: a new paradigm for antimicrobial therapy. *Nature chemical biology* **3**, 541-548
139. Bailey, L., Gylfe, A., Sundin, C., Muschiol, S., Elofsson, M., Nordstrom, P., Henriques-Normark, B., Lugert, R., Waldenstrom, A., Wolf-Watz, H., and Bergstrom, S. (2007) Small molecule inhibitors of type III secretion in *Yersinia* block the *Chlamydia pneumoniae* infection cycle. *FEBS letters* **581**, 587-595
140. Kauppi, A. M., Nordfelth, R., Uvell, H., Wolf-Watz, H., and Elofsson, M. (2003) Targeting bacterial virulence: inhibitors of type III secretion in *Yersinia*. *Chemistry & biology* **10**, 241-249
141. Keyser, P., Elofsson, M., Rosell, S., and Wolf-Watz, H. (2008) Virulence blockers as alternatives to antibiotics: type III secretion inhibitors against Gram-negative bacteria. *Journal of internal medicine* **264**, 17-29
142. Bieber, D., Ramer, S. W., Wu, C. Y., Murray, W. J., Tobe, T., Fernandez, R., and Schoolnik, G. K. (1998) Type IV pili, transient bacterial aggregates, and virulence of enteropathogenic *Escherichia coli*. *Science* **280**, 2114-2118
143. Beatson, S. A., Whitchurch, C. B., Sargent, J. L., Levesque, R. C., and Mattick, J. S. (2002) Differential regulation of twitching motility and elastase production by Vfr in *Pseudomonas aeruginosa*. *Journal of bacteriology* **184**, 3605-3613
144. Darzins, A. (1994) Characterization of a *Pseudomonas aeruginosa* gene cluster involved in pilus biosynthesis and twitching motility: sequence similarity to the chemotaxis proteins of enterics and the gliding bacterium *Myxococcus xanthus*. *Molecular microbiology* **11**, 137-153
145. Reichow, S. L., Korotkov, K. V., Hol, W. G., and Gonen, T. (2010) Structure of the cholera toxin secretion channel in its closed state. *Nature structural & molecular biology* **17**, 1226-1232

146. Battesti, A., and Bouveret, E. (2012) The bacterial two-hybrid system based on adenylate cyclase reconstitution in *Escherichia coli*. *Methods* **58**, 325-334
147. Hoang, T. T., Karkhoff-Schweizer, R. R., Kutchma, A. J., and Schweizer, H. P. (1998) A broad-host-range Flp-FRT recombination system for site-specific excision of chromosomally-located DNA sequences: application for isolation of unmarked *Pseudomonas aeruginosa* mutants. *Gene* **212**, 77-86
148. Asikyan, M. L., Kus, J. V., and Burrows, L. L. (2008) Novel proteins that modulate type IV pilus retraction dynamics in *Pseudomonas aeruginosa*. *Journal of bacteriology* **190**, 7022-7034
149. Kus, J. V., Tullis, E., Cvitkovitch, D. G., and Burrows, L. L. (2004) Significant differences in type IV pilin allele distribution among *Pseudomonas aeruginosa* isolates from cystic fibrosis (CF) versus non-CF patients. *Microbiology* **150**, 1315-1326
150. Schneider, C. A., Rasband, W. S., and Eliceiri, K. W. (2012) NIH Image to ImageJ: 25 years of image analysis. *Nature methods* **9**, 671-675
151. Karimova, G., Dautin, N., and Ladant, D. (2005) Interaction network among *Escherichia coli* membrane proteins involved in cell division as revealed by bacterial two-hybrid analysis. *Journal of bacteriology* **187**, 2233-2243
152. Wolfgang, M., Lauer, P., Park, H. S., Brossay, L., Hebert, J., and Koomey, M. (1998) PilT mutations lead to simultaneous defects in competence for natural transformation and twitching motility in piliated Neisseria gonorrhoeae. *Mol Microbiol* **29**, 321-330
153. Bose, N., Payne, S. M., and Taylor, R. K. (2002) Type 4 pilus biogenesis and type II-mediated protein secretion by *Vibrio cholerae* occur independently of the TonB-facilitated proton motive force. *Journal of bacteriology* **184**, 2305-2309
154. Abendroth, J., Mitchell, D. D., Korotkov, K. V., Johnson, T. L., Kreger, A., Sandkvist, M., and Hol, W. G. (2009) The three-dimensional structure of the cytoplasmic domains of EpsF from the type 2 secretion system of *Vibrio cholerae*. *Journal of structural biology* **166**, 303-315
155. McLaughlin, L. S., Haft, R. J., and Forest, K. T. (2012) Structural insights into the Type II secretion nanomachine. *Current opinion in structural biology* **22**, 208-216
156. Py, B., Loiseau, L., and Barras, F. (1999) Assembly of the type II secretion machinery of *Erwinia chrysanthemi*: direct interaction and associated conformational change between OutE, the putative ATP-binding component and the membrane protein OutL. *Journal of molecular biology* **289**, 659-670
157. Wolfgang, M., Lauer, P., Park, H. S., Brossay, L., Hebert, J., and Koomey, M. (1998) PilT mutations lead to simultaneous defects in competence for

natural transformation and twitching motility in piliated *Neisseria gonorrhoeae*. *Molecular microbiology* **29**, 321-330

158. Carbonnelle, E., Helaine, S., Nassif, X., and Pelicic, V. (2006) A systematic genetic analysis in *Neisseria meningitidis* defines the Pil proteins required for assembly, functionality, stabilization and export of type IV pili. *Molecular microbiology* **61**, 1510-1522
159. Carbonnelle, E., Helaine, S., Prouvensier, L., Nassif, X., and Pelicic, V. (2005) Type IV pilus biogenesis in *Neisseria meningitidis*: PilW is involved in a step occurring after pilus assembly, essential for fibre stability and function. *Molecular microbiology* **55**, 54-64
160. Lee, H. M., Wang, K. C., Liu, Y. L., Yew, H. Y., Chen, L. Y., Leu, W. M., Chen, D. C., and Hu, N. T. (2000) Association of the cytoplasmic membrane protein XpsN with the outer membrane protein XpsD in the type II protein secretion apparatus of *Xanthomonas campestris pv. campestris*. *Journal of bacteriology* **182**, 1549-1557
161. Lu, C., Korotkov, K. V., and Hol, W. G. (2014) Crystal structure of the full-length ATPase GspE from the *Vibrio vulnificus* type II secretion system in complex with the cytoplasmic domain of GspL. *Journal of structural biology* **187**, 223-235
162. Gray, M. D., Bagdasarian, M., Hol, W. G., and Sandkvist, M. (2011) In vivo cross-linking of EpsG to EpsL suggests a role for EpsL as an ATPase-pseudopilin coupling protein in the Type II secretion system of *Vibrio cholerae*. *Molecular microbiology* **79**, 786-798
163. Paschos, A., den Hartigh, A., Smith, M. A., Atluri, V. L., Sivanesan, D., Tsolis, R. M., and Baron, C. (2011) An *in vivo* high-throughput screening approach targeting the type IV secretion system component VirB8 identified inhibitors of *Brucella abortus 2308* proliferation. *Infection and immunity* **79**, 1033-1043
164. Smith, M. A., Coincon, M., Paschos, A., Jolicoeur, B., Lavallee, P., Sygusch, J., and Baron, C. (2012) Identification of the binding site of *Brucella* VirB8 interaction inhibitors. *Chemistry & biology* **19**, 1041-1048
165. Simon, R., Priefer, U., Pulher, A. (1983) A broad host range mobilisation system for *in vivo* genetic engineering: transposon mutagenesis in Gram-negative bacteria. *Nat Biotech* **1**, 784-791
166. Kus, J. V., Kelly, J., Tessier, L., Harvey, H., Cvitkovitch, D. G., and Burrows, L. L. (2008) Modification of *Pseudomonas aeruginosa* Pa5196 type IV Pilins at multiple sites with D-Araf by a novel GT-C family Arabinosyltransferase, TfpW. *Journal of bacteriology* **190**, 7464-7478
167. Winsor, G. L., Lam, D. K., Fleming, L., Lo, R., Whiteside, M. D., Yu, N. Y., Hancock, R. E., and Brinkman, F. S. (2011) *Pseudomonas* Genome Database: improved comparative analysis and population genomics capability for Pseudomonas genomes. *Nucleic acids research* **39**, D596-600

168. Clamp, M., Cuff, J., Searle, S. M., and Barton, G. J. (2004) The Jalview Java alignment editor. *Bioinformatics* **20**, 426-427
169. Waterhouse, A. M., Procter, J. B., Martin, D. M., Clamp, M., and Barton, G. J. (2009) Jalview Version 2--a multiple sequence alignment editor and analysis workbench. *Bioinformatics* **25**, 1189-1191
170. Douzi, B., Filloux, A., and Voulhoux, R. (2012) On the path to uncover the bacterial type II secretion system. *Philosophical transactions of the Royal Society of London. Series B, Biological sciences* **367**, 1059-1072
171. Durand, E., Bernadac, A., Ball, G., Lazdunski, A., Sturgis, J. N., and Filloux, A. (2003) Type II protein secretion in *Pseudomonas aeruginosa*: the pseudopilus is a multifibrillar and adhesive structure. *Journal of bacteriology* **185**, 2749-2758
172. Robert, V., Hayes, F., Lazdunski, A., and Michel, G. P. (2002) Identification of XcpZ domains required for assembly of the secreton of *Pseudomonas aeruginosa*. *Journal of bacteriology* **184**, 1779-1782
173. Winston, S. E., Mehan, R., and Falke, J. J. (2005) Evidence that the adaptation region of the aspartate receptor is a dynamic four-helix bundle: cysteine and disulfide scanning studies. *Biochemistry* **44**, 12655-12666
174. Seeger, M. A., von Ballmoos, C., Eicher, T., Brandstatter, L., Verrey, F., Diederichs, K., and Pos, K. M. (2008) Engineered disulfide bonds support the functional rotation mechanism of multidrug efflux pump AcrB. *Nature structural & molecular biology* **15**, 199-205
175. Bass, R. B., Butler, S. L., Chervitz, S. A., Gloor, S. L., and Falke, J. J. (2007) Use of site-directed cysteine and disulfide chemistry to probe protein structure and dynamics: applications to soluble and transmembrane receptors of bacterial chemotaxis. *Methods in enzymology* **423**, 25-51
176. Arts, J., de Groot, A., Ball, G., Durand, E., El Khattabi, M., Filloux, A., Tommassen, J., and Koster, M. (2007) Interaction domains in the *Pseudomonas aeruginosa* type II secretory apparatus component XcpS (GspF). *Microbiology* **153**, 1582-1592
177. Robert, V., Filloux, A., and Michel, G. P. (2005) Subcomplexes from the Xcp secretion system of *Pseudomonas aeruginosa*. *FEMS microbiology letters* **252**, 43-50
178. Leighton, T. L., Dayalani, N., Sampaleanu, L. M., Howell, P. L., and Burrows, L. L. (2015) A novel role for PilNO in type IV pilus retraction revealed by alignment subcomplex mutations. *Journal of bacteriology*
179. Careaga, C. L., and Falke, J. J. (1992) Thermal motions of surface alpha-helices in the D-galactose chemosensory receptor. Detection by disulfide trapping. *Journal of molecular biology* **226**, 1219-1235
180. Careaga, C. L., and Falke, J. J. (1992) Structure and dynamics of *Escherichia coli* chemosensory receptors. Engineered sulfhydryl studies. *Biophysical journal* **62**, 209-216; discussion 217-209

181. Wang, X., Pineau, C., Gu, S., Guschinskaya, N., Pickersgill, R. W., and Shevchik, V. E. (2012) Cysteine scanning mutagenesis and disulfide mapping analysis of arrangement of GspC and GspD protomers within the type 2 secretion system. *The Journal of biological chemistry* **287**, 19082-19093
182. Simon, V., and Schumann, W. (1987) *In vivo* formation of gene fusions in *Pseudomonas putida* and construction of versatile broad-host-range vectors for direct subcloning of Mu d1 and Mu d2 fusions. *Applied and environmental microbiology* **53**, 1649-1654
183. Nguyen, Y., Sugiman-Marangos, S., Harvey, H., Bell, S. D., Charlton, C. L., Junop, M. S., and Burrows, L. L. (2014) *Pseudomonas aeruginosa* Minor Pilins Prime Type IVa Pilus Assembly and Promote Surface Display of the PilY1 Adhesin. *The Journal of biological chemistry*
184. Martin, P. R., Watson, A. A., McCaul, T. F., and Mattick, J. S. (1995) Characterization of a five-gene cluster required for the biogenesis of type 4 fimbriae in *Pseudomonas aeruginosa*. *Molecular microbiology* **16**, 497-508
185. Leighton, T. L., Yong, D. H., Howell, P. L., and Burrows, L. L. (2016) Type IV Pilus Alignment Subcomplex Components PilN and PilO Form Homo- and Heterodimers *In Vivo*. *The Journal of biological chemistry*
186. Walter, T. S., Meier, C., Assenberg, R., Au, K. F., Ren, J., Verma, A., Nettleship, J. E., Owens, R. J., Stuart, D. I., and Grimes, J. M. (2006) Lysine methylation as a routine rescue strategy for protein crystallization. *Structure* **14**, 1617-1622
187. Minor, W., Cymborowski, M., Otwinowski, Z., and Chruszcz, M. (2006) HKL-3000: the integration of data reduction and structure solution--from diffraction images to an initial model in minutes. *Acta crystallographica. Section D, Biological crystallography* **62**, 859-866
188. Winn, M. D., Ballard, C. C., Cowtan, K. D., Dodson, E. J., Emsley, P., Evans, P. R., Keegan, R. M., Krissinel, E. B., Leslie, A. G., McCoy, A., McNicholas, S. J., Murshudov, G. N., Pannu, N. S., Potterton, E. A., Powell, H. R., Read, R. J., Vagin, A., and Wilson, K. S. (2011) Overview of the CCP4 suite and current developments. *Acta crystallographica. Section D, Biological crystallography* **67**, 235-242
189. Chen, V. B., Arendall, W. B., 3rd, Headd, J. J., Keedy, D. A., Immormino, R. M., Kapral, G. J., Murray, L. W., Richardson, J. S., and Richardson, D. C. (2010) MolProbity: all-atom structure validation for macromolecular crystallography. *Acta crystallographica. Section D, Biological crystallography* **66**, 12-21
190. Adams, P. D., Afonine, P. V., Bunkoczi, G., Chen, V. B., Davis, I. W., Echols, N., Headd, J. J., Hung, L. W., Kapral, G. J., Grosse-Kunstleve, R. W., McCoy, A. J., Moriarty, N. W., Oeffner, R., Read, R. J., Richardson, D. C., Richardson, J. S., Terwilliger, T. C., and Zwart, P. H. (2010) PHENIX: a comprehensive Python-based system for macromolecular structure

solution. *Acta crystallographica. Section D, Biological crystallography* **66**, 213-221
191. Krissinel, E., and Henrick, K. (2004) Secondary-structure matching (SSM), a new tool for fast protein structure alignment in three dimensions. *Acta crystallographica. Section D, Biological crystallography* **60**, 2256-2268
192. Dyson, H. J., and Wright, P. E. (2002) Coupling of folding and binding for unstructured proteins. *Current opinion in structural biology* **12**, 54-60
193. Matilla, M. A., Ramos, J. L., Duque, E., de Dios Alche, J., Espinosa-Urgel, M., and Ramos-Gonzalez, M. I. (2007) Temperature and pyoverdine-mediated iron acquisition control surface motility of *Pseudomonas putida*. *Environmental microbiology* **9**, 1842-1850